공학박사 학위논문

Sulfur Modification

for Battery and Optical Applications

차세대 배터리 및 광학 응용을 위한 황의 개질에

관한 연구

2016년 8 월

서울대학교 대학원

화학생물공학부

김 의 태

Abstract

Understanding and developing a new sulfur chemistry give great opportunities for the synthesis of advanced functional materials, because of the strong relationship between sulfur and the environment on the Earth, as well as the economic demands to address surplus problem of sulfur from oil refinery industry. Although there are a number of superior functionalities with sulfur, such as high refractive index and electrochemical activity, its utilization and processing are challenging due to the poor physico-chemical properties resulted from its orthorhombic molecular crystalline nature. There have been several efforts to incorporate sulfur into amorphous polymeric materials, but simple preparation methods for high sulfur content polymers are still lacking.

In this thesis, extremely simple chemistry to prepare high sulfur content copolymers is introduced, and various kinds of their applications, including IR optical devices and cathodes for Li-S batteries, are demonstrated with the significantly improved processibility and performances of the sulfur copolymers. Moreover, based on these sulfur copolymers, novel hybridization strategies are proposed for the enhanced functionalities, and finally, a couple of conformal coating methods are reported to stabilize the surface of sulfur copolymers when they are utilized in electrochemical electrodes.

After a brief introduction on unique characteristics and challenging issues of sulfur, in chapter 1, the novel synthetic chemistry of sulfur copolymers, and their properties

are discussed in chapter 2, followed by facile processing the polymers for the various applications. By the '*inverse vulcanization*', high sulfur contents copolymers were synthesized, and their completely amorphous and viscous nature was analyzed. A melt process was conducted with these amorphous polymers using PDMS imprint nano pattering technique, and solution process was also possible due to the solubility of the copolymers at increased temperature. By using these processing methods, the sulfur copolymers were utilized in various applications, such as IR lens, transistors, photonic crystals, and Li-S batteries. Superior functionalities of the copolymers were attributed to the intrinsic properties of elemental sulfur.

Hybridization of sulfur copolymers with functional nanomaterials were introduced in chapter 3, with a novel bi-functionality of oleylamine which is a comonomer for the sulfur copolymeric matrices. Because the double bond in the middle of oleylamine links to linear polysulfide, and amine functional group is attached the surface of inorganic nanoparticles, the nanocomposites with sulfur copolymers were prepared by adding inorganic salts into the copolymer mixture. The reaction mechanism facilitating simple one-pot synthesis of the sulfur copolymeric nanocomposites were revealed by various characterization tools.

In chapter 4, the preparation of graphene sulfur copolymeric nanocomposites are exhibited based on similar dual reactivity of oleylamine. Especially, significant enhancement in battery performance was demonstrated with these nanocomposites due to the intense electrical contact facilitated by graphene within the copolymers.

The surface modification of sulfur copolymers is discussed in chapter 5, more

focused on the potential application in Li-S batteries. Because the interface interaction between sulfur cathode and electrolyte is a serious problem in Li-S batteries, direct deposition of protecting layers on sulfur cathode was demonstrated with drastically enhanced cycle performance of the polymer coated sulfur cathodes. Polymer conformal coating methods such as layer-by-layer (LbL) deposition on top of the sulfur cathode are introduced to further increase the capacity retention of Li-S batteries.

Keyword : sulfur copolymer, hybridization, surface modification, lithium-sulfur battery, conformal coating

Student Number : 2010-22808

Contents

List of Figures

List of Tables

Chapter 1. Introduction

1.1. Utilization of sulfur as an alternative feedstock

Sulfur is everywhere. It is the sixth most abundant element in the Earth.[1] Sulfur occurs as organosulfur compounds, sulfide, sulfate minerals or elemental sulfur in crustal rocks, in the Earth's mantle, near volcanoes, in ocean water, or in the atmosphere.[2-4] Sulfur is also an essential ingredient in living things including human body, necessary for protein synthesis.[5] Because sulfur has variable valence states (i.e. S^{2-} (H_2S), S^{6+} (SO_4^{2-}), and S^0), it is a common ore former from the deep geological fluids, and it continuously circulates through ocean, atmosphere, and living systems by thermochemical, or biological reduction/oxidation.[6] This global cycle of sulfur species is called as "sulfur cycle", and it strongly affect the environment and the ecosystem of the Earth. Therefore the understanding of the sulfur chemistry draws general scientific curious.

The development of new sulfur chemistry is also of great interest to chemists and engineers as well, due to the economic importance of sulfur in the relevant industries. Nowadays, most of the sulfur produced worldwide is a by-product from petroleum refineries, and oil producing countries still have difficulty in figuring out what to do with sulfur. Even though it mainly produced from crude oil which is thought to be

on the brink of depletion, ironically, sulfur itself is currently suffering from excessive surplus and low price. Despite the large scale conversion of sulfur as a feedstock for sulfuric acid and downstream fertilizers, there typically remains an annual surplus of approximately 7 million tons,[7] much of which is stored in massive above ground deposits as shown in **Figure 1.1**. These sulfur deposits lead to the serious environmental issue, because sulfur sublimes and oxidizes in the atmosphere to form SO_2, which is the primary cause of acid rain. Therefore the utilization of abundant sulfur instead of oil, as an alternative feedstock for the synthesis of advanced materials and a higher value-added business provides unique opportunities.

Figure 1.1 Example of an exposed deposit of elemental sulfur from hydro-desulfurization in petroleum refining processes.

1.2. Unique properties and application of sulfur

There are numerous useful and superior characteristics of sulfur relevant to advanced functional materials, when it is incorporated into organic/inorganic compounds, or as elemental sulfur, by itself. Similar to oxygen, sulfur is a common heteroatom consisting organic molecules or polymers, and also a popular source for inorganic semiconductors (metal chalcogenides) as well. Furthermore, elemental sulfur has attracted great attention recently, due to its unique electrochemistry.

1.2.1 Optical and optoelectronic applications

Sulfur is combined with organic/inorganic compounds for the enhanced optical and optoelectronic functionalities. Refractive index (n) is an intrinsic property of material, which describe how light propagates through the medium. Higher n means larger refraction of light, resulting in more efficient dispersion or focusing of light with the same medium path length. Therefore, high n is required in various optical, or optoelectronic devices such as LEDs, solar cells, cameras, and sensors.[8] Elemental sulfur is the lightest solid chalcogen on Earth, and it is highly polarizable on the applied electro-magnetic field due to the unpaired electrons in its valent shell.[9] Therefore it exhibits high refractive index (n=1.9-2.1) which is comparable to that of ceramics, and much higher than that of typical hydrocarbons or glasses. Therefore sulfur is frequently utilized in optical devices, especially in infrared optics, because the low phonon energy of sulfur bonds leads to its IR transparency.[10] Typically, other

inorganic elements, such as As or Se, are combined with sulfur to fabricate into glasses for the enhancement of optical functionalities and mechanical stabilities.[9, 11-12] However, because of the difficulties in processing and fabrication of elemental sulfur into the well-defined optical devices due to the molecular crystallinity of sulfur, in general, these IR glasses based on elemental sulfur are not widely utilized in micro/nano scale devices which require a precise control of shapes and thicknesses of the glasses.

In the micro/nano scale devices, hydrocarbon polymers are employed as a high *n* material, due to their various options of processing methods, and capabilities of precise morphological control. In these cases, sulfur is often utilized as a heteroatom in the polymers, in order to enhance the optical properties of the polymers, because the molar refraction of sulfur atom is much higher (R_m=8) than other heteroatoms (R_m=1-2).[13] Therefore, when the sulfur contents in the polymers increase, the average *n* drastically increase. Although a large number of efforts have been devoted to increase *n* of the polymer by increasing sulfur contents, however, there is still a limitation of *n* below 2 due to the lack of chemical synthetic methods to increase sulfur contents.[14-15] In order to increase *n* of the polymers over 2, high-*n* inorganic nanoparticles has been introduced as a filler within the polymeric matrices.[15] Ceramic fillers such as ZrO_2 or TiO_2 were hybridized with high-*n* polymeric resins, and greatly increased the *n* values with facile processing methods.[16-18] Sulfur containing metal chalcogenides (metal sulfides) such as PbS, CdS, and ZnS are also included in the high-n nanocomposites as well,[19-20] and especially, PbS/polymer

nanohybrid materials exhibit ultra-high *n* due to the superior optical property of PbS (*n*=4.2).[21]

Metal sulfides are also well-known semiconductors, which are frequently utilized in optoelectronic devices such as LED, solar cells, and photo detectors.[22-24] Recently, great number of synthetic methods using sulfur for metal sulfide nanocrystals with various shape (quantum dots, nanorods, nanowires, and tetrapods) have been reported with precise control of their size and shape.[20, 25-33] By tuning the bandgap and electron/hole mobility of metal sulfides nanocrystals, the performance of the optoelectronic devices are optimized. Elemental sulfur was recently turned out to be photoactive, and capable of acting as a hole conductor.[34] Therefore it was utilized as a photo detector,[35] and an electrolyte of dye sensitized solar cell.

1.2.2 Electrochemical applications

Sulfur has superior electrochemical properties because it is the most electro-negative solid on Earth, and it has unique and variable valent states, so that it is often employed in various electrochemical devices including secondary batteries. When elemental sulfur (S_8) dissolves in electrolytes of galvanic cells, the cascade cathodic reduction takes place at -0.48 V (SHE), and S_8 converts into polysulfide anions (S_x^{2-}, x=2-8) and is finally reduced into S^{2-}.[36-38] These electrochemical process produces large amount of electricity when combined with lithium metal as an anode, generating 2.57 V vs Li/Li^+, and 1675 mAh/g of theoretical discharge capacity, which is 7 times higher than those of today's lithium ion batteries based on $LiCoO_2$

cathodes.[39] Hence, lithium-sulfur (Li-S) secondary battery has been considered as one of the most promising candidates for the next generation energy storages such as electric vehicles or large scale electric energy storage systems (ESS). Furthermore the unique cascade redox reaction of sulfur was also utilized as an electrolyte in electrochemical capacitors[40] and photo-electrochemical cells[41].

On the other hand, it is still considered as a daunting task to achieve the theoretical capacity from the Li-S batteries because of irreversible loss of polysulfide active materials, the low electrical conductivity of sulfur (10-15 Ω·m),[42] and the mechanically induced damage to electrodes incurred from volumetric expansion of lithiated discharge products. In particular, higher order discharge products ranging between S_8 and Li_2S from the electrochemical reaction, polysulfides, are highly soluble in the electrolyte medium, thus they are continuously dissolved until Li_2S is finally precipitated on the cathode during battery operation. When the polysulfides are precipitated as Li_2S on the cathode during the redox reaction, they easily form chalks at the surface of the cathode without electrical contacts. The electrical isolation of the precipitated active species results in the serious loss of capacity by further impeding the electrochemical reaction. Moreover, the diffusion of these polysulfides through the electrolyte phase also leads to the migration onto the Li anode side to form inactive deposits on the surface of Li metal, retarding the charging back to higher order polysulfides (i.e., polysulfide shuttle).[43]

In order to solve these critical issues, significant efforts have been placed particularly on tailoring the morphology of active sulfur species on the nanoscale.

Significant improvements have been made by the use of sulfur/carbon composites,[44-50] where nano-sized sulfur was chemically or physically entrapped by carbonaceous materials. Carbonaceous encapsulation of sulfur has been reported to preserve the polysulfides within the vicinity of the cathode side as well as to enhance the electrical conductivity of the cathode. The most representative one among the carbonaceous materials is graphene due to its superior electrical conductivity and extremely small occupied volume. However, both graphene and sulfur are intrinsically poor materials for processing, so the chemically oxidized graphene, graphene oxide (GO), was mostly utilized for the preparation of sulfur/GO composites.[51-56] Even though the reduction of GO was able to recover the original electrical property of graphene, the high quality nanocomposites with sulfur and reduced GO for Li-S batteries were rarely reported.[57-60]

1.2.3 Other applications

Because there is an intimate relation between sulfur and living organisms, sulfur has been utilized in biological application since a long time ago. Sulfur is a traditional fertilizer due to its anti-bacterial property, which are closely related to the cascade electrochemical redox reaction of sulfur, which disturbs the activities of the cells in the bacteria.[61-62] Various organosulfur compounds, and sulfur nanoparticles were developed for the improvement in anti-bacterial function with bio-compatibility and selectivity.[63-65]

Sulfur also works for a mercury capture, when an ionic complex is formed with

polysulfide.[66-67] The polysulfide dianions associate with metal cations and form a gel in organic polar solvents. After supercritical drying of the gel, porous aerosol, named as “chalcogel”, was obtained, and it exhibited efficient capability of mercury capture. The reason for that is the strong interaction between linear polysulfide chains and mercury vapor.[68]

Sulfur is known as an insulator, but it is able to response on an applied electric field.[69-70] Therefore sulfur was utilized as a nano-patterning material, by applying a high electric field on the defined regions of sulfur film.[71] When electric field is applied on sulfur, the S_8 rings are opened, and linear chains of sulfur with diradical ends initiate the homopolymerization of sulfur. As a result, polymeric sulfur is formed according to the nano-pattern by the applied electric field, and further modification is possible on the patterned film because polymeric sulfur is insoluble in any organic solvent, while as elemental sulfur is removable with solvents.

The incorporation of sulfur into electro-active organic molecule is able to tune the electrical performance. For example, pentacene is known as a common organic semiconductor, and it was simply combined with sulfur to form hexathiapentacene, which exhibited a modified carrier mobility and on/off ratio when utilized as an active material of the organic thin film transistor.[72-73]

1.3. Old chemistry for incorporation of sulfur into polymers

Although there is a number of useful properties with sulfur as shown in chapter 1.2, the synthesis and fabrication with sulfur for the preparation of functional advanced materials are still challenging, due to the intrinsic poor physicochemical properties of sulfur. The most stable molecular form of elemental sulfur in the atmosphere at room temperature is a ring of S_8, and the S_8 molecules form orthorhombic crystal structure with a weak intermolecular interaction.[74] Therefore the mechanical strength of sulfur is very weak compared to inorganics and polymers, and it easily sublimes even at room temperature. Due to its crystallinity, the morphology control of sulfur in a nano-scale is difficult. Furthermore, the solubility or miscibility of sulfur is very poor, so the solution processing or melt processing is limited.

Hence, in order to enlarge the options of synthetic and processing methods with sulfur, the physico-chemical modification of sulfur is required. Since about a half century ago, many scientists have attempted to make polymers with sulfur, or incorporate sulfur into the polymers.

1.3.1 Homopolymerization of sulfur

Sulfur (S_8) melts at 119 ^oC, and the S_8 ring opens to form linear chains with di-radical ends at 159 ^oC. At this point, sulfur di-radicals spontaneously connect each other by the free radical polymerization, to form long chain polymeric sulfur. The

viscosity of molten sulfur increase abruptly at 159 ºC, but when the temperature is further increased, the viscosity slowly decrease. On the other hand, the contents of polymeric sulfur linearly increase, as a function temperature. These phenomena imply that the average chain length of the polymeric sulfur is maximum at 159 ºC, and it gradually decompose into shorter chain polymers as increasing temperature. Therefore this reaction is considered as an equilibrium homopolymerization of sulfur, which strongly depends on the temperature.[75-77]

The polymeric sulfur depolymerize and slowly come back to S_8 when it is cooled down to room temperature, because the linear sulfur chains are unstable at lower temperature below 159 ºC. However, when it is quickly quenched with dry ice or liquid nitrogen, the polymeric sulfur remains without depolymerization for a few days. The properties of polymeric sulfur are very different from those of elemental sulfur. It is absolutely insoluble in any organic solvent, and that is why it is called as "insoluble sulfur". The mechanical strength of polymeric sulfur is much harder than elemental sulfur.[78-79]

Although polymeric sulfur is not widely utilized for the material synthesis, the chemistry behind the polymeric sulfur has been often referred by the researchers who has tried to copolymerize sulfur with other monomers.

1.3.2 Vulcanization of rubber

Vulcanization is one of the most popular and oldest chemistry for the copolymerization of sulfur, although the reaction mechanism is still controversy.

When sulfur is heated above 140 °C with a natural rubber or synthetic rubbers such as polybutadiene or polyisoprene, an elastomer is formed by the cross-linking reaction with linear sulfur linkages.

Vulcanization is often conducted with accelerators, which catalyze the reaction by opening the S_8 ring, and control the quality of the products by fractionation and rearrangement of the sulfur linkages.[80-81] Generally, tertiary amines, thiols, and organo-metallic compounds are used as accelerators. Therefore there are two different types of vulcanization, which are accelerated, and unaccelerated vulcanization. The reaction mechanism of vulcanization is explained with two different pathways. The first one is a radical reaction near the double bonds of the rubber, occurred by sulfur radicals which are formed by a homolytic scission of S_8. Another one is polar addition to the double bonds by sulfur cations which are formed by a heterolytic scission of S_8.[82] In general, both of them are involved in the reaction process, but they depend on the type of the vulcanization, and the accelerator used.

The chemical stability and mechanical strength of the vulcanizated rubber is strongly depends on the sulfur contents.[83] With high sulfur contents (32%), linear sulfur chain is unstable due to the long chain length, so the crosslinking density is poor, and it easily depolymerize to form elemental sulfur on the surface of rubber (sulfur blooming). The optimum fraction of sulfur is known to be only 2%, in order to achieve high crosslinking density and chemical stability.

1.3.3 Copolymerization of sulfur with monomers

Using a similar chemistry to vulcanization, there has been many synthetic methods proposed for the sulfur copolymers with olefinic monomers which have analogue molecular structure with synthetic rubbers. The double bonds of olefinic monomers such as styrene, butadiene, and cyclohexene react with elemental sulfur, similar to vulcanization.[84-87] However, in this case, the yield of polymeric species is too small, and the main products of the reaction is oligomers or dimers, as a form of bis-alkyl akenyl sulfides.[88-89] These differences could come from the different reaction condition of olefin/sulfur in dilute organic solution, due to the immiscibility of each other, in which solvents could suppress the growth of the polymers.

Sulfur copolymers were synthesized by the oxidative condensation of dithiol monomers.[90-91] The sulfur contents of these polymers are very low, although they exhibit unique self-healing properties due to their dynamic covalent sulfur bonds. Furthermore, the addition of elemental sulfur into these disulfide polymers were also introduced using liquid sulfur as a reactive medium.[92-94] Similar to the vulcanization, elemental sulfur associate to the disulfide bonds, and combined with them by insertion. However the functionalities of these polymers are limited, and the processing methods with them are lacking.

Sulfur also anionically reacts with olefins in the presence of strong base such as Li or Na metal.[95-97] Well-defined sulfur copolymers with propylene sulfide were reported, and the kinetics of polymerization and the characterization of the products were successfully conducted.[98-99] However these reactions require very low

temperature and inert environment to suppress side reaction.

Therefore, the facile synthetic method of high sulfur content polymeric materials with chemical stability and mechanical strength is still absent, to the best of my knowledge. In this thesis, we present extremely simple synthetic method to prepare high sulfur content copolymers by bulk reaction of sulfur with olefin monomers in melt, and thereby provide various facile processing methods for utilization of sulfur in a number of applications as advanced materials. Furthermore, an enhancement of the functionalities of the sulfur copolymers is demonstrated by the fabrication of sulfur copolymers into hybrid nanocompoistes using unique dual reaction chemistry of the olefin monomer. Finally, we report on the surface modification of the sulfur copolymers using various polymer coating techniques and a novel chemistry, for the enhanced functionalities of sulfur copolymers as well. These efforts are expected to address the critical issues on sulfur surplus problem, and to give a meaningful insight on understanding chemistry of sulfur, which is closely related to human beings.

Chapter 2. Unique Properties & Applications of Sulfur Copolymers

2.1. Introduction

Since more than one and a half centuries ago, petroleum has been widely consumed throughout the world for major resources of energy and chemical products. Nowadays, petroleum is no more an attractive resource because it is on the brink of depletion and its price keeps rising. Ironically, sulfur itself is suffering from rather surplus and its lowering price even though it is mainly produced from petroleum refinery process. People still don't know what to do with abundant and cheap sulfur except for little utilization of it in agriculture and some chemical products including rubbers. Sulfur exhibits a number of useful properties relevant to advanced materials, such as high refractive index for optical devices,[8] and electrochemical activity for high capacity lithium-sulfur batteries.[46, 54, 100] However, due to its inherently poor solubility, brittle nature, and being readily subject to sublimation, synthesis and processing methods with sulfur to prepare well-defined functional materials are currently limited.

Previous researchers have tried to get polymeric forms of sulfur for easy handling. By heating above 159 ^{o}C, sulfur transforms from eight-membered ring (S_8) into

linear polysulfide chains with diradical ends, which subsequently polymerize into high molecular weight polymers with plastic behavior.[75-79] When the polymeric sulfur is stored in ambient condition, however, it readily depolymerizes back to polysulfide diradicals and then to S_8 ring. When small amount of sulfur is added into the polymers such as polybutadiene or polyisoprene at over 140 ^oC, the double bonds of the polymers react with sulfur to form crosslinked elastic polymers. This process is known as vulcanization that has been well investigated in the synthetic rubbers industry.

Similarly to this chemistry, there have been lots of efforts to stabilize the linear polymeric chains of sulfur by copolymerization with olefin monomers.[84-89, 95-97, 101] Nevertheless, most of the products exhibited poor processability and the low degrees of sulfur incorporated into the final copolymer. The reason behind the failure of copolymerization is thought to be due to the immiscibility of sulfur with the monomers and consequent use of solvent as a reaction medium. The solvents used in the copolymerization seemingly suppress the growth of the copolymers by the stabilization of radicals or cations of monomers.

Herein, we report on successful synthesis of sulfur copolymer by using molten sulfur as a reaction medium, and by adding miscible comonomers into molten sulfur.[102-104] This extremely simple method realizes processable high sulfur content copolymers. Therefore by using this copolymers various processing techniques are demonstrated, and ultimately, a number of applications of the copolymers are introduced.

2.2. Experimental section

2.2.1 Synthesis of sulfur copolymers

Sulfur (sublimed powder) was purchased from Sigma-Aldrich. 1,3-Diisopropenyl benzene (DIB) was obtained from TCI Chemical.

Poly(S-r-DIB) copolymer (SDIB) was synthesized by adding 10 wt%, 20 wt%, 30 wt%, and 50 wt% of DIB into molten sulfur in a vial at 185 ºC with vigorous stirring. The reaction was stopped by cooling down to room temperature after the reaction product solidify, and the stirring stopped by the increased viscosity of the product.

Differential scanning calorimeter (DSC) data was obtained using a DSC 4000 (PerkinElmer) at a heating rate of 10 ^{o}C/min under nitrogen atmosphere. Thermal gravimetric analysis (TGA) was carried out by a TGA Q500 (TA Instruments) at a heating rate of 10 ^{o}C/min under nitrogen atmosphere. Elemental analysis was performed using a Flash1112 (CE Instrument, Italy) with CHNS-Porapack PQS columns. X-ray diffraction (XRD) measurements were obtained using a New D8 Advance model (Bruker) at room temperature with a CuKα radiation source at 18 kW.

2.2.2 Processing of sulfur copolymers

1,2-dichlorobenzene (DCB) was purchased from Junsei Chemical. Spin-casting of SDIB copolymers was conducted after dissolving 10 wt%, 20 wt%, 30 wt%, and 50 wt% DIB contents of SDIB copolymers into DCB as a solvent (300mg/ml). The

solution was heated at 130 ^{o}C for the complete dissolution, and then promptly spun at 2000 rpm for 40 sec, followed by 6000 rpm for 2 min, on a glass, or silicon substrate, which were pre-heated at 185 ^{o}C. As-spun film of SDIB copolymer was annealed at 180 ^{o}C for 5 min, and then 100 ^{o}C for 24 h.

Nanoimprinting of SDIB copolymers was performed using PDMS mold. Sulfur was heated in a vial at 130 ^{o}C, and 20 wt% of DIB was added into the molten sulfur with vigorous stirring at 130 ^{o}C. When the reaction mixture became homogeneous, red colored, it was taken from the vial, and then promptly dropped on to a glass, or silicon substrate which was pre-heated at 185 ^{o}C. A PDMS mold was slowly placed on top of the SDIB pre-polymer, and then another glass was placed on top of the PDMS mold, followed by pressing the glass with a clip. After 2 h, the fully polymerized SDIB copolymer with patterns was cooled to room temperature, and the PDMS mold was removed.

Micro-lens pattern was prepared with SDIB film, casted as described above. A PDMS mold was placed on top of SDIB film which was pre-heated at 185 ^{o}C. After 2 h, the film was cooled to room temperature, and PDMS mold was removed. The patterned SDIB film was further heated at 185 ^{o}C for 24 h.

Sulfur initiated polymerization was carried out by the dispense of polyethylene glycol divinyl ether (PEGDVE) on to the bulk SDIB copolymers, or SDIB cathode, and followed by heating at 60 ^{o}C for 24 h.

^{1}H NMR spectra were obtained with a Bruker Avance III 500 MHz spectrometer using $CDCl_3$ as a solvent. Differential scanning calorimeter (DSC) data was obtained

using a DSC 4000 (PerkinElmer) at a heating rate of 10 ^{o}C/min under nitrogen atmosphere. Thermal gravimetric analysis (TGA) was carried out by a TGA Q500 (TA Instruments) at a heating rate of 10 ^{o}C/min under nitrogen atmosphere. Elemental analysis was performed using a Flash1112 (CE Instrument, Italy) with CHNS-Porapack PQS columns. X-ray photoelectron spectroscopy (XPS) was conducted using Axis-HSi (Kratos) with Mg/Al dual anode at 15 kV and 10 mA. Fourier-transform infrared (FTIR) spectra were obtained with FT-IR/NIR Frontier Spectrum 400 (PerkinElmer).

Atomic force microscopy (AFM) was carried out with Nanowizard (JPK Instruments). Scanning electron microscopy (SEM) images were obtained with JSM-6701F (JEOL). UV-visible absorption spectra were measured with LS-55 (PerkinElmer).

2.3. Results and discussions

2.3.1 Synthesis of sulfur copolymers

High sulfur content sulfur copolymers were synthesized by extremely simple chemistry by using elemental sulfur in melt and DIB as comonomers with different composition (10-50 wt% of DIB) as shown in **Figure 2.1.** Even only 10 wt% of DIB results in homogeneous polymeric materials, which is completely different from traditional vulcanization chemistry. This novel chemistry is named as "inverse vulcanization",[102, 104] because the composition ratio of sulfur to organics is totally reversed. In the chemistry of traditional vulcanization, when sulfur contents increase, the linear sulfur chain becomes unstable, which results in decomposition and depolymerization of sulfur. In the chemistry of inverse vulcanization, however, very long chain (~22 S) of sulfur is stable due to both bi-functionality and miscibility of DIB molecule, which strongly interacts and stabilize the linear sulfur chain. Moreover, the copolymerization takes place in a bulk state, so the molecular weight of the polymer reaches to the maximum without depolymerization, while as the solution reaction of sulfur with other olefin monomer results in continuous depolymerization.

DSC thermograms of SDIB copolymers were compared with elemental sulfur in **Figure 2.2.** Elemental sulfur undergoes melting transition at 119 ^{o}C, and crystallization at ~ 21 ^{o}C. However, with SDIB copolymers of all composition, there is no melting & crystallization peak, that confirms the amorphous nature of SDIB

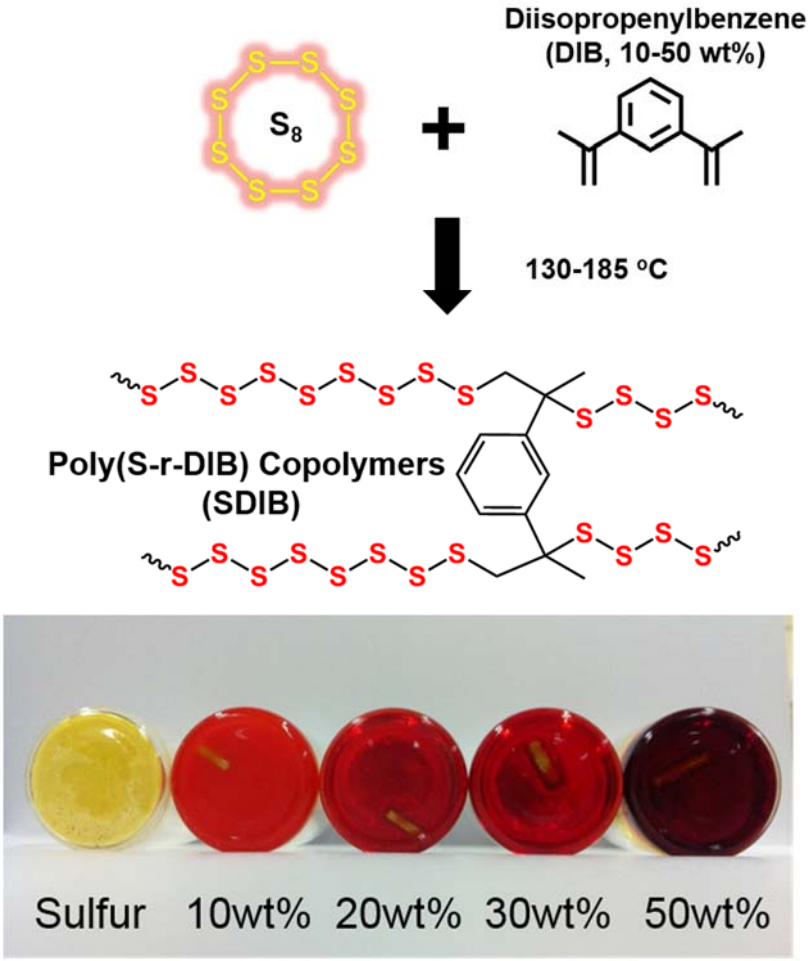

Figure 2.1 Synthesis of Poly(S-r-DIB) copolymers with different composition (10 wt% to 50 wt% of DIB)

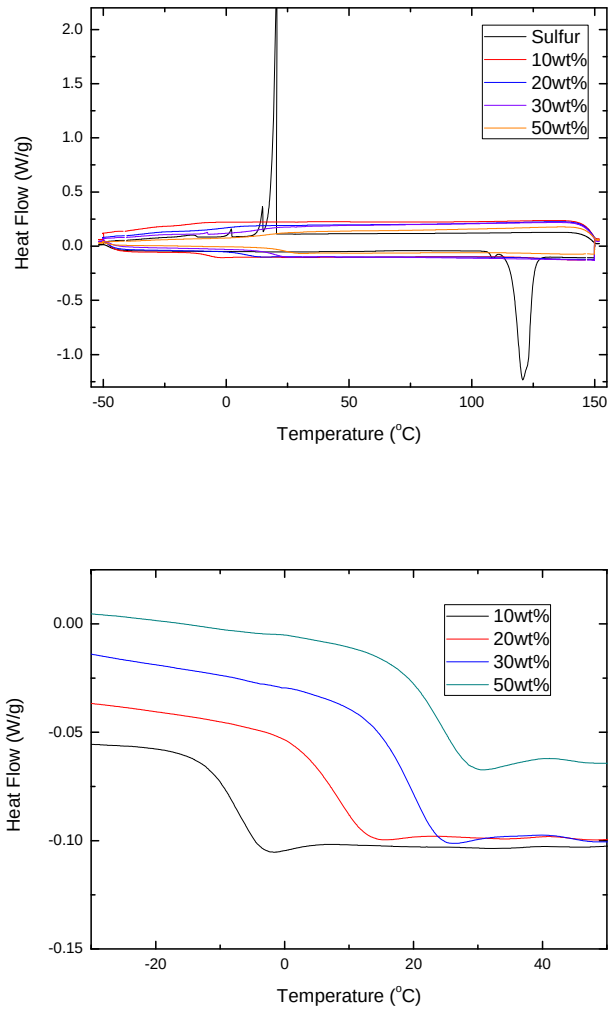

Figure 2.2 DSC thermograms of elemental sulfur and SDIB copolymers of 10 wt%, 20 wt%, 30 wt%, and 50 wt% DIB contents.

copolymers. Moreover, the glass transition temperature of these copolymers were gradually increase from -10 ^{o}C to 25 ^{o}C as a function of DIB contents from 10 wt% to 50 wt%. That is explained by the increased crosslinking density of the copolymer as increasing DIB contents.

XRD patterns of SDIB copolymers with different DIB contents were demonstrated in **Figure 2.3.** Interestingly, the diffraction pattern of elemental sulfur was also observed with 10 wt% SDIB copolymer, which implies that small amount of elemental sulfur is included in 10 wt% SDIB copolymer although the melting or crystallization peak was hidden in DSC curve in **Figure 2.2.**

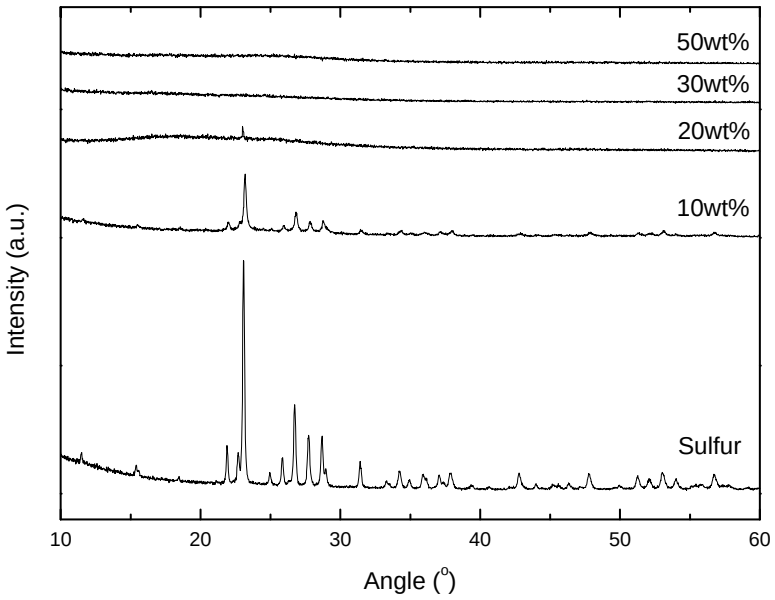

Figure 2.3 XRD Patterns of elemental sulfur and SDIB copolymers of 10 wt%, 20 wt%, 30 wt%, and 50 wt% DIB contents.

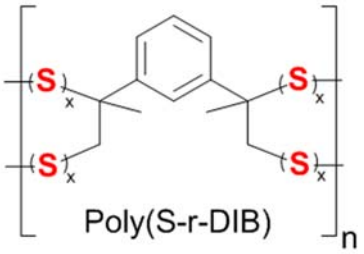

DIB Contents	Avg. x (Ranks) by Calculation
10 wt%	***22.2***
20 wt%	***9.87***
30 wt%	***5.76***
50 wt%	***2.47***

Table 2.1 Average sulfur atoms in the polysulfide chains of SDIB copolymer with different DIB Contents.

2.3.2 Unique properties of sulfur copolymers

The synthesized SDIB copolymers are capable of solution processing and melt processing due to the thermoplastic, and amorphous property of the copolymers which is the significant differences from elemental sulfur. We demonstrate two representative processing methods using SDIB copolymers, spin-casting of SDIB copolymers for thin film fabrication, and nanoimprinting of the polymers for patterning.

The solubility of SDIB copolymer in 1,2-dichlorobenzene (DCB) as a solvent at room temperature is shown in **Figure 2.4.** 50 wt% SDIB copolymer completely dissolves in DCB, while as the other copolymers are partly insoluble, and the solubility of the copolymers increases as a function of DIB contents. The reason is presumably that shorter sulfur chain in high DIB content copolymers takes advantages in miscibility with organic solvents. When the solutions of 10-30 wt% SDIB copolymers in DCB are heated up to 130 ^{o}C, they become homogenous, and the copolymers completely soluble at increased temperature. Therefore, spin-casting of these copolymers was possible by dispensing the hot solution on to the hot substrates, followed by spinning. However, the spinning step and post-annealing process is critical for the high quality uniform surfaces of the SDIB copolymer films. Otherwise, the copolymer films get rough, and heterogeneous after a few days as shown in **Figure 2.5.** The reason of these changes is thought to be due to the depolymerization of sulfur to form elemental sulfur in the films, which is confirmed

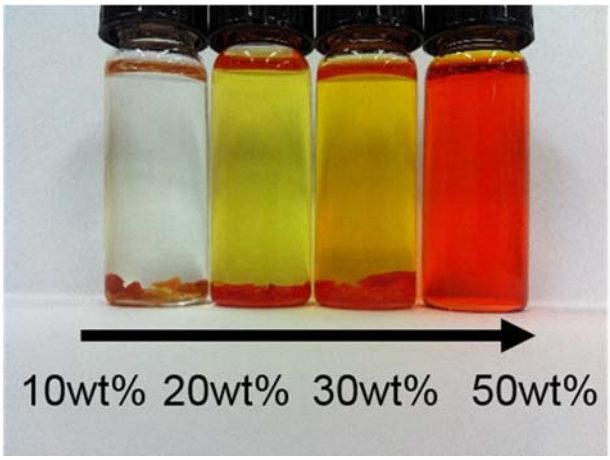

Figure 2.4 SDIB copolymers of 10 - 50 wt% DIB contents, dissolved in DCB as a solvent.

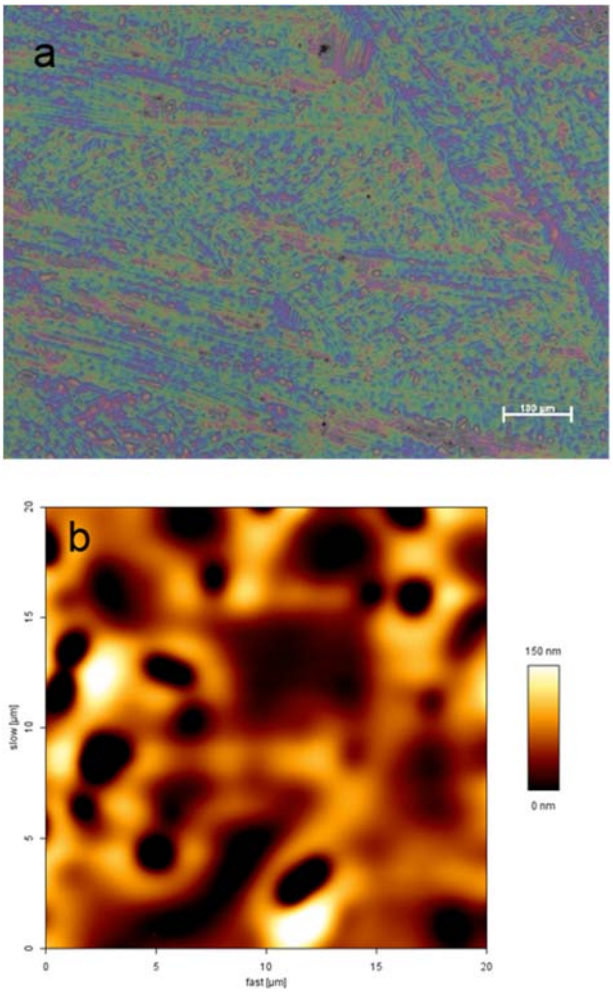

Figure 2.5 a) Optical microscopy of SDIB copolymer (20 wt%) obtained by improper spinning and annealing processes. b) AFM image of SDIB copolymer (20 wt%) obtained by improper spinning and annealing processes.

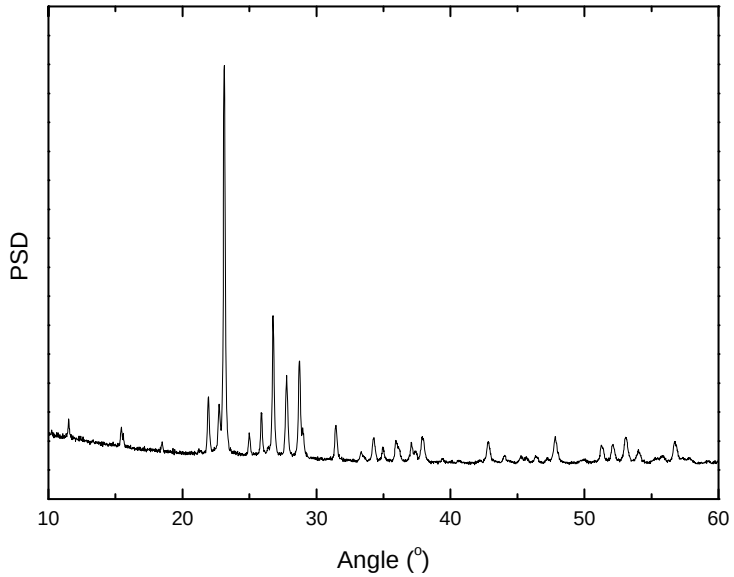

Figure 2.6 XRD pattern of SDIB copolymer (20 wt%), after heating at 130 oC and cooling in DCB solvent.

by XRD characterization in **Figure 2.6**. When the SDIB solution is cooled down to room temperature and heating at 130 ^{o}C, precipitates are formed from the solution, which are turn out to be elemental sulfur. Therefore linear sulfur chains in SDIB copolymers are instable in the solvent at lower temperature, so complete removal of solvent during the spinning, and thorough annealing are required to prevent depolymerization sulfur in the films. **Figure 2.7**. demonstrate the uniform film formed after fast and complete removal of solvent, and this film is stable without morphological changes after 1 month. UV-vis absorption spectra of the SDIB copolymer films and solutions in comparison with elemental sulfur solution is shown in **Figure 2.8**. SDIB copolymers, with all weight fraction range, exhibit a characteristic peak at 432 nm, which is absent for elemental sulfur. Therefore it is thought to come from the linear sulfur chains.

Due to the thermoplastic property of SDIB copolymer, it was able to be fabricated into nanopatterns using PDMS mold. Simple molding is conducted with pre-polymers of SDIB, which were synthesized as described in chapter 2.3.1, but lower temperature of 130^{o}C to impede the polymerization rate and facilitate controlling the polymer viscosity. The pre-polymer was dispensed on to the hot glass substrate, at the point between becoming a homogeneous red and solidifying. PDMS mold was placed on to the pre-polymer, and after heating for a hour and cooling, it was removed. The micrometer sized pillar patterns were uniformly appeared on the surface SDIB copolymer films as shown in SEM image (**Figure 2.9**). Micro lens patterns were also prepared with the same PDMS mold and SDIB thin films as shown

in **Figure 2.10**. SDIB thin films were prepared as described above, and PDMS mold were placed and heated. After removal of PDMS mold, the pillar shaped patterns of SDIB films were further heated at 185 ^{o}C to induce flows of the patterned polymers to deform from pillars to round lens-like shapes. It was found that post deformation of SDIB polymers are possible due to their thermos-plasticity.

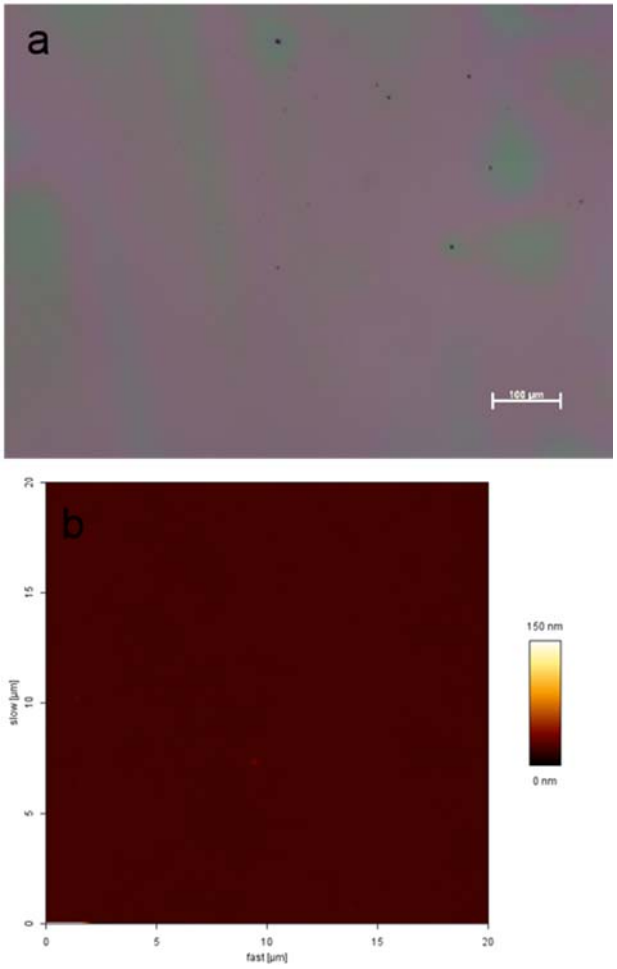

Figure 2.7 a) Optical microscopy of SDIB copolymer (20 wt%) obtained by optimum spinning and annealing processes. b) AFM image of SDIB copolymer (20 wt%) obtained by optimum spinning and annealing processes.

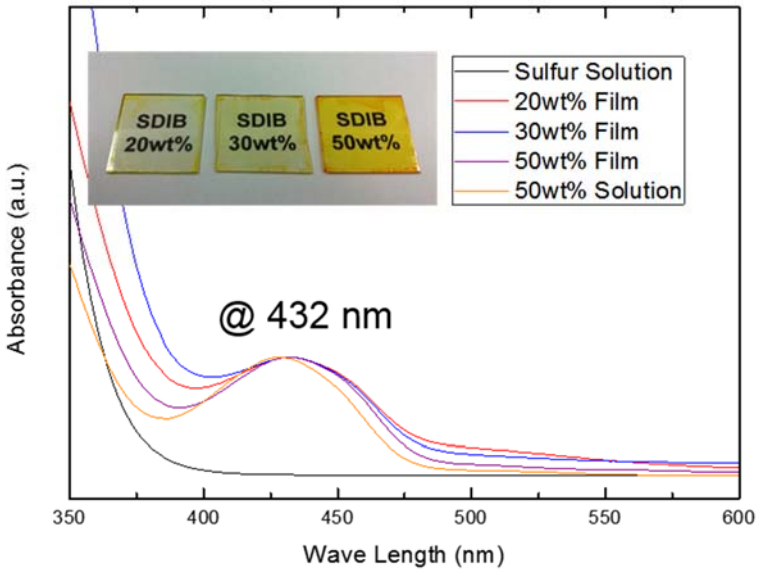

Figure 2.8 UV-vis spectra of SDIB copolymer films (20, 30, and 50 wt%) and solution (50 wt%) compared with sulfur solution.

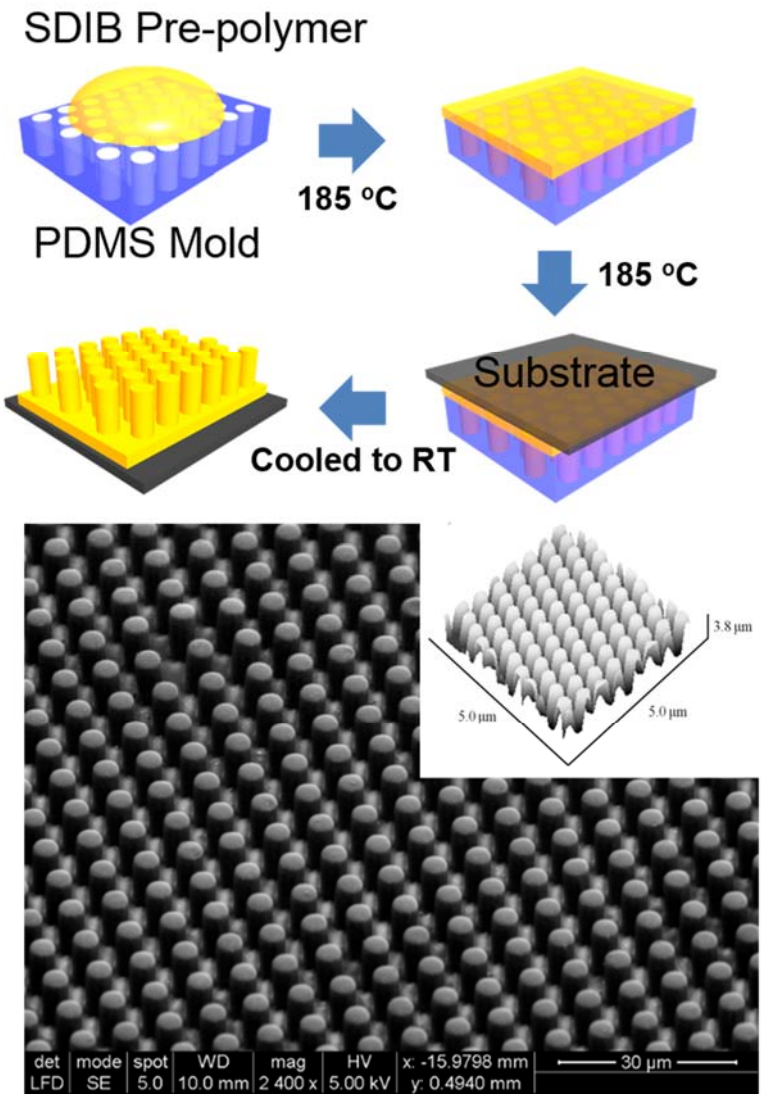

Figure 2.9 A schematic illustration of PDMS patterning of SDIB copolymers and SEM image of patterned SDIB copolymer.

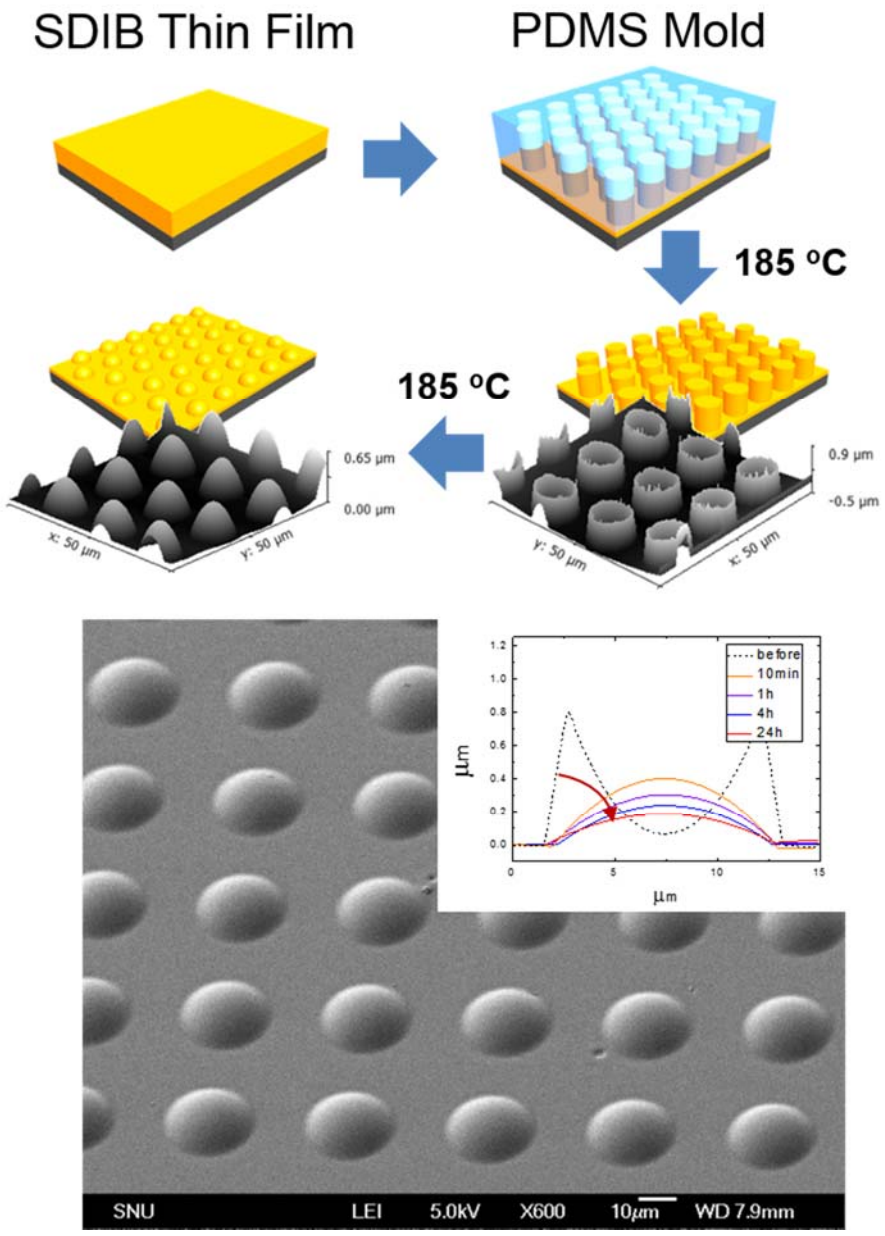

Figure 2.10 A schematic illustration of PDMS patterning of SDIB copolymer films for micro lens pattern and SEM image of patterned SDIB copolymer.

2.3.3 Application of sulfur copolymers

Due to the improved physico-chemical properties of SDIB copolymers which facilitate processing of the polymers, there could be various application to utilize SDIB copolymers as advanced materials.

As mentioned in chapter 1.2.1, sulfur exhibits high refractive index (*n*), and IR transparency, so SDIB copolymers with high sulfur contents are utilized in IR optics as a high *n* lens.[105-106] The n of SDIB copolymer decreases as a function of DIB contents due to the decrease of sulfur contents. Transmission of SDIB copolymer in IR region also decreases with DIB contents, because the C-H bonds in hydrocarbons including DIB monomer strongly absorb the IR radiation. Therefore 20 wt% SDIB copolymer exhibited superior optical characteristic (n=1.85), due to the high sulfur contents, and processability. The IR lens of SDIB copolymer was prepared by PDMS molding, and utilized as a lens in IR camera as shown in **Figure 2.11**. In general, polymers with hydrocarbon is impossible to utilize in IR optics due to the IR absorption and low refractive index. On the other hand, typical inorganic materials for IR optics such as Ge, or GaN is too expensive, challenging to process. Therefore, this is the first example of the polymer for IR optics exhibiting superior functionality, with low cost, facile processing and extremely simple chemistry.

Sulfur also exhibit high dielectric constant (ε = 3.2) compared to hydrocarbon polymers.[69] Therefore, SDIB copolymers are also utilized as a dielectric layer in transistors to give high capacitance. SDIB copolymers were simply spin-casted on to the substrates followed by annealing, and fabricated into two types of dielectrics,

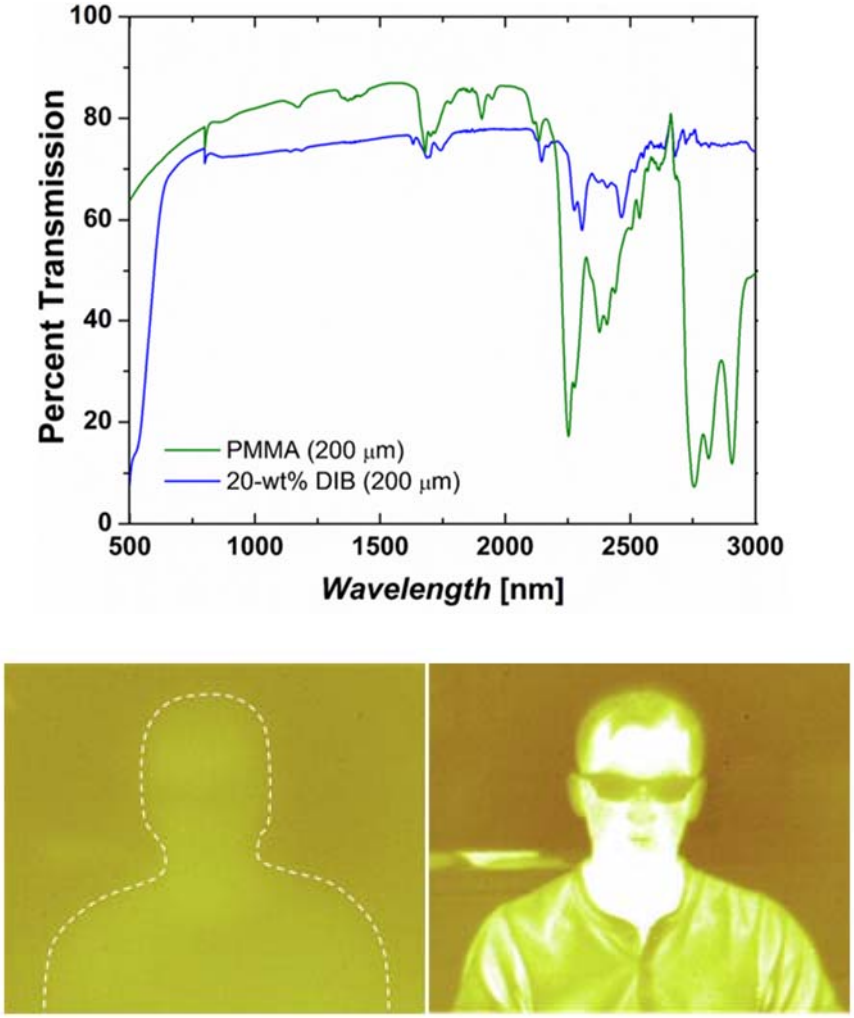

Figure 2.11 (top) IR Transmission spectra of PMMA and SDIB (20 wt%) copolymer lens. (left) A picture taken from IR camera with PMMA lens. (right) A picture taken from IR camera with SDIB copolymer (20 wt%) lens.

for MIM (metal-insulator-metal) capacitors, and thin film transistors (TFT). Dielectric constant measured with SDIB copolymer (50 wt%) in MIM was even higher (ε =3.45) than elemental sulfur. Furthermore, the leakage current of MIM with SDIB copolymers was extremely low compared to the typical polymer dielectrics (PMMA), and it is independent on a film thickness. With this superior dielectric properties, TFT with SDIB copolymer (50 wt%) also works as comparable to typical SiO_2 dielectrics as shown in **Figure 2.12**.

Combining the high refractive index and facile processability of SDIB copolymers, they could be utilized in unique optical devices such as 2-D photonic crystals. When hundreds nanometers thin films of two materials with different refractive index are stacked alternatively, the multilayered film exhibits unique optical properties known as bragg refraction.[107-108] By controlling the thickness of the each film, the wave length of light passing through the multilayer is determined, by the reflection within the films. Specific range of the wave length can't pass through the films, such like the films absorb the range of light, which is called as photonic band gap (PBG).[109-110] using these unique properties, 2-D photonic crystals are utilized in lasers, sensors, and IR mirrors.[107, 109, 111] For the intense and efficient generation of the PBG, large difference in *n* between two materials are necessary. Using a high *n* of SDIB copolymers (*n*=1.7 for 50 wt%), 2-D photonic crystals were fabricated in combination with cellulose acetate (CA) as low *n* polymer (*n*=1.4) as shown in **Figure 2.13**. SDIB/CA multilayers were fabricated by spin-casting up to 10 bilayers, with different thickness of SDIB films. The PBG of the multilayer were able to be

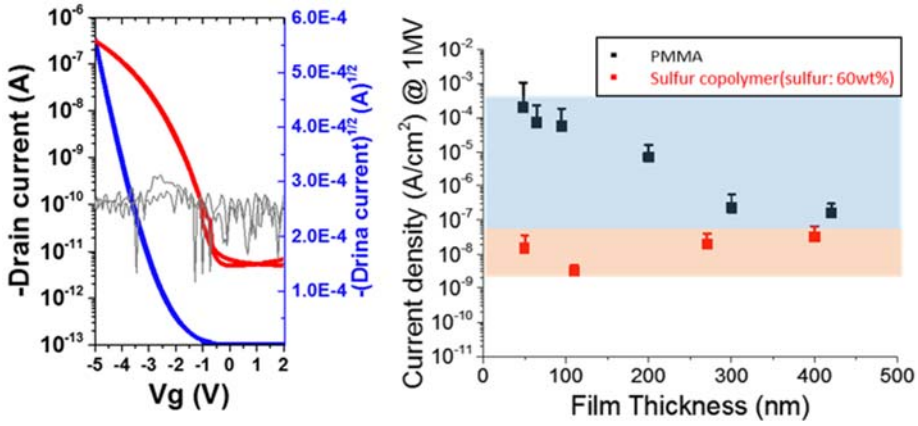

Figure 2.12 (left) TFT gate dielectric performance of SDIB copolymer (50 wt%). (right) MIM leakage current density of SDIB copolymer compared with PMMA as a dielectric layer.

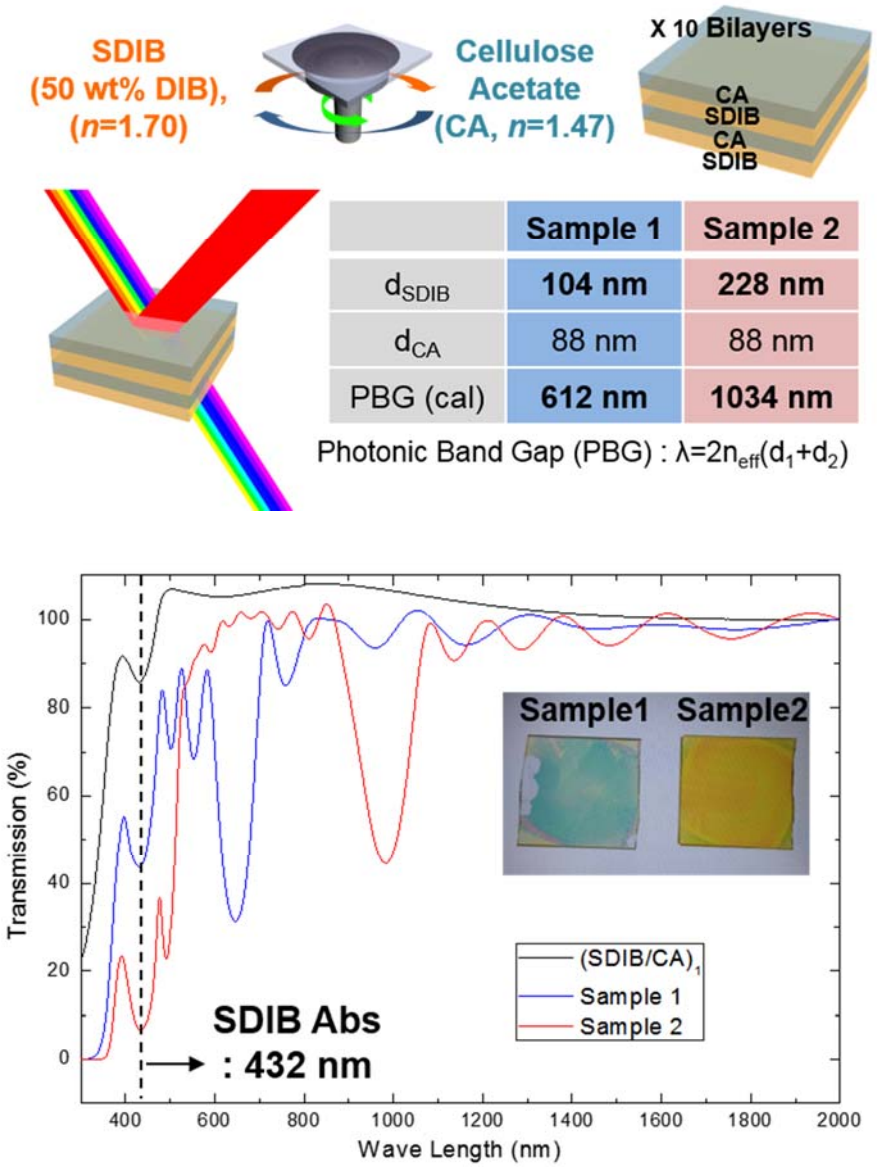

Figure 2.13 Schematic description of the preparation of SDIB/CA photonic crystals and UV-Vis transmission spectra of SDIB/CA photonic crystals with different thickness of SDIB copolymer (50 wt%).

tuned by the thickness control (PBG=645nm for 100 nm SDIB film, and PBG=980 nm for 230 nm SDIB film), and these results are well fitted with the theoretical simulation of PBG.

One of the most important applications of sulfur is cathodes of Li-S batteries. As introduced in chapter 1.2.2, utilization of sulfur as a cathode material is challenging, in spite of its high theoretical capacity. The main challenging issue is capacity fading during the cycles due to the diffusion of soluble polysulfide, which results electrical contact loss between carbon framework and active sulfur species. SDIB copolymers were utilized as cathode materials, and significantly improve the cyclic stability of Li-S batteries compared to the cathode with elemental sulfur (**Figure 2.14**), by retaining the stable cathode structure during cycles.[42, 112-114] A proposed electrochemical reaction of SDIB copolymer cathode is shown in **Figure 2.15**, in which Li^+ reacts with linear sulfur chains of SDIB copolymer during discharge until Li_2S forms, and DIB molecules bound to sulfur is well mixed with Li_2S phase. Therefore these DIB moieties act as stabilizers in the cathode, facilitating stable redox reaction with electrical contact during the repeated cycles. However, the rate capability of SDIB copolymer cathode is poor, due to the absence of electrical pathway inside the polymer, and still there is a slight capacity fading on prolonged cycles due to the polysulfide dissolution. Therefore, in the next chapters, we will focus on the improvement of the SDIB cathodes by addressing these challenging issues with strategies of hybridization and surface modification.

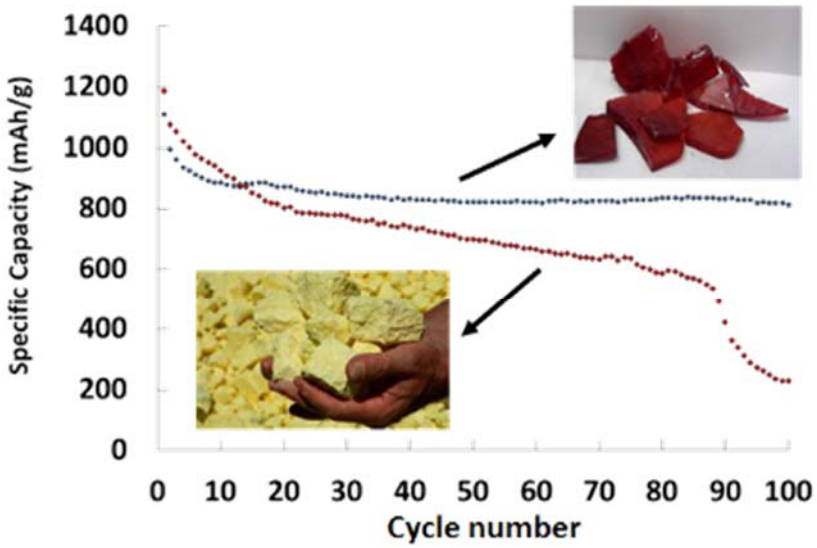

Figure 2.14 Cyclic performance Li-S battery cells of SDIB copolymer cathode (10 wt%), in comparison with elemental sulfur cathode.

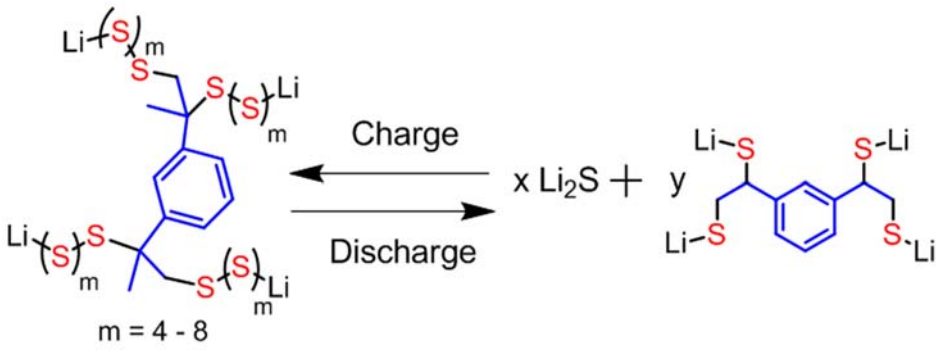

Figure 2.15 Proposed electrochemical reaction of SDIB copolymer cathode during charge/discharge of Li-S battery.

2.4. Conclusions

In this chapter, we report on the synthesis of SDIB sulfur copolymer with extremely simple chemistry to give thermoplastic, amorphous and high sulfur contents polymers. With the physico-chemically enhanced properties of this copolymers, melt process of PDMS patterning, and solution process of spin-casting were described. Finally, with the facile processing methods, various kinds of applications were introduced to realize intrinsically superior functionalities of sulfur. In the following chapters, we will discuss further on the enhancement of functionalities of this sulfur copolymers by introducing novel chemistry and surface coating technique for hybridization and surface modification, respectively.

Chapter 3. Incorporation of Sulfur Copolymers into Nanohybrid Materials

3.1. Introduction

The development of chemistry and processing methods for the utilization of elemental sulfur into polymeric materials provides a unique opportunity for addressing the substantial surfeit of sulfur generated via petroleum refining. Despite the large scale conversion of sulfur as a feedstock for sulfuric acid and downstream fertilizers, there typically remains an annual surplus of approximately 7 million tons,[7] much of which is stored in massive above ground deposits. However, there exists a paucity of synthetic and processing methods to modify or chemically convert elemental sulfur into polymeric materials, primarily due to the limited miscibility and solubility of elemental sulfur with a majority of commonly used chemical reagents.[75-79]

To address the inherent chemical challenges associated with using elemental sulfur to prepare polymers, we examined the use of molten liquid sulfur as a reaction medium and comonomer. We demonstrated the use of liquid sulfur both as the solvent and reducing agent medium for the synthesis of noble metal nanoparticles.[103] These sulfur-colloidal dispersions were then polymerized by treatment with

divinylbenzene to prepare the nanocomposite. In chapter 2, chemically stable copolymer materials using a methodology, termed, inverse vulcanization, were developed via the bulk copolymerization of molten sulfur with 1,3-diisopropenylbenzene.[102, 104] Similar efforts by Block et al.,[93] reported the use of liquid sulfur as a solvent or a reagent for the synthesis of allyl-terminated oligosulfides.

However, the development of alternative bulk or solution methods to prepare novel sulfur-based polymers and nanocomposites remains an important challenge in the field. Furthermore, S-S bonds (like the types found in polymeric sulfur) are difficult to characterize using conventional spectroscopic methods, which further complicates the development of new chemistry and materials based on sulfur.[84-89, 95-97, 101] In particular, symmetrical S-S bonds are largely IR inactive and ^{33}S NMR is complicated by the low sensitivity and abundance of ^{33}S nuclei. Hence, the discovery of new comonomers that are miscible and reactive with elemental sulfur is an opportunity to develop new chemistry and materials utilizing sulfur as a chemical feedstock.

The chemistry of oleylamine and elemental sulfur has previously been explored in the context of preparing chalcogenide-based semiconductor nanocrystals.[28] In these nanocrystal synthesises, the reaction of oleylamine and sulfur served to generate hydrogen sulfide (H_2S) as the sulfur source to promote the metal chalcogenide formation. Ozin et al.[115] investigated the mechanistic aspects of this reaction via model reactions of saturated aliphatic amines and sulfur, which were

reported to afford (thio)amide-based compounds. While the reaction of oleylamine and sulfur has been investigated for nanoparticle reactions, exploitation of this system to prepare high sulfur content polymeric materials has not been fully exploited.

Herein, we report on the copolymerization of sulfur with oleylamine to prepare nanocomposite materials consisting of high content sulfur copolymers and lead sulfide (PbS) nanoparticles. In the current study, we report on the ability of oleylamine to form chemically stable copolymers via the copolymerization with elemental sulfur, along with the in-situ formation of PbS nanoparticles (NPs) to prepare PbS-sulfur copolymer nanocomposites (**Figure 3.1**). In this system, the one-pot reaction of oleylamine and sulfur in the presence of PbS NP precursors enabled the in-situ formation of chalcogenide NPs, with efficient dispersion of colloidal inclusions throughout the sulfur copolymer matrix. We previously demonstrated that the one-pot reactions of sulfur with Au(I) salts, followed by the inverse vulcanization of the sulfur phase with styrenic comonomers afforded Au NPs dispersed in a sulfur copolymer matrix.[103] In the current chapter, this concept was applied using different chemistry to prepare dispersed chalcogenide NPs in a poly(oleylamine-random-sulfur) copolymer (poly(OLA-r-S)) matrix. This one-pot synthetic process highlights the ability of both sulfur and oleylamine to react both by free radical and oxidative processes to form polymeric and metal chalcogenide materials.

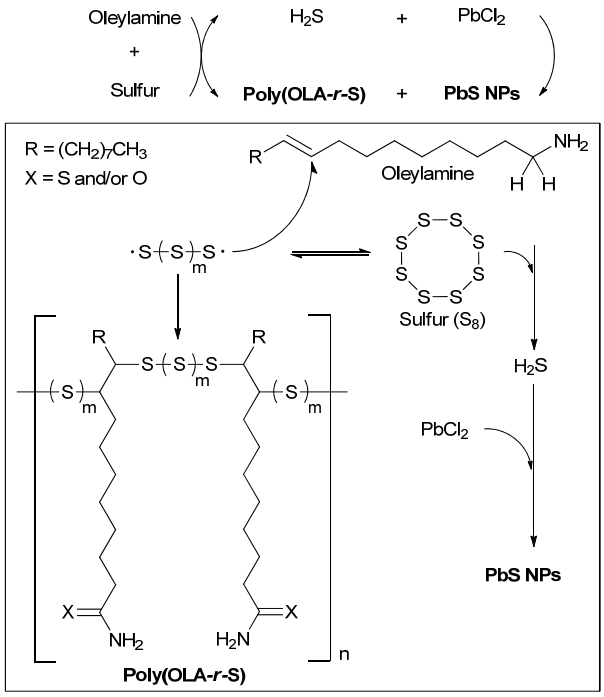

Figure 3.1 Proposed overall reaction scheme for the in-situ synthesis of PbS/poly(OLA-r-S) nanocomposites.

3.2. Experimental section

3.2.1 Materials and Characterizations

Sulfur (colloidal powder), oleylamine (OLA, 70%, technical grade), 1,2-Dichlorobenzene (DCB, 99%, anhydrous), and Lead(II) chloride ($PbCl_2$, 99.99%, trace metals basis) were purchased from Aldrich and used as received. It is important to note the low purity of the technical grade oleylamine (Aldrich), as reactions conducted at larger scales may exhibit different kinetics, or afford unexpected side products when acquired from different vendors.

^{1}H NMR spectra were obtained with a Bruker Avance III 500 MHz spectrometer using $CDCl_3$ as a solvent. Gel permeation chromatography (GPC) measurements were performed by YL9100 (Young Lin Instrument) using THF (HPLC grade) as a solvent with columns (Waters Styragel HR3 and HR4) at a flow rate of 1 mL/min with a UV-Vis spectrometer (254 nm). The normalization on the series of trace curves were conducted by setting DCB peaks on 22.02 min as a reference. The calibration curve was constructed with a series of monodisperse polystyrene standards (Shodex). Differential scanning calorimeter (DSC) data was obtained using a DSC-Q1000 (TA Instruments) at a heating rate of 10 °C/min under nitrogen atmosphere. Thermal gravimetric analysis (TGA) was carried out by a TGA Q500 (TA Instruments) at a heating rate of 10 °C/min under air atmosphere. Elemental analysis was performed using a Flash1112 (CE Instrument, Italy) with CHNS-Porapack PQS columns. X-ray diffraction (XRD) measurements were obtained using

a M18XHF-SRA model (MAC Science Co) at room temperature with a CuKα radiation source at 18 kW.

Transmission electron microscopy (TEM) images were recorded on a JEOL-JEM2100 at an operating voltage of 200 kV. For the cross-sectional views of TEM, the composite films were lifted off from the substrates by immersing in HF solution (5 %). The freestanding films were placed on a pre-cured epoxy resin, and then embedded by pouring a fresh epoxy resin on the top of the films after drying in a vacuum oven. The resin mixture for molding was prepared by mixing 25.6 g of Embed 812 resin, 13.51 g of dodecenyl succinic anhydride, 10.9 g of Nadic® methyl anhydride, and 1 g of DMP-30. All the components were purchased from Electron Microscopy Sciences. The cured resins were sliced with a microtome (Leica Microsystems). The 70 nm-thick slices were prepared with a diamond-coated knife (DiATOME) at an angle of 6 ° and a cutting velocity of 0.1 mm/s. The slices were suspended in water and supported on a Cu grid.

3.2.2 Synthesis of Poly(OLA-r-S)

In these reactions, molar feed ratios of 2:1 to 33:1 of [Sulfur]/[Oleylamine] were investigated. In a typical preparation, sulfur (1.6 g, 50 mmol) and oleylamine (0.4 g, 1.5 mmol) were mixed with DCB (4 mL), and heated up to 180 °C with vigorous stirring. The color of the mixture became transparent yellow within a minute, and slowly converted into black solution within 10 min and allowed to react for 30 min at T = 180 °C . For the ^{1}H NMR and GPC measurements, aliquots were removed via

syringe and dissolved in deuterated chloroform and THF, respectively. Purification of the copolymer was achieved by addition of n-hexane (6 mL) into the reaction mixture to induce precipitation of excess sulfur. The precipitated sulfur was removed by centrifugation at 3,000 rpm for 5 min, and the remained DCB mixture was poured into 20 mL of methanol, followed by centrifugation at 17,000 rpm for 10 min. The supernatant in methanol was decanted and the precipitate (black rubbery solid) was dried in a vacuum oven at room temperature overnight (yield = 0.43 g).

3.2.3 Synthesis of PbS/Poly(OLA-r-S) nanocomposites

A Pb precursor solution was first prepared by the addition of varying amounts of $PbCl_2$ (0.04-0.12 g, 0.14-0.43 mmol) was added to oleylamine (0.4 g, 1.5 mmol) and heated to 180 °C with vigorous stirring until a white milky dispersion was formed. Separately, a poly(OLA-r-S) was synthesized as described above, where sulfur (1.6 g, 50 mmol) and oleylamine (0.4 g, 1.5 mmol) were mixed with DCB (4 mL) and heated up to 180 °C with vigorous stirring. After 30 min, the Pb precursor solution was injected into the poly(OLA-r-S)/DCB solution. The mixture was stirred at 180 °C for 5 min, and then purified by the method described above affording a black rubbery solid (yield = 0.36 g).

The nanocomposites prepared above were dissolved in THF (5 wt%), and the solution was spin-coated on a glass substrate at a spin rate of 2,000 rpm for 1 min. The films were heated on a hotplate at 180 °C for 5 min. The thickness of the resulting films measured by ellipsometry was in the range from 500 to 600 nm. For

the preparation of free-standing films, the 5 wt% nanocomposite solution (10 mL) was poured into a PTFE mold, and the solvent was evaporated in ambient condition for overnight. The resulting film was further heated at 180°C for 5 min and removed from the PTFE mold to afford a free-standing film.

Oleylamine-capped PbS NPs were synthesized as described in the literature.[28] $PbCl_2$ (0.28 g, 1 mmol) was added to 5 mL of oleylamine and was heated to 90 °C under vacuum for 5 min. Sulfur (0.016 g, 0.5 mmol) was separately dissolved in 2.5 mL of oleylamine and the solution was injected into the Pb-oleylamine complex solution at 90 °C. The mixture was heated to 220 °C for 1h and 100 mL of ethanol was added into the resulting mixture, followed by centrifugation at 7,000 rpm for 5 min. The precipitate was dried in a vacuum oven.

For the preparation of blends, the oleylamine-capped PbS NPs (0.004 g) and 0.2 g of poly(OLA-r-S) were separately dissolved in THF (5 mL) and then mixed together. The blends were drop casted on TEM grids or spin-casted on glass substrates, followed by heating at 180 °C for 5 min.

3.3. Results and discussions

The general synthetic strategy employed for this study was initial investigation into the synthesis of poly(oleylamine-random-sulfur) (poly(OLA-r-S)) copolymers, followed by the utilization of these conditions to further introduce soluble Pb(II) complexes to promote PbS NP formation (**Figure 3.2**). The key to this one-pot and tandem step process was the use of elemental sulfur to react with vinyl bonds of oleylamines to form polymers while also reacting with α-protons in oleylamines to convert the primary amine groups to (thio)amides. The formation of (thio)amides generates H_2S which is critical as the sulfur atom source to form PbS NPs.

3.3.1 Synthesis of Poly(OLA-r-S)

Solution polymerization of S_8 and oleylamine was conducted at different molar ratios of [S]/[oleylamine] in 1,2-dichlorobenzene (DCB) at T = 180 °C to retain the homogeneity of polymeric products and those of Pb(II) complexes used in the one-pot reaction to form PbS/poly(OLA-r-S) nanocomposites. In these reaction mixtures, the color of the solution changed from yellow to red and then to black. UV-Vis absorption spectra of the solutions were recorded as a function of reaction time (**Figure 3.3**). As the reaction proceeded, the absorption shoulder moved to longer wavelength showing the broader range of absorption wavelength. The reaction mixture was then poured into excess n-hexane to remove unreacted sulfur, followed by the precipitation of soluble copolymers into methanol to yield a black rubbery

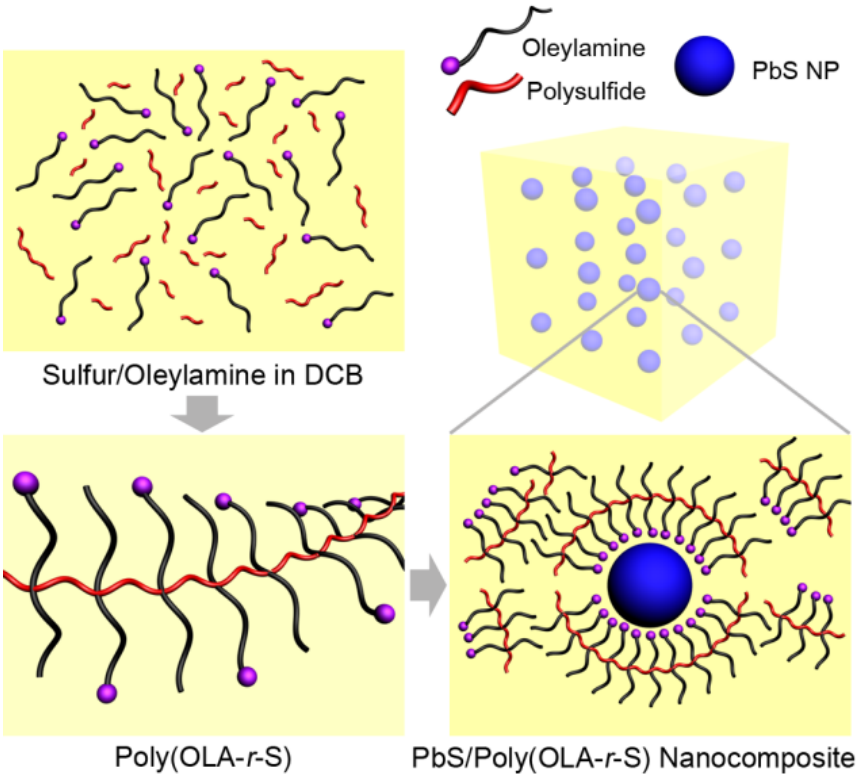

Figure 3.2 Schematic illustration of the in-situ synthesis of PbS/poly(OLA-r-S) nanocomposites.

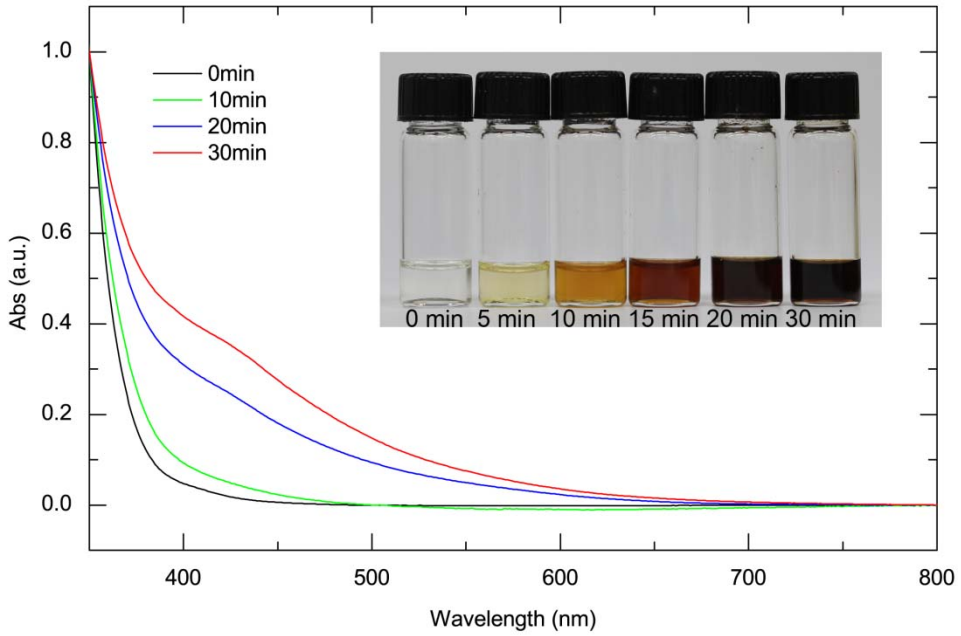

Figure 3.3 UV-Vis absorption spectra of the solution copolymerization of oleylamine and sulfur in DCB at T=180 °C for [oleylamine]:[sulfur] = 1:33 in mole ratio taken at different reaction time.

solid. The origin of the black color is thought to originate from linear polysulfide radicals in the copolymers, as observed in sulfur species at high temperature or those dissolved in amine solutions.[115-118]

The aliquots of the reaction mixture ([S]/[oleylamine], for 33:1 molar feed ratio) were periodically withdrawn for size exclusion chromatography (SEC) and ^{1}H nuclear magnetic resonance spectroscopy (NMR) to determine the number average molecular weight (Mn) as well as oleylamine conversion. 1H NMR kinetic measurements revealed the complex consumption of oleylamines during the copolymerization after 30 min of reaction, as noted by a progressive decrease in the integration of vinyl and allylic α-CH_2 protons at 5.35 and 2.01 ppm, respectively (**Figure 3.4**). In addition, the conversion of S_8 in the copolymerization was quantitatively determined using UV-Vis spectral detection, set at 254 nm, in SEC measurements of reaction mixture aliquots at 24.5 min of S_8 elution time (16 % conversion of total S_8, as shown in **Figure 3.5a**. A progressive increase in the copolymer molar mass determined by SEC characterization was observed with the increase in reaction time, confirming the formation of poly(OLA-r-S) copolymers (**Figure 3.5b**). In general, these copolymers exhibited low number average molecular weight with broad molecular weight distribution (Mn = 1,130 g/mol; Mw/Mn = 1.58). The SEC characterization along with the conversion curves of the aliquots with different feed ratios ([oleylamine : sulfur] = 1:2, 1:8, and 1:33 in molar ratio were also conducted as shown in **Figure 3.6** and **Figure 3.7**.

Characterization of poly(OLA-r-S) was further carried out via elemental analysis

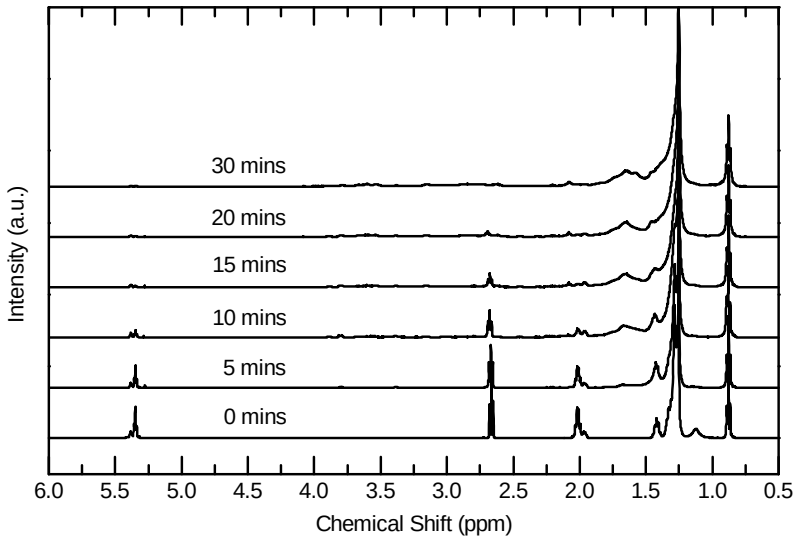

Figure 3.4 1H NMR spectra of solution copolymerization of oleylamine and S8 ([S]/[oleylamine] : 33) in DCB at T = 180 °C at different reaction times.

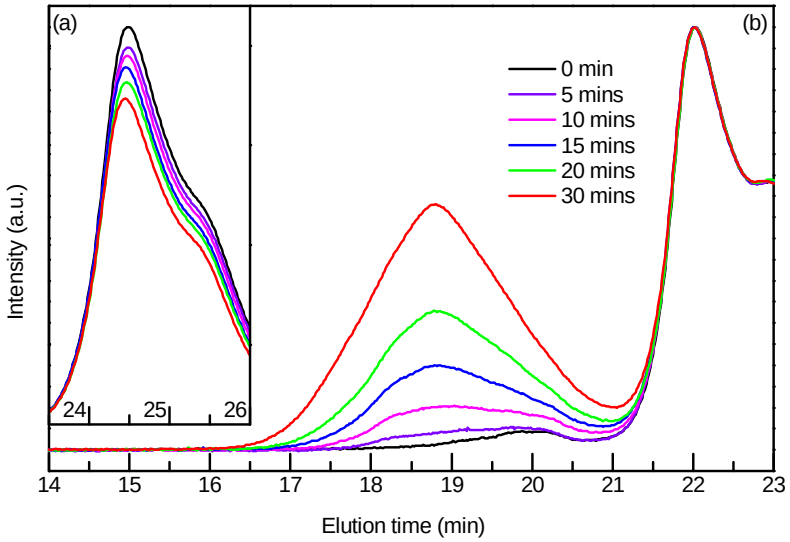

Figure 3.5 SEC of aliquots from the copolymerization of oleylamine and S8 ([S]/[oleylamine] : 33) in DCB at T = 180 °C at different reaction time: (a) Enlarged trace curves for sulfur consumption, (b) Copolymerization trace curves for poly(OLA-r-S). Normalization was conducted with solvent (DCB) peaks at 22.02 min of elution time as a reference.

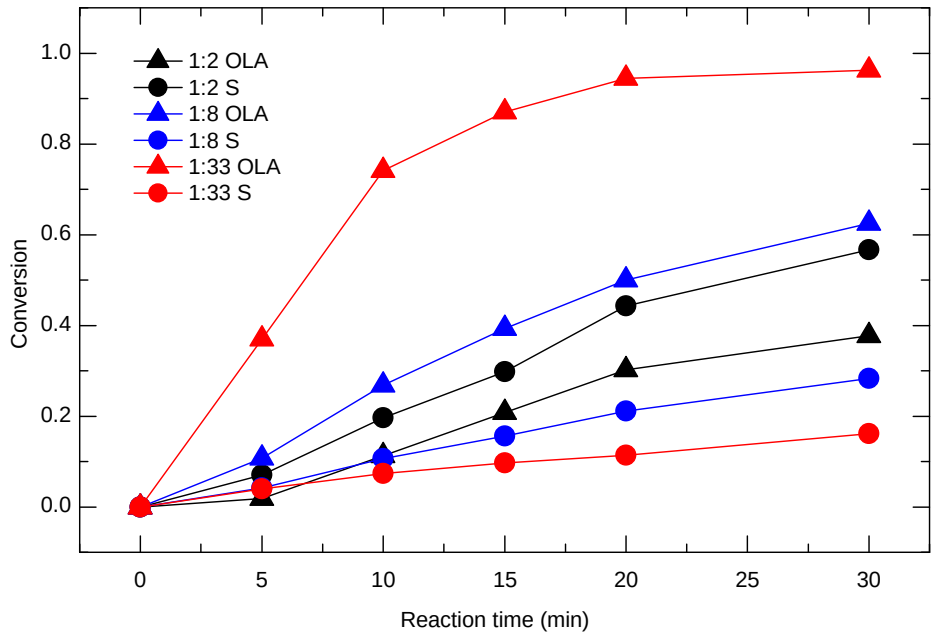

Figure 3.6 Conversion curves of solution copolymerization of oleylamine and sulfur in DCB at T = 180 °C at different reaction time. ([oleylamine : sulfur] = 1:2 (black), 1:8 (blue), and 1:33 (red)). Conversions of oleylamine with different molar ratios are shown in colored triangles, which were determined from 1H NMR. Conversions of sulfur with different molar ratios are shown in colored circles, which were determined by SEC.

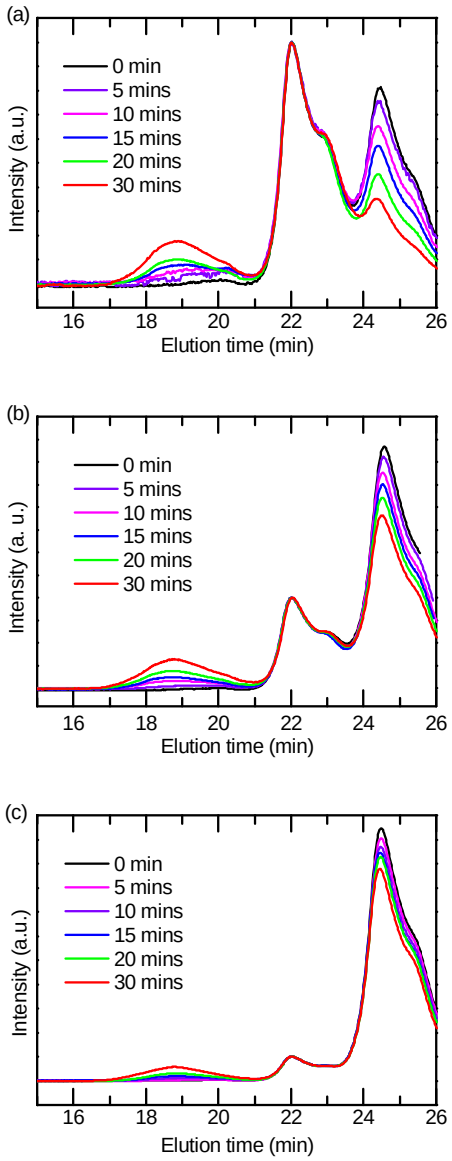

Figure 3.7 SEC of aliquots removed from the solution copolymerization of oleylamine and sulfur in DCB at T=180°C at different reaction time (0 to 30 min) with different feed ratios: (a) [oleylamine : sulfur] = 1:2; (b) 1:8; (c) 1:33 in molar ratio.

and DSC. The composition of the copolymer product measured by elemental analysis indicates the following weight percentages: N: 2.772±0.061 %, C: 53.68±0.10 %, H: 7.954±0.131 %, S: 35.60±0.12 %. From the elemental weight percentage data, it was determined that the copolymers prepared consist of approximately 4 to 5 S-units on average per oleylamine comonomer units. DSC of the poly(OLA-r-S) copolymers were also conducted to confirm that S-units in the copolymers are not in the form of crystalline sulfur. During the heating scans thermal transitions for elemental sulfur assigned to melting transitions at 108 °C (for orthorhombic α-sulfur) and 118 °C (for monoclinic β-sulfur) were observed. During the cooling cycles, crystallization of α- and β-sulfur are observed at 28 °C and 42 °C, respectively. However, DSCs of poly(OLA-r-S) were found to be largely featureless for both heating and cooling scans, indicative of the formation of amorphous copolymers despite the presence of a high content (37 wt%) of sulfur (**Figure 3.8**).

It was initially anticipated at our reaction condition (T = 180 °C) that the homolytic ring opening of S_8, followed by the addition of sulfur diradicals to vinylic groups of oleylamines would be the primary mechanistic pathway to form poly(OLA-r-S) copolymers, with retention of primary amines as side chain functional groups. However, throughout the copolymerization, it was observed by ^{1}H NMR that α-CH_2 protons adjacent to the amine functional groups at 2.61 ppm were also consumed in this reaction indicating the concurrence of additional chemistry (**Figure 3.4**). Hence, these ^{1}H NMR studies confirmed that the conversion of amine side chain groups from oleylamines into some other functionality during

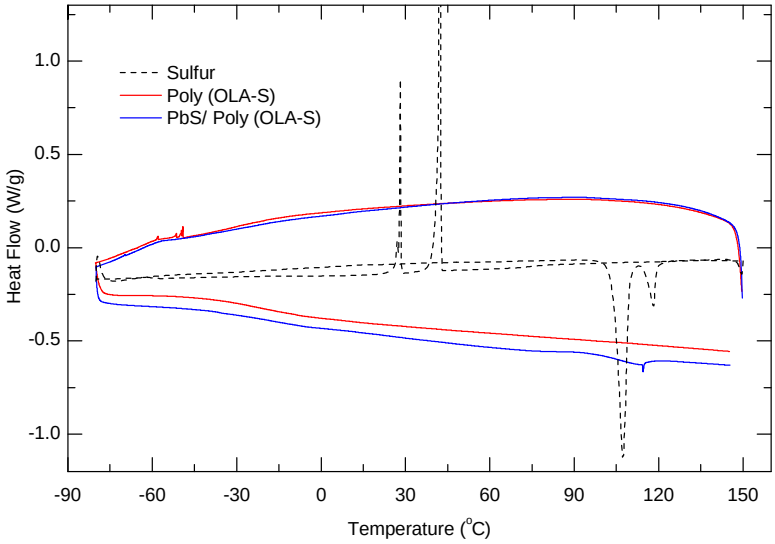

Figure 3.8 DSC thermograms of purified poly(OLA-r-S) with a feed molar ratio of [oleylamine]:[sulfur] = 1:33 and a PbS/poly(OLA-r-S) nanocomposite obtained by adding 0.144 M of $PbCl_2$, dissolved in 0.4 g of oleylamine, into poly(OLA-r-S) solution after 30 min of copolymerization.

the copolymerization, which was consistent with the findings by Ozin et al. as previously discussed.[115] While ^{1}H NMR, SEC, elemental analysis and DSC of these materials confirmed the formation of true copolymers, the structural identification of the side chain functionality in the copolymers required more rigorous investigation of model reactions and ^{13}C NMR spectroscopy, especially since IR spectroscopy did not definitely confirm the presence of a distinct functionality.

In order to confirm if (thio)amide groups were formed by the proposed mechanism of Ozin et al., ^{13}C NMR measurements of crude copolymerization mixtures of oleylamine and S_8 were conducted in deuterated 1,2-dichlorobenzene-d4. These measurements revealed the presence of ^{13}C NMR resonances at δ= 205.4 and 184.9 ppm, which were in good agreement with assignments from Ozin et al., corresponding to thioamide and amide functional groups (**Figure 3.9**).[115] While the exact ratio of these functional groups could not be quantified using ^{13}C NMR, these experiments nevertheless confirmed that the primary amine groups from oleylamines were also converted into chain moieties of the copolymers, presumably consisting of the mixtures of thioamides and amide side chain groups. To further support this assignment, the cross-coupling reactions with oleylamines and 4-t-butylbenzyl amine in the presence of S_8 were conducted, followed by the analysis with ^{13}C NMR spectroscopy. This additional model reaction revealed the presence of a single resonance at δ= 198 ppm, corresponding to the formation of substituted (thio)amides from the cross-coupling of benzylic and aliphatic amines (**Figure 3.10**). The reactivity and spectroscopic characterization of a pure substance, such as, 4-t-

butylbenzyl amine was beneficial for these studies, since the commercially available oleylamine contains of number of impurities (technical grade ~ 70% purity, Aldrich).

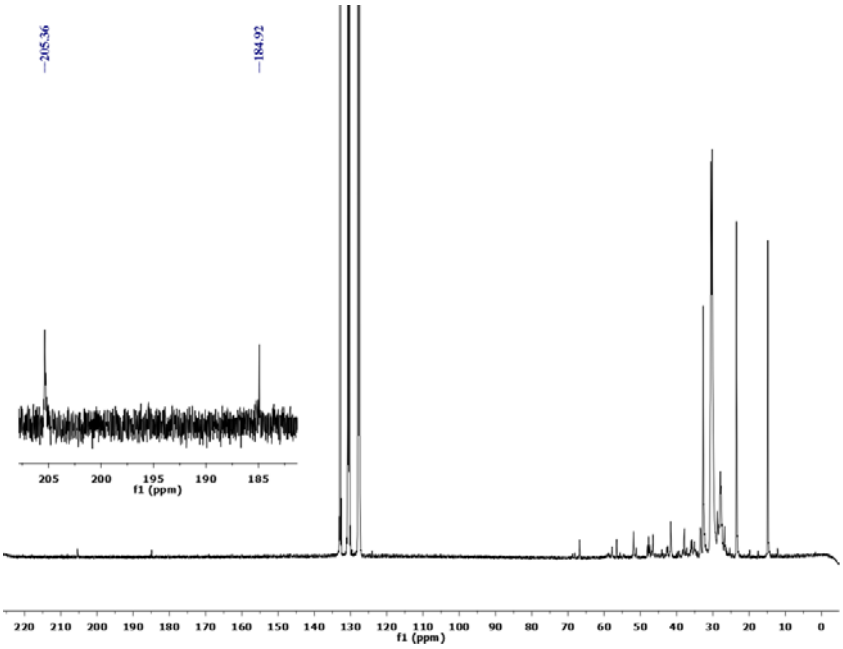

Figure 3.9 ^{13}C NMR spectrum of a copolymer consisting of oleylamine and sulfur polymerized in 1,2-dichlorobenzene-d4 at T=180 °C for [oleylamine]:[sulfur] = 1:33 in mole ratio, after 30 min of copolymerization.

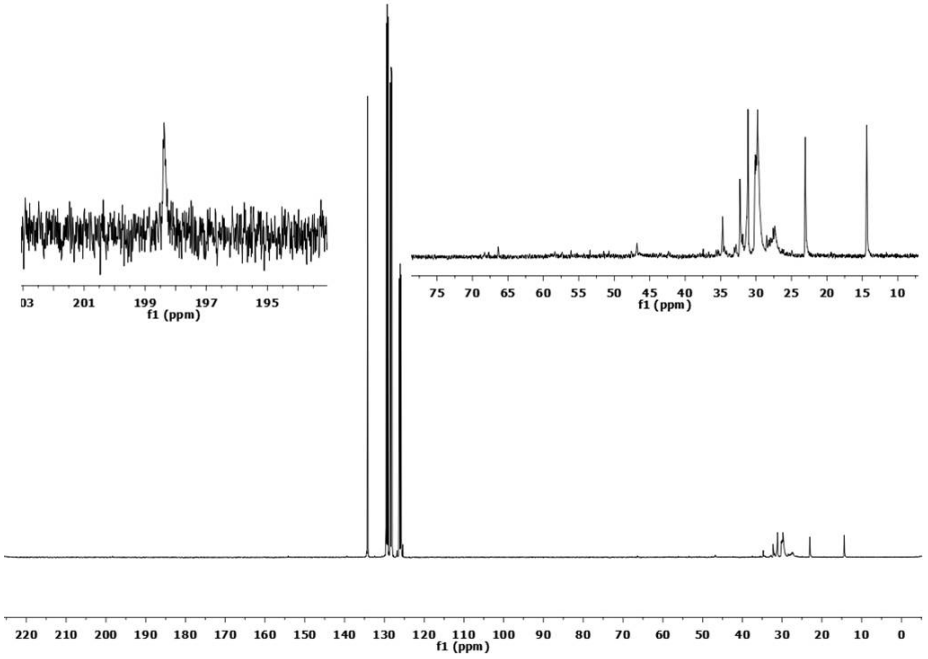

Figure 3.10 ^{13}C NMR spectrum of reaction mixture synthesized from cross-coupling reaction of 4-*tert*-butylbenzylamine and oleylamine with sulfur. NMR sample was prepared by dissolving reaction mixture in chlorobenzene-d_5 and peak at δ = 198.4 ppm corresponds to a single substituted thioamide functional group.

3.3.2 Synthesis of PbS/Poly(OLA-r-S) nanocomposites

Upon the optimization of reaction conditions to prepare poly(OLA-r-S) copolymers, the one-pot method to prepare PbS/poly(OLA-r-S) nanocomposites was then investigated. The key novelty and advantage of this one-pot process is the ability to prepare well-dispersed NPs within high sulfur content polymer matrices. Due to the dual reactivity of oleylamines toward both formations of sulfur copolymers and PbS NPs, the direct addition of preformed Pb(II)Cl_2 complexes with oleylamines to reaction mixtures with sulfur in DCB were conducted. An earlier report by Hyeon et al.[28] demonstrated the preparation of PbS nanocrystals using $PbCl_2$ complexes in the presence of sulfur and oleylamine. In this example, the reaction of sulfur and oleylamine was solely intended to generate H_2S in-situ to promote PbS NP formation. Furthermore, it is noted that a low feed ratios of sulfur was used in this reaction.

In the one-pot preparation of these nanocomposites $PbCl_2$/oleylamine complex solutions were injected into the copolymerization mixtures of sulfur and oleylamine at different initial feed ratios of oleylamine and sulfur ([S]/[oleylamine] 2:1, 8:1, and 33:1 in molar ratio) to determine optimal conditions to prepare well-dispersed NP nanocomposites. The optimal feed ratio was found to be 33:1, as an excess amount of sulfur along with higher conversion of oleylamine at the moment of PbS NP formation facilitated the stable dispersion of NPs within sulfur copolymer matrices. Under these conditions, the Pb(II) precursors were injected in a series of separate

reactions after allowing oleylamines and sulfur to copolymerize for 5, 10, 15, 20 and 30 min to determine the optimal reaction time to induce the PbS NP reaction. TEM images of the aliquots taken from different crude reaction mixtures revealed that the dispersion of PbS NPs within sulfur copolymer matrices was significantly improved when the Pb(II)-oleylamine complexes were injected after a reaction time of 30 min in the initial copolymerization step (**Figure 3.11d**). Due to the in-situ generation of H2S from the reaction of oleylamine and sulfur, PbS NPs were observed to form within 5 min. Furthermore, the TEM images in Figure 3.5 confirmed that the PbS NPs formed were comparable in size (diameter (D) = 7.4±1.9 nm, Figure 3.5d) and XRD confirmed the formation of halite (cubic) PbS phases (**Figure 3.12**).

To further demonstrate the advantage of our one-pot process to prepare well-defined and highly dispersed PbS/poly(OLA-r-S) nanocomposites, blending experiments with preformed PbS NPs with free poly(OLA-r-S) were conducted. Preformed NPs were prepared by the synthesis of PbS NPs using oleylamine as capping ligands, as previously described by Hyeon et al.[28] Blends with PbS NPs and poly(OLA-r-S) were then prepared in solution followed by casting onto carbon-coated TEM grids. The TEM image confirmed that the preformed oleylamine-capped PbS NPs tended to aggregate within the poly(OLA-r-S) matrices (**Figure 3.11a**). The massive NP aggregation in this case was attributed to both enthalpic immiscibility of oleylamine-capped PbS NPs with the copolymer matrices as well as the depletion demixing of poly(OLA-r-S) with PbS NP inclusions. Hence, in our one-pot reactions, by forming PbS NPs in the presence of poly(OLA-r-S) copolymers in

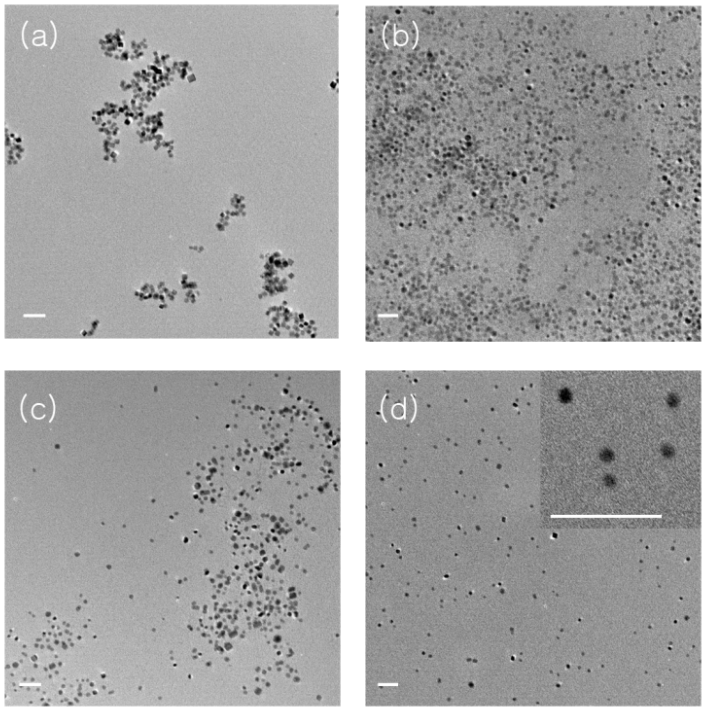

Figure 3.11 Plan view TEM images of: (a) blends of oleylamine-capped PbS NPs (2 wt%) with poly(OLA-r-S) copolymers. The NP size is 8.4±1.1 nm. (b) A PbS/poly(OLA-r-S) nanocomposite by the addition of $PbCl_2$-oleylamine solution into the oleylamine-sulfur mixture without polymerization of poly(OLA-r-S). The NP size is 9.2±1.5 nm. (c) A PbS/poly(OLA-r-S) nanocomposite by the addition of PbCl2-oleylamine solution into the poly(OLA-r-S) solution after copolymerization for 15 min. The NP size is 8.7±2.2 nm. (d) A PbS/poly(OLA-r-S) nanocomposite by the addition of PbCl2-oleylamine solution into the poly(OLA-r-S) solution after copolymerization for 30 min. The NP size is 7.4±1.9 nm. All the scale bars are 50 nm.

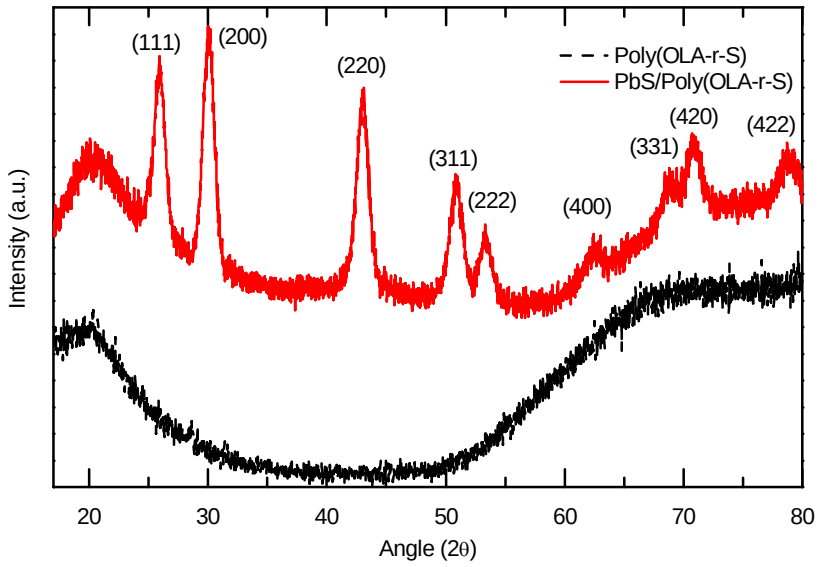

Figure 3.12 XRD spectra of PbS/poly(OLA-r-S) nanocomposites. Cubic (Fm3m) lattice planes of PbS NPs were assigned to the diffraction peak.

DCB solution, we propose that the amide/thioamide side chain groups of the sulfur copolymers are able to sufficiently associate and stabilize PbS NPs, which are, in turn, miscible with the sulfur copolymer matrices when cast as films.

To further demonstrate the advantages of this synthetic process to prepare NP-sulfur nanocomposites, the variation of PbS NP loading within poly(OLA-r-S) films was demonstrated by varying the concentration of $PbCl_2$ in oleylamine (0.288, 0.576, and 0.864 M) injected into the reaction mixtures (**Figure 3.13**). The TEM images confirmed the concurrent increase in number particle density as a direct function of Pb(II) precursor loading into the reaction mixtures, where the NP size remain almost constant at D = 7.4 nm. The TGA analysis of the nanocomposites revealed PbS NP loadings of 1, 3.5, and 14 wt% as a function of different Pb(II) precursor concentration of 0.288, 0.576, and 0.864 M, respectively (**Figure 3.14**). The influence of the molar feed ratios ([oleylamine] : [sulfur]) on the internal morphologies of the PbS NPs were also demonstrated in **Figure 3.15**. These PbS/poly(OLA-r-S) nanohybrids were found to readily dissolve in THF and toluene, enabling facile solution processing of these materials into thin films on glass substrates or free-standing films, as demonstrated in **Figure 3.16**.

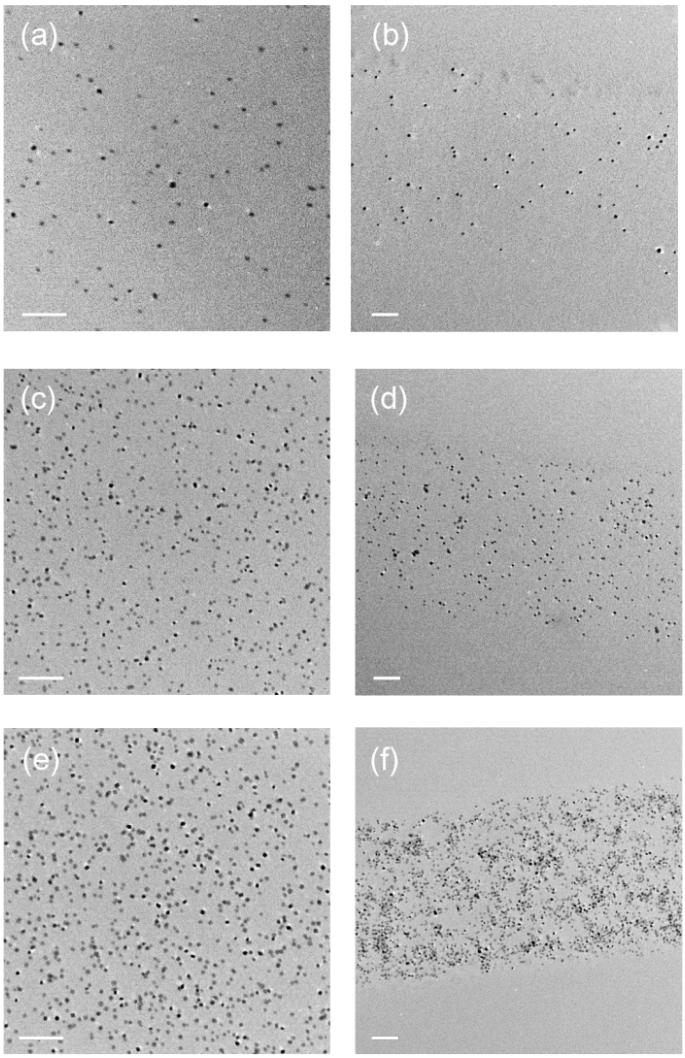

Figure 3.13 Cross-sectional TEM images of PbS/poly(OLA-r-S) nanocomposites with different concentration of PbCl2 ((a), (c), and (e)), and their spin-cast films ((b), (d), and (f)): (a) and (b) 0.288 M of PbCl2 added. The NP size is 7.4±1.9 nm. (c) and (d) 0.576 M. The NP size is 7.4±1.3 nm. (e) and (f) 0.864 M. The NP size is 7.4±0.1 nm. All the scale bars are 100 nm.

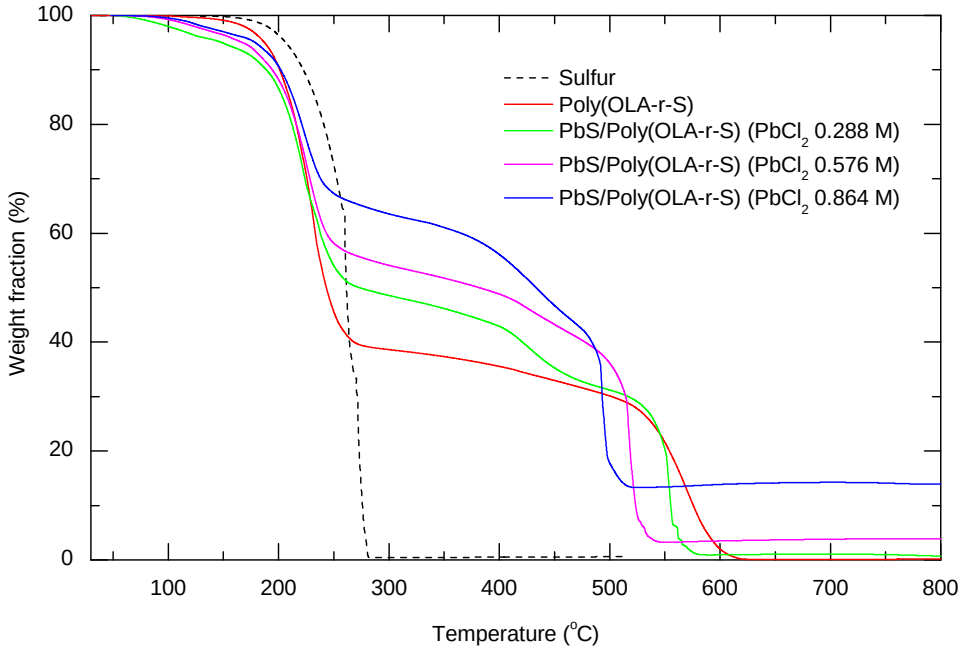

Figure 3.14 TGA curves of PbS/poly(OLA-r-S) nanocomposites obtained by adding different amount of $PbCl_2$ (0.288, 0.576, and 0.864 M) dissolved in 0.4 g of oleylamine into poly(OLA-r-S) solution with a molar feed ratio of [oleylamine]:[sulfur] = 1:33, after 30 min of copolymerization.

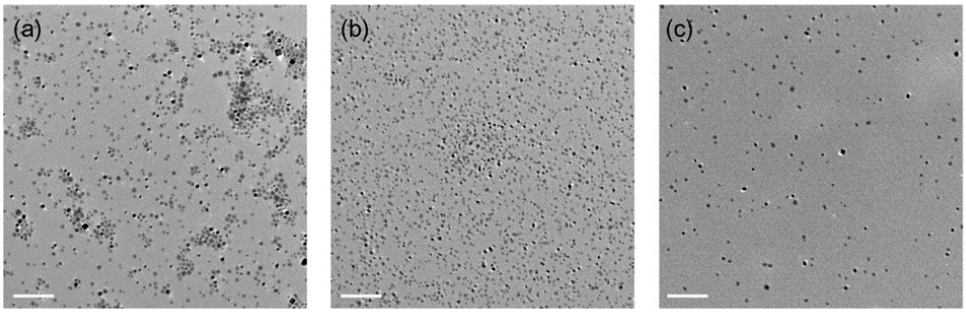

Figure 3.15 TEM images of PbS/poly(OLA-r-S) nanocomposites by the addition of $PbCl_2$-oleylamine solution (0.288 mmol of $PbCl_2$ dissolved in 0.4 g of oleylamine) into poly(OLA-r-S) solution (after 30 min of copolymerization) with different molar feed ratios: (a) [oleylamine]:[sulfur] = 1:2; (b) 1:8; (c) 1:33.

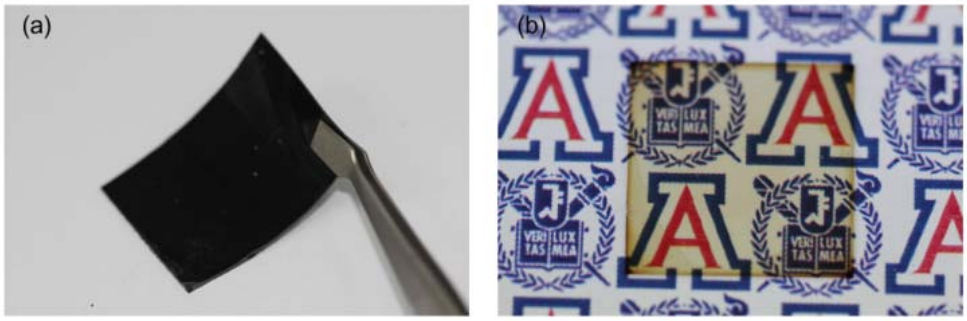

Figure 3.16 Photo images of PbS/poly(OLA-r-S) nanocomposite films: (a) A free-standing film prepared by solvent evaporation (film thickness = 1 mm). (b) A spin-cast film on a glass substrate (film thickness = 600 nm).

3.4. Conclusions

We report on the first one-pot synthetic method to prepare well-defined NP/sulfur nanocomposites containing PbS NPs well-dispersed within high sulfur content copolymer matrices by employing oleylamines as a comonomer for sulfur copolymers as well as a H2S generating precursor for NP synthesis. We demonstrate the dual role or reactivity of oleylamines for the first time toward applications of sulfur copolymerization and the synthesis of chalcogenide NPs. Various kinds of NP/sulfur nanocomposites are anticipated to be prepared using poly(OLA-r-S). This general approach is a new synthetic advance in the emerging area of sulfur utilization by the direct modification of elemental sulfur as a novel feedstock for materials synthesis.

Chapter 4. Reduced Graphene Oxide / Sulfur Copolymer Nanocomposites for Li-S Batteries

4.1. Introduction

Lithium-sulfur (Li-S) batteries have been attracted much attention for a decade, because they are expected to achieve a significant breakthrough in energy storage industries including electric vehicles, due to the large specific capacity (1575 $mAhg^{-1}$) of sulfur cathodes. However, there are still many challenging problems to overcome for the commercialization of Li-S batteries. The most serious issues in sulfur cathodes come from the electrically insulating property of sulfur, as well as the unique electrochemical reaction in the cathode during the charge/discharge cycles. The intermediate products of sulfur, polysulfides, easily dissolve in the electrolyte, and they continuously diffuse out from the electrode. Moreover, the fully lithiated product of the dissolved polysulfides, lithium sulfide (Li_2S), is also insulating solid, which irreversibly precipitate on the electrode surface without electrical contact. Those electrochemical processes involving liquid and solid phases lead to gradual decomposition of the electrical conducting path, reaching to the active sulfur species inside the cathode, and that results in rapid capacity fading during the repeated charge/discharge cycles.

To address these issues, we developed high sulfur content copolymers, poly(S-r-DIB) (SDIB), via the inverse vulcanization, as new cathode materials for Li-S batteries. In these copolymers, the small contents of monomer (DIB), cross-linked with linear polysulfide chains, act as a binder to prevent irreversible dissolution of polysulfides, and also stabilize the lithiated product phases of the cathode during the electrochemical reaction. As a result, homogeneous contact between carbon and the copolymers could be retained during the repeated charge/discharge cycles. Therefore these polymer cathodes exhibited high capacity retention until more than 500 cycles.[102, 104, 113, 119] However, the enhancement of high C-rate capability with SDIB copolymer is still hard to achieve due to the absence of electrically conducting pathway inside the copolymers.

There have been a large number of the strategies developed for the incorporation of conductive carbon materials with sulfur to improve the rate capabilities of Li-S cells. The most representative methods come along with graphene due to its superior electrical conductivity and extremely small occupied volume. However, both graphene and sulfur are intrinsically poor materials for processing, so the chemically oxidized graphene, graphene oxide (GO), was mostly utilized for the preparation of sulfur/GO composites.[51-56] Even though the reduction of GO was able to recover the original electrical property of graphene, the high quality nanocomposites with sulfur and reduced GO for Li-S batteries were rarely reported.[57-60] Moreover, the macromolecular sulfur/graphene nanocomposite material have not been introduced yet, that is expected to afford a variety of options for the electrode fabrication

methods.

Herein we demonstrate improvements of rate capability and specific energy of SDIB polymer cathode by introducing simple nano-scale inclusion of reduced GO (rGO) into SDIB polymeric matrix. A facile method to include functional nanomaterials within polymeric sulfur matrices were introduced by our group.[103, 120] By using unique dual interaction between oleylamine (OLA) and sulfur, PbS NP/sulfur copolymer nanocomposites were synthesized in a one-pot manner. The double bond in the middle of OLA chain copolymerized with sulfur diradical to form polymeric matrix of the nanocomposites, and at the same time, the amine functional group at the end of OLA chain was attached to the surface of PbS NP to stabilize the interfaces. In this work, the similar chemistry was employed for SDIB/rGO nanocomposites by using dual interaction of OLA, which binds to both sulfur and GO (**Figure 4.1**). For the homogeneous dispersion of rGO in SDIB polymer matrix, OLA was attached on to GO, and the OLA modified GO (oGO) was subsequently reduced with trioctylphosphine (TOP), as a reducing agent. Lee et al.[121] reported that these modification and reduction steps afforded good miscibility and processability of rGO in 1,2 dichlorobenzene (DCB). Therefore, simple mixing of rGO and SDIB polymers at 150 °C resulted in the homogeneous nanocomposite materials after purification. Furthermore, the OLA molecules, binding to rGO, copolymerized with SDIB in the mixing step, to generate nano-scale electrical contact between rGO and SDIB polymer.

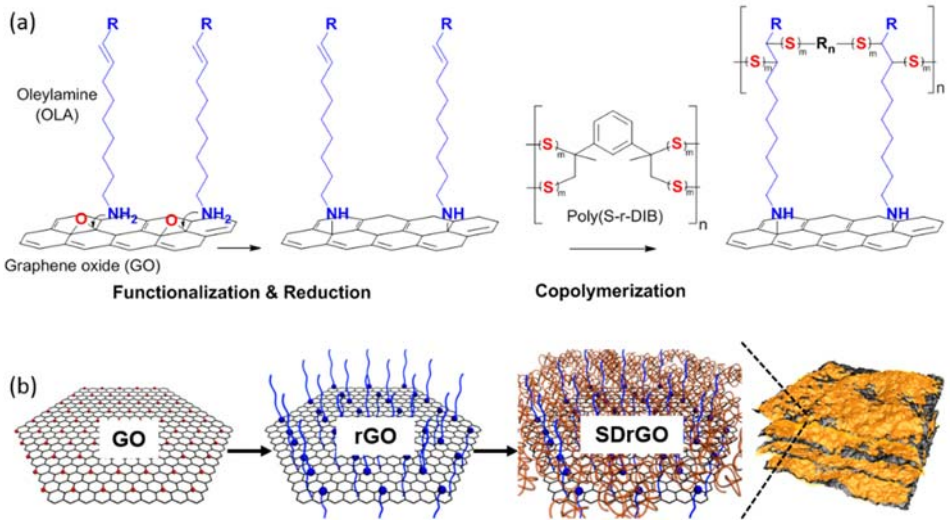

Figure 4.1 a) overall reaction scheme for the synthesis of poly(S-r-DIB)/rGO nanocomposites. b) Schematic illustration of the synthesis of SDrGO.

4.2. Experimental section

4.2.1 Materials

Graphite powder (<45 microns), sulfur, potassium permanganate ($KMnO_4$), oleylamine (OLA, 70% technical grade), trioctylphosphine (TOP, 90% technical grade), and N,N-dimethylformamide (DMF) were purchased from Sigma-Aldrich. Hydrochloric acid (HCl) was provided from Samchun Chemical. Concentrated sulfuric acid (H_2SO_4) was obtained from PFP Chemicals. Hydrogen peroxide (H_2O_2) and 1,2-dichlorobenzene (DCB) was purchased from Junsei Chemical. 1,3-Diisopropenyl benzene (DIB) was obtained from TCI Chemical.

4.2.2 Synthesis of SDrGO nanocomposites

GO was prepared from natural graphite by the modified Hummer's method according to the previous reports.[122-124] 2 g of graphite and 46 mL of H_2SO_4 were added into the flask placed in ice bath with stirring. After 10 min, 6 g of $KMnO_4$ was slowly added to the mixture, while being kept below 20 ^oC. After 16 h, 92mL of deionized water was slowly added and heated to 35 ^oC for 2 h. The reaction was terminated with 280 mL of deionized water and 5 mL of H_2O_2 at 60 ^oC. The reaction product was filtrated and washed several times with 500 mL of 5 % HCl solution. The fractionated GO dispersion in water (1 mg/mL) were obtained by ultra-sonication at 40 % amp. for 30 min in the presence of ice bath. The final product was freeze-dried for 3 days for further use.

oGO and rGO were prepared following the previous paper by Lee and coworkers.[121] 0.2 g of GO and 2 mL of OLA were added into 50 mL of DMF, and the mixture was subjected to sonication for 1 h, followed by heating at 80 ^{o}C for 24 h. For purification, 50 mL of ethanol was added and oGO suspension was precipitated by centrifugation at 4500 rpm for 20 min. This process was repeated twice after the re-dispersion of the precipitates in 20 mL of n-hexane. The final product was dried in vacuum oven overnight.

For the preparation of rGO, 0.1 g of oGO and 5 mL of TOP were added into 50 mL of DCB, and the mixture was subjected to sonication for 1 h, followed by heating at 100 ^{o}C for 24h. The purification and drying process was the same as that for oGO.

SDIB copolymer was synthesized according to the previous reports.[102, 104, 113, 119] 4.5 g of sulfur and 0.5 g of DIB were heated at 185 ºC with vigorous stirring until the mixture became homogeneous and vitrified. The reaction was stopped by cooling down to room temperature after the reaction product solidify, and the stirring stopped by the increased viscosity of the product.

For SrGO, 0.05 g of rGO and 0.45 g of sulfur were added in 5 mL of DCB, and the mixture was subjected to sonication for 1 h, followed by heating at 150 ^{o}C for 24 h. After the reaction, 10 mL of methanol was added and the product was precipitated by centrifugation at 4500 rpm for 20 min. The product was dried in vacuum oven overnight.

SDrGO was synthesized with 0.05 g of rGO and 0.45 g of SDIB copolymer added in 5 mL of DCB. The reaction and purification steps were the same as that for SrGO.

4.2.3 Electrochemical characterization of SDrGO nanocomposites

^{1}H NMR spectra were obtained with a Bruker Avance III 500 MHz spectrometer using $CDCl_3$ as a solvent. Differential scanning calorimeter (DSC) data was obtained using a DSC 4000 (PerkinElmer) at a heating rate of 10 ^{o}C/min under nitrogen atmosphere. Thermal gravimetric analysis (TGA) was carried out by a TGA Q500 (TA Instruments) at a heating rate of 10 ^{o}C/min under nitrogen atmosphere. Elemental analysis was performed using a Flash1112 (CE Instrument, Italy) with CHNS-Porapack PQS columns. X-ray diffraction (XRD) measurements were obtained using a New D8 Advance model (Bruker) at room temperature with a CuKα radiation source at 18 kW.

X-ray photoelectron spectroscopy (XPS) was conducted using Axis-HSi (Kratos) with Mg/Al dual anode at 15 kV and 10 mA. Fourier-transform infrared (FTIR) spectra were obtained with FT-IR/NIR Frontier Spectrum 400 (PerkinElmer). Atomic force microscopy (AFM) was carried out with Nanowizard (JPK Instruments). Raman spectra were taken with T64000 (Horiba) using Ar laser (514 nm).

Transmission electron microscopy (TEM) images were recorded on a JEOL-JEM2100 at an operating voltage of 200 kV. For the cross-sectional views of TEM, the samples were placed on a pre-cured epoxy resin, and then embedded by pouring a fresh epoxy resin on the top of the films after drying in a vacuum oven. The resin mixture for molding was prepared by mixing 25.6 g of Embed 812 resin, 13.51 g of

dodecenyl succinic anhydride, 10.9 g of Nadic® methyl anhydride, and 1 g of DMP-30. All the components were purchased from Electron Microscopy Sciences. The cured resins were sliced with a microtome (Leica Microsystems). The 70 nm-thick slices were prepared with a diamond-coated knife (DiATOME) at an angle of 6 ^{o} and a cutting velocity of 0.1 mm/s. The slices were suspended in water and supported on a Cu grid.

The cathodes were fabricated from slurries dispersed in N-methyl-2-pyrrolidone (2 ml). The prepared slurry was cast onto an aluminum foil using a doctor blade method. The cathodes were transferred to an Ar-filled glove box and were assembled in a 2032 type coin cell. The mass loading of all samples was ~1 mg of active material. The electrolyte was 1.0 M LiTFSI (lithium bis-trifluoromethanesulfonimide) and 0.1 M LiNO3 (lithium nitrate) with DOL (dioxolane) and DME (dimethyl ether) 1:1 volume ratio (Panax Etec, Korea). The separator was supplied from SK Innovation corporation (Korea), and lithium metal was used as a counter electrode. Electrochemical properties were measured with a WBCS3000 cycler (Won-A Tech, Korea). The voltage window for electrochemical measurements was fixed between 1.7 - 2.8 V vs. Li+/Li (all the voltages below are vs. Li+/Li).

4.3. Results and discussions

4.3.1 Synthesis of SDrGO nanocomposites

The XRD patterns were obtained to confirm the successive modification and reduction of GO (**Figure 4.2a**). As-synthesized GO has a diffraction peak at 2θ = 11.7 °, corresponding to 7.56 Å of the basal plane distance (001) due to the oxygen containing functional groups in graphene interlayers. After the modification with OLA, the interlayer distance increased to 23.4 Å, which is attributed to the length of alkyl chains of OLA intercalated between the GO interlayers.[125] When oGO reduced with TOP (rGO), a new broad peak centered at 20.8 ° (4.27 Å), closer to that of natural graphite (3.34 Å), appeared in the XRD pattern as a result of re-stacking of reduced graphene interlayers.[121] As-synthesized rGO were re-dispersible in DCB and other organic solvents, due to the remaining OLA grafted on GO, after the reduction. The AFM height images were obtained after spun on silicon wafer using water for GO solution, and DCB for oGO and rGO solutions, and that also confirmed the OLA grafting on GO after the reduction as shown in **Figure 4.2b**. The thickness of GO measured by AFM was about 1 nm, while as those of oGO and rGO were roughly 2 to 2.5 nm. The 4 point probe measurement revealed the significant enhancement in the electrical conductivity of rGO. The electrical resistivity of GO (7.43 X 105 Ω·cm) slightly decreased after OLA modification (3.20 X 104 Ω·cm), and after the reduction, it drastically decreased into 6.06 Ω·cm.(**Figure 4.3**) Further characterization of rGO were conducted by XPS (**Figure 4.4**).

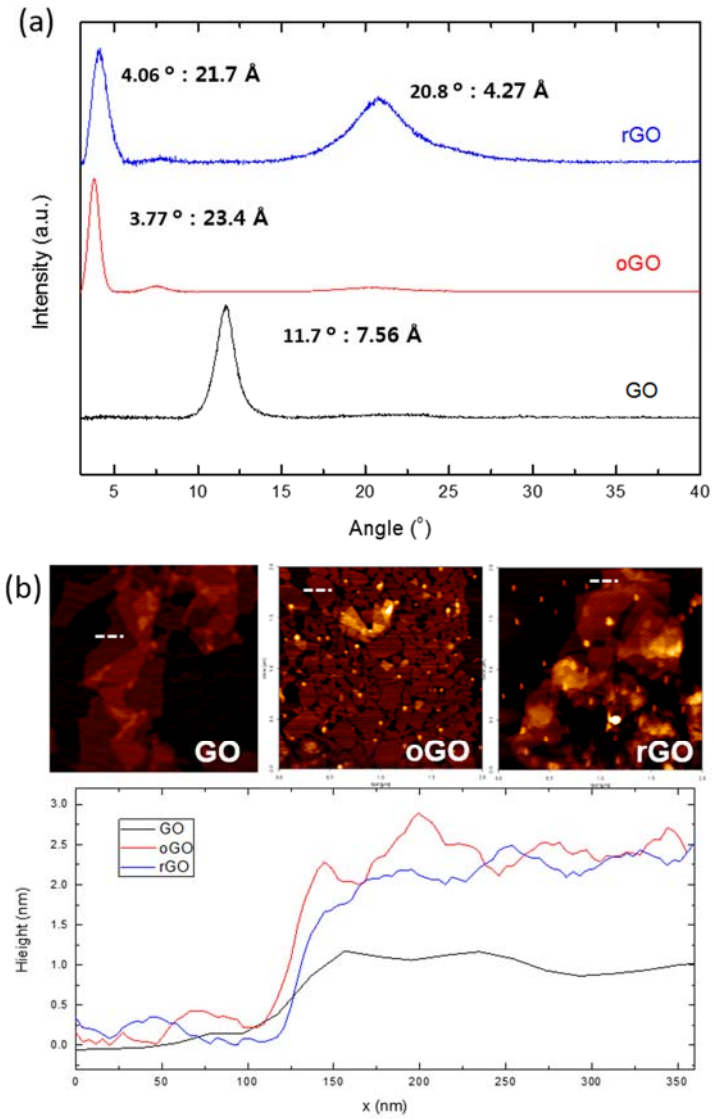

Figure 4.2 (a) XRD patterns and (b) AFM height measurements of GO, oGO, and rGO

GO	7.43 X 10^5 Ω·cm
oGO	3.20 X 10^4 Ω·cm
rGO	*6.06 Ω·cm*

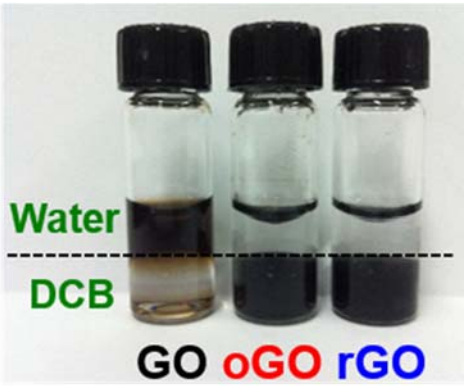

Figure 4.3 Electrical resistivity of GO, oGO, and rGO measured by 4-point probe (left), and photo image dispersed in water/DCB layered media.

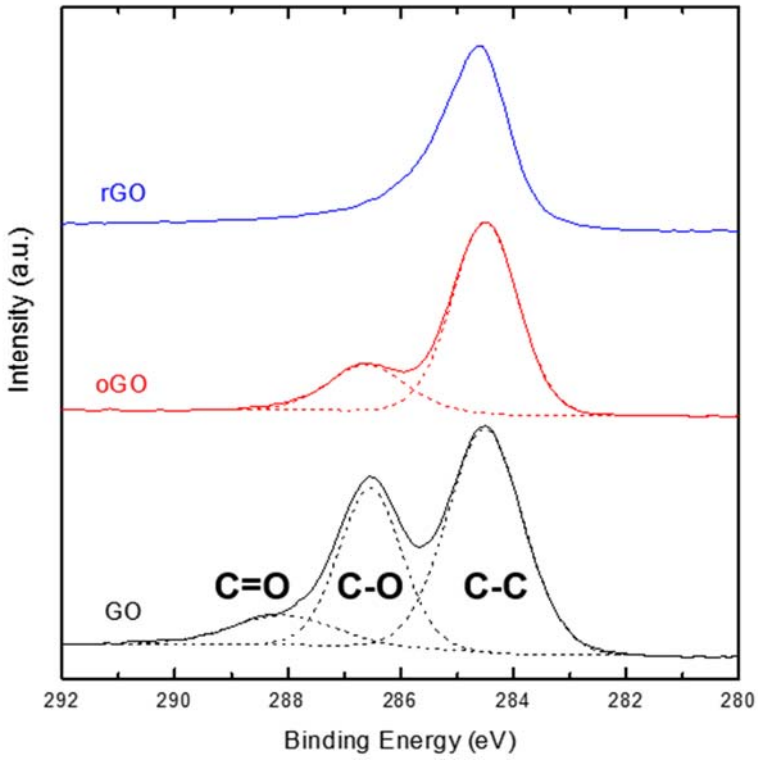

Figure 4.4 XPS Spectra (C1s) of GO, oGO, and rGO.

As-synthesized rGO was utilized for sulfur/rGO (SrGO) or SDIB/rGO (SDrGO) nanocomposites, which were obtained by simply mixing of sulfur or SDIB, respectively, with rGO in DCB. The contents of sulfur in SDIB polymer used in the synthesis were 90 wt%, which was proved to exhibit the best capacity retention behaviour among all the feed ratio ranges,[102, 104] and 10 wt% of rGO was additionally included in the SrGO and SDrGO nanocomposites. The chemical bonds between polysulfides and OLA of rGO were expected to be formed during the mixing step, as previously reported.[120] The additional experiment with SDIB/OLA mixtures at the same condition revealed the consumption of the OLA double bond to afford S-DIB-OLA copolymers. TGA curves confirmed the 10 wt% of rGO incorporation in the nanocomposites after the purification. About 90 wt% and 80 wt% of sulfur was contained in the SrGO and SDrGO nanocomposites, respectively (**Figure 4.5a**). The π-π stacking of the reduced graphene layers and OLA intercalation, observed in the XRD pattern of the rGO, were disappeared in SrGO and SDrGO, which support the homogeneous dispersion of rGO sheets in the sulfur polymeric matrices, The STEM images along with the EDS elemental maps were also demonstrated to show identical location of both sulfur and carbon signals, and that implies the nano-scale electrical contact between active sulfur of SDIB and carbon of rGO (**Figure 4.5b**).

The chemical bonds between sulfur copolymer and OLA of rGO were formed during the mixing step, as confirmed by FTIR spectrum of SDrGO, in which alkyl CH=CH stretching band of OLA in rGO disappeared after the reaction with SDIB copolymers (**Figure 4.6**). The additional experiment of ^{1}H NMR measurement with

SDIB/OLA mixtures at the same condition also revealed the consumption of the vinyl and allylic α-CH_2 protons of OLA to afford SDIB-OLA copolymers (**Figure 4.7**).

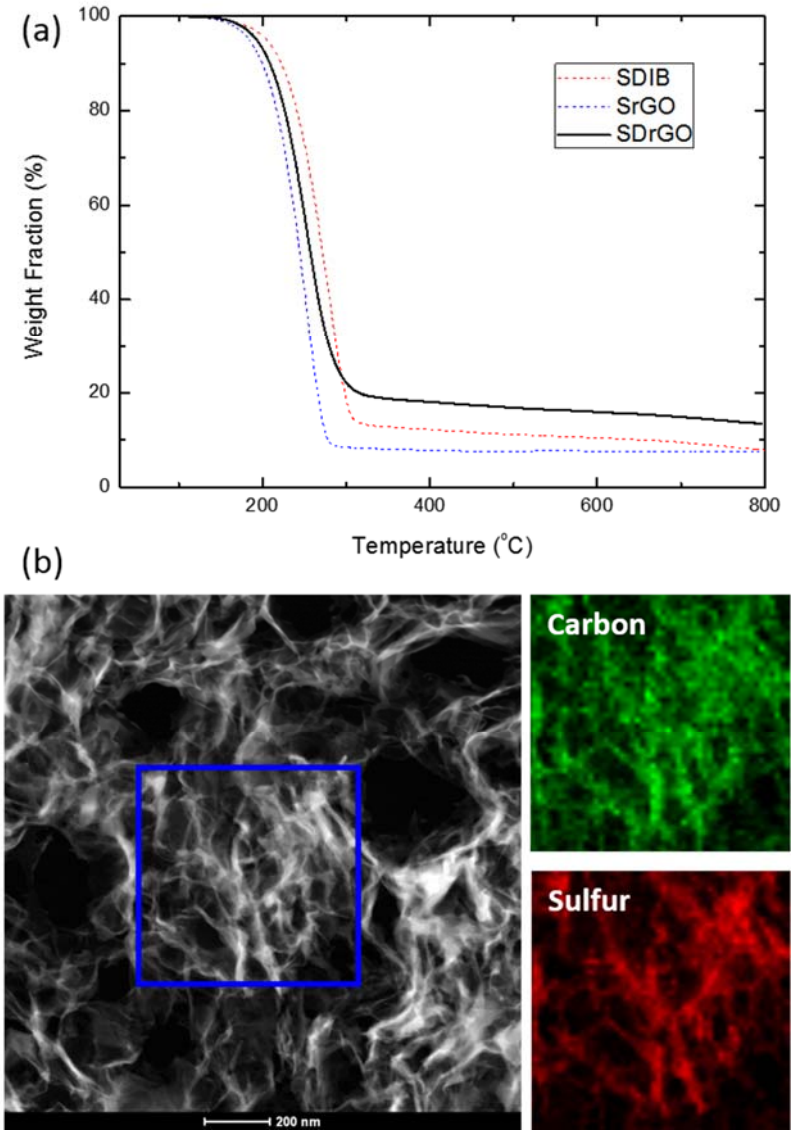

Figure 4.5 (a) TGA curves of Poly(S-r-DIB), Sulfur/rGO nanocomposites, and Poly(S-rDIB)/rGO nanocomposites. (b) STEM image and EDS elemental map of Poly(S-rDIB)/rGO nanocomposites.

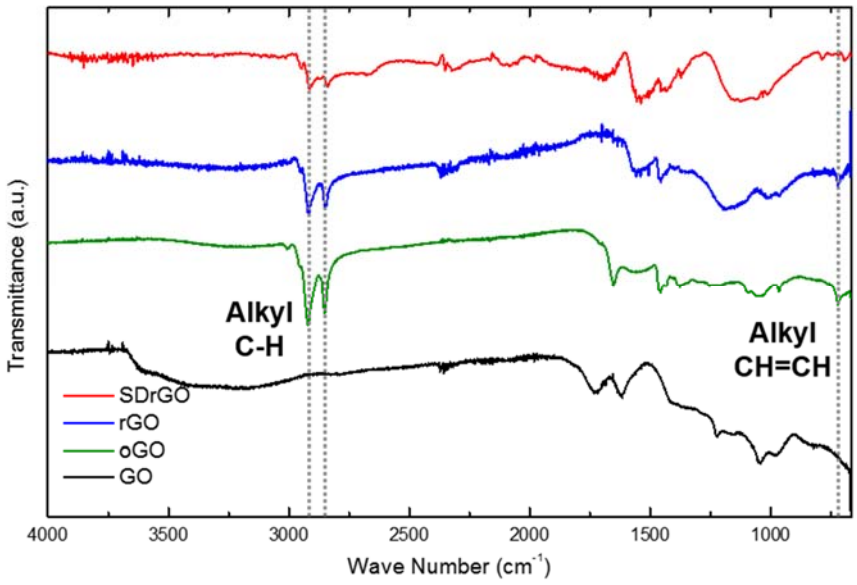

Figure 4.6 FTIR spectra of SDrGO nanocomposite in comparison with GO, oGO, and rGO.

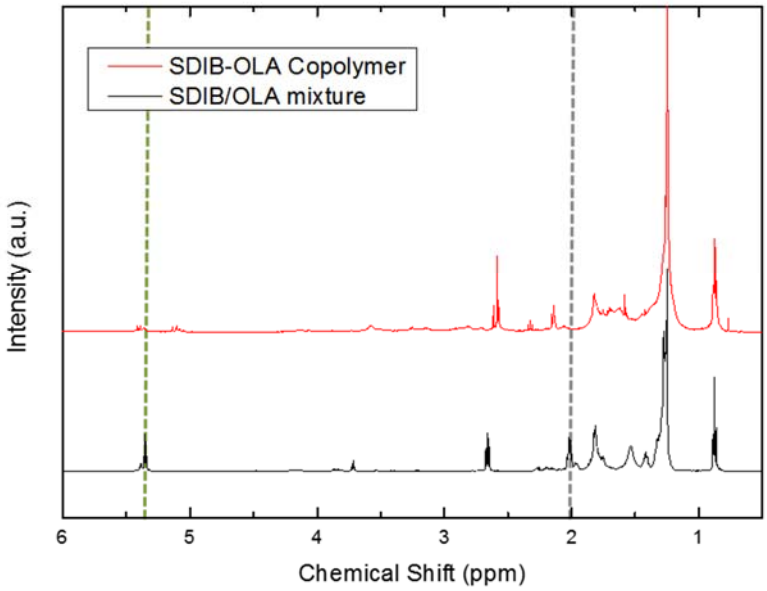

Figure 4.7 ^{1}H NMR spectra of SDIB-OLA copolymer with the same reaction condition for the synthesis of SDrGO Nanocomposites.

4.3.2 Electrochemical Characterization of SDrGO nanocomposites

The SDIB, SrGO, and SDrGO cathodes for electrochemical analysis were separately prepared by mortar mixing of each with super P carbon and PVDF binder. In order to fix the total sulfur contents as 72 wt% in each of the cathodes, the addition of super P carbon in SDrGO cathode was reduced into 5 wt%, while as 15 wt% of super P carbon was added in each of SDIB and SrGO cathodes (**Table 4.1**). The charge-discharge voltage profiles and the cycling performance of the cathodes at 0.5 C-rate (1C = 1,675 mA/g) are shown in **Figure 4.8**, and **Figure 4.9**, respectively. Stable capacity retention during 300 cycles was observed with SDIB cathode (850 mAh/g, at 300 th cycle), although the initial capacity (985 mAh/g) was relatively low. On the other hand, the SrGO cathode exhibited high initial capacity (1,219 mAh/g), but it underwent severe capacity fading during the cycles (598 mAh/g at 300 th cycle). The SDrGO cathode exhibited not only high initial capacity (1,180 mAh/g), but also superior capacity retention (960 mAh/g at 300 th cycle) compared to the others. Both of the DIB containing composite cathodes (SDIB and SDrGO) exhibited great capacity retention, and that is attributed to the role of DIB in the cathodes, as reported previously.[104] Additionally, the rGO in the composite cathodes enhances the electrical conductivity of the cathodes and that is supposed to increase the initial capacity of the SrGO and SDrGO by sufficient utilization of active sulfur at the initial stage. The rate performances of the composite cathodes on varying C-rates (0.1, 0.2, 0.5, and 1 C) is shown in **Figure 4.9b**, that also confirms the significant improvement of rate capability of the SDIB cathode, by the incorporation

with rGO. More interesting features of the composite cathodes are demonstrated in the charge/discharge profiles on varying C-rates as shown in **Figure 4.10**. The lower operating voltages and higher charging voltages, resulted from a severe polarization as increasing C-rates, was observed in SDIB cathode, while as SrGO and SDrGO cathode exhibited only negligible polarization at increased C-rate. These different voltage profiles are directly related to the overall performance of the Li-S cells, because the specific energy and specific power of the cells are estimated by the integration of the operating voltage values by the generated charges (**Figure 4.11**). The electrochemical reaction kinetics of the composite cathodes were further characterized with cyclic voltammetry (CV), and the positive and negative peak currents vs. square root scan rates ($\nu 1/2$) were plotted. The faster reaction kinetics of the rGO containing composite cathodes were shown at all scan rates of CV. The electrochemical impedance spectroscopy (EIS), measured before the cycling, also support the lower charge transfer resistance of SrGO and SDrGO cathodes compared to that of SDIB. These are the clear evidences of the enhanced electrical contact between rGO and active sulfur, achieved by the OLA medicated nano-scale inclusion of rGO in sulfur matrices. Furthermore, SDrGO cathode preserved high capacity retention during the cycles at high C-rate, due to the synergetic effect of DIB crosslinker with rGO, which resulted in the drastic improvements in specific energy and specific power of the Li-S cells.

	SDIB	SrGO	SDrGO
Active Material	***80 wt%***	***80 wt%***	***90 wt%***
Carbon	***15 wt%***	***15 wt%***	***5 wt%***
Binder	5 wt%	5 wt%	5 wt%
Sulfur Contents	**72 wt%**	**72 wt%**	**72 wt%**

Table 4.1 Compositions of the cathodes for the electrochemical characterization

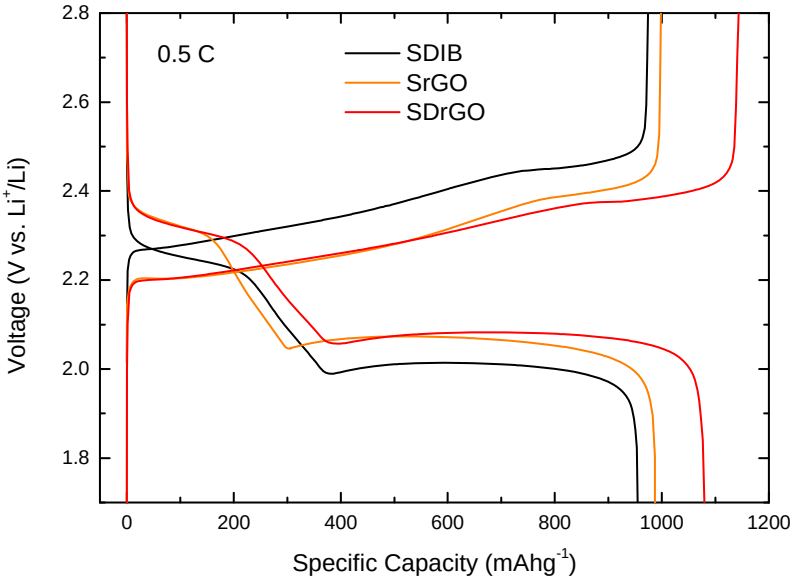

Figure 4.8 Charge/discharge voltage profiles of the cathodes at 10th cycle, 0.5 C.

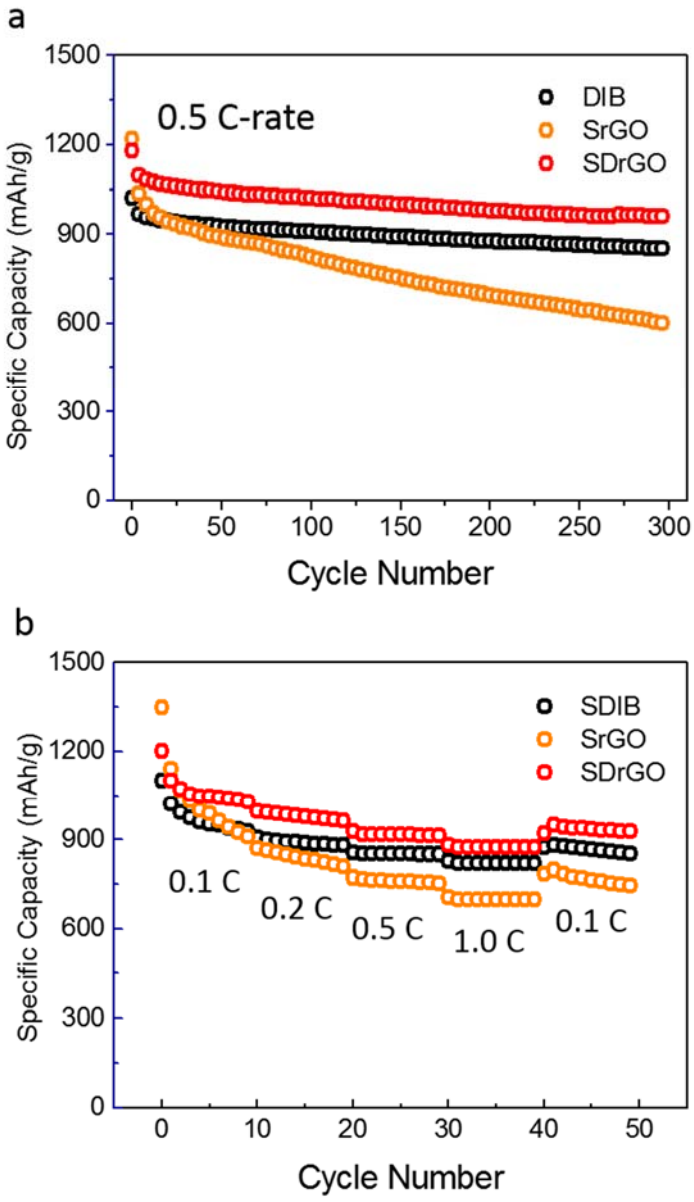

Figure 4.9 (a) Cycling performances of SDIB, SrGO, and SDrGO cathodes at 0.5 C.

(b) Rate capabilities of SDIB, SrGO, and SDrGO cathodes at varying C-rates.

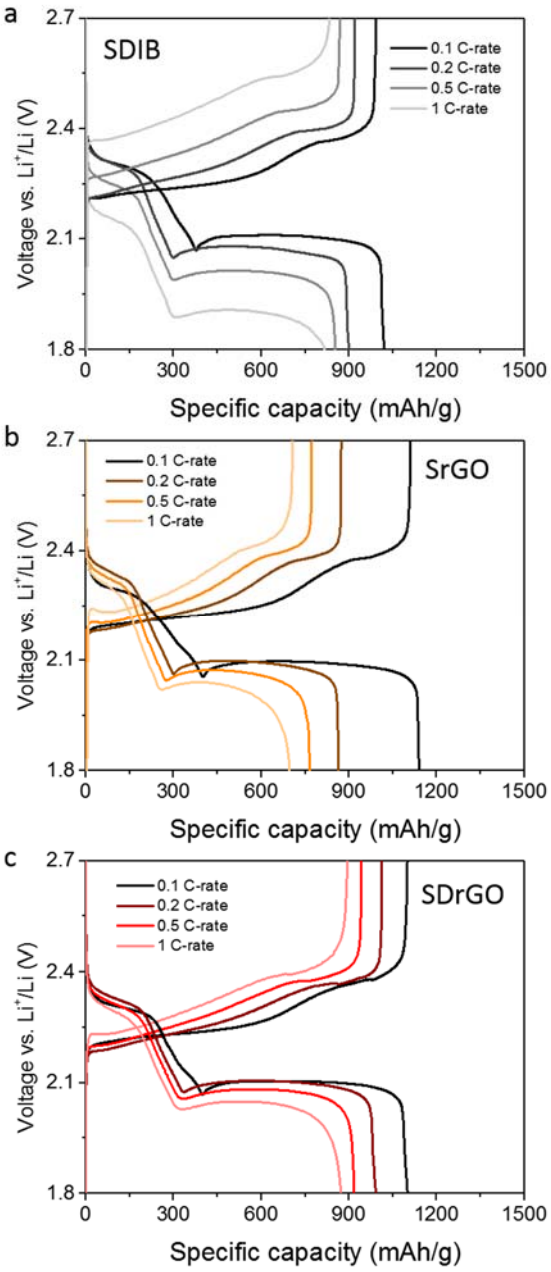

Figure 4.10 Charge/discharge voltage profiles at constant current (0.1, 0.2, 0.5, and 1 C) of (a) SDIB, (b) SrGO, (c) SDrGO cathodes.

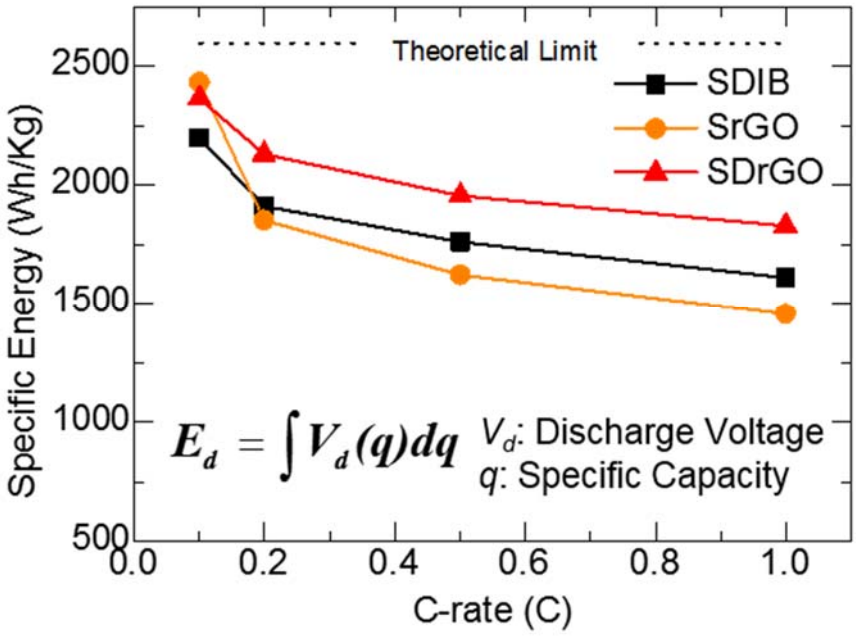

Figure 4.11 Specific energy of the cathodes as a function of C-rate, calculated from the charge/discharge voltage profiles at constant current.

4.4. Conclusions

We report on significant improvements in rate capability of polymeric sulfur cathode for the high energy Li-S batteries. The enhanced electrical contact in the cathode by nano-scale inclusion of rGO in SDIB polymers was facilitated by employing the dual reactivity of OLA, and that resulted in both faster electrochemical reaction kinetics and stable cycling performances at high C-rate.

Chapter 5. Surface Coating Layers on Sulfur Copolymers

5.1. Introduction

Lithium-sulfur (Li-S) batteries are considered as one of the most promising candidates for the next generation energy storage systems due to their high theoretical specific capacity (1,675 $mAhg^{-1}$). However, it is still considered as a daunting task to achieve the theoretical capacity from the Li-S batteries because of irreversible loss of polysulfide active materials, the low electrical conductivity of sulfur (~ 10-15 Ω·m),[42] and the mechanically induced damage to electrodes incurred from volumetric expansion of lithiated discharge products. In particular, higher order discharge products ranging between S_8 and Li_2S from the electrochemical reaction, polysulfides, are highly soluble in the electrolyte medium, thus they are continuously dissolved until Li_2S is finally precipitated on the cathode during battery operation. When the polysulfides are precipitated as Li_2S on the cathode during the redox reaction, they easily form chalks at the surface of the cathode without electrical contacts. The electrical isolation of the precipitated active species results in the serious loss of capacity by further impeding the electrochemical reaction. Moreover, the diffusion of these polysulfides through the electrolyte phase also leads to the

migration onto the Li anode side to form inactive deposits on the surface of Li metal, retarding the charging back to higher order polysulfides (i.e., polysulfide shuttle).[43]

In order to solve these critical issues, significant efforts have been placed particularly on tailoring the morphology of active sulfur species on the nanoscale. Significant improvements have been made by the use of sulfur/carbon composites,[44-50] where nano-sized sulfur was chemically or physically entrapped by carbonaceous materials. Carbonaceous encapsulation of sulfur has been reported to preserve the polysulfides within the vicinity of the cathode side as well as to enhance the electrical conductivity of the cathode. We reported on the chemical modification of elemental sulfur (S_8) into copolymeric materials to prepare improved cathode materials for Li-S batteries.[112-114, 119] These high sulfur content copolymers were prepared via a process termed, inverse vulcanization, where a small amount of organic comonomers were copolymerized with elemental sulfur and stabilized the interphases between the lithiated and de-lithiated sulfur products during Li-S battery cycling. Highly stable capacity retention during several hundred cycles was achieved with this extremely simple synthetic chemistry.

From the macroscopic viewpoint of sulfur cathodes, the polysulfides dissolved into electrolyte could remain within the bulk cathode, by adding interlayers between the cathode and a separator.[126-131] Mostly, layers of carbonaceous materials or polymer electrolytes were deposited on the separators with the additional layers facing toward the sulfur cathode to prevent or minimize the diffusion of polysulfides. When applying the blocking interlayer in the Li-S batteries, conformal contacts

between the sulfur cathode and the interlayer should be taken into account, otherwise, the dissolved polysulfides could be irreversibly lost.

Layer-by-layer (LbL) deposition using various polymers[132-136] is known as an effective technique to produce conformal coating layers on various substrates with tunable thickness in the nm scale. There are many options of functional materials for the multilayer deposition based on the adsorption of one component on top of the other using various interactions such as electrostatic attraction, hydrogen bonding, or covalent bonding. Polyethylene oxide (PEO) has frequently been utilized in combination with polyacrylic acid (PAA) to form hydrogen-bonded PEO/PAA multilayers for ion conductive membranes, exhibiting superior lithium ion diffusion characteristics compared to other electrostatic multilayers using cationic polyelectrolytes such as polyallylamine hydrochloride (PAH) or polyethylenimine (PEI).[137-139] However, LBL deposition has not been utilized to modify cathode electrodes to improve upon the properties of Li-S batteries which is the effort of the currently study.

Herein, we demonstrate a new strategy enabling the conformal coating that is directly deposited onto sulfur cathode for Li-S batteries surface by layer-by-layer (LbL) deposition (**Figure 5.1**). The utilization of surface protecting layers conformally coated on the sulfur cathodes has not been reported. In a LbL deposition, the polymer multilayers were designed to have a composition of PAH/PAA/(PEO/PAA)n (n = 1, 3, and 5), and conformally deposited on the sulfur cathodes. We note that the multilayer-coated cathodes effectively prevented the

irreversible loss of polysulfides while providing Li ionic conduction without the need for lithium nitrate ($LiNO_3$) in the electrolyte. These advances offer a facile, inexpensive methodology to improve the performance of sulfur based cathodes that can suppress polysulfide shuttling without the aid of electrolyte additives.

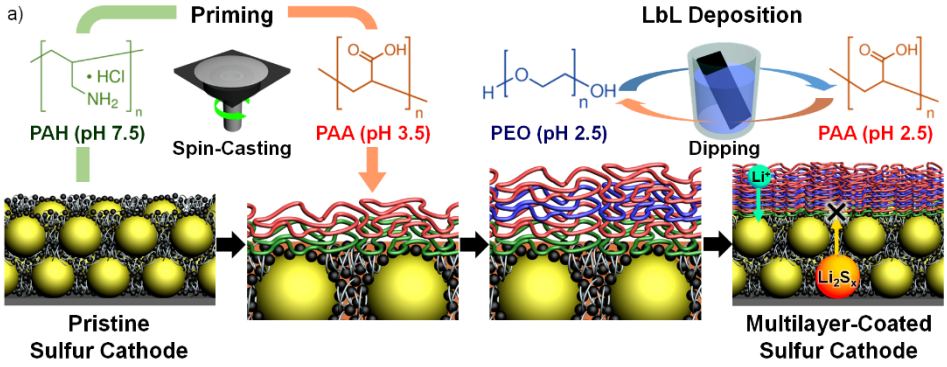

Figure 5.1 A schematic illustration of the layer-by-layer (LbL) deposition of a priming layer and (PEO/PAA) multilayers on sulfur cathodes.

5.2. Experimental section

5.2.1 Conformal coatings on sulfur cathodes

Materials: Polyallylamine hydrochloride (PAH, Mw = 15 000 g mol-1), polyacrylic acid (PAA, Mw = 50,000 g mol-1), polyethylene oxide (PEO, Mw = 300,000 g mol-1), and bis(trifluoromethane)sulfonamide lithium salt (LiTFSI) were purchased from Sigma-Aldrich.

Preparation of substrates: The sulfur powder (325 mesh) was purchased from Alfa Aesar. Super P carbon and polyvinylidene fluoride (pvdf) were provided from SK innovation. The slurry mixture was prepared by mortar mixing of sulfur (60 wt%) , super P (20 wt%), and pvdf (20 wt%), and then casted on an aluminum foil using doctor blade method, followed by drying in a vacuum oven for 12 hours. The carbon+binder substrates were prepared by the same procedure as described above for the sulfur cathode, but without sulfur powder inclusion. The sulfur substrate was fabricated by spin-casting of sulfur in carbon disulfide solution on gold substrate.

Layer-by-layer deposition: The polymer solutions for layer-by-layer deposition were prepared by dissolving polymers in 18MΩ Milli-Q wtater (1 mg mL^{-1}), and pH of each solution was adjusted using 0.1 M of HCl and NaOH. The rinsing solutions corresponding to each polymer solution with the same pH were prepared with Milli-Q water. LiTFSI (0.1 M) was added to all polymer and rinsing solutions. For the deposition of priming layers, the sulfur cathodes were initially dipped into PAH (pH = 7.5) solution for 5 min and then spun at 1500 rpm for 30 s, followed by rinsing

with the Milli-Q water of the same pH at the same rpm. The PAA (pH = 3.5) solution was spun at the same condition, and then washed with the rinsing solution with the same pH. The layer-by-layer deposition was conducted on top of the priming layers with PEO (pH = 2.5) and PAA (pH = 2.5), by dipping for 5 min in each polymer solution and 1 min in rinsing solution, respectively. The cycle was repeated for the required number of bi-layers. After deposition, the cathodes were dried overnight in vacuum oven at 50 °C.

5.2.2 Characterizations

Morphology Characterization: Water contact angles were measured using a DE/DSA100 contact angle analyzer (Fruss Inc.). Scanning electron microscopy (SEM) images were obtained with JSM-6701F (JEOL). X-ray photoelectron spectroscopy (XPS) was conducted using Axis-HSi (Kratos) with Mg/Al dual anode at 15 kV and 10 mA.

Electrochemical Characterization: All cathodes were punched into circular disks (diameter ~11mm) and assembled in a 2032 type coin cell. The electrolyte was prepared with 0.1 M lithium nitrate (LiNO3) and 1.0 M lihtium bistrifluoromethane-sulfonimide (LiTFSI) in dioxolane (DIOX) and dimethyl ether (DME) 1:1 volume ratio mixture (PanaxEtec, Korea). Electrochemical properties were measured with a WBC300 cycler (Won-A Tech, Korea). The potential window was fixed to 1.7 V-2.8 V vs. Li+/Li. The electrochemical impedance spectroscopy (EIS) was performed at open-circuit voltage between 100 kHz to 100 mHz with fluctuations of 10 mV.

5.3. Results and discussions

5.3.1 Conformal coatings on sulfur cathodes

In general, the first adhesion or priming layer was the critical step to enable the stable growth of LbL multilayers. Particularly, the direct LbL deposition of hydrophilic (PEO/PAA)n multilayers on the sulfur cathodes was challenging due to the hydrophobicity and the lack of uniformity of the cathode surfaces coated using S_8. Therefore, prior to the LbL deposition, PAH/PAA priming layers were first spin-coated using aqueous solutions of PAH (pH 7.5) and PAA (pH 3.5) with 0.1 M of LiTFSI added salt. The molecular causality of the initial priming of PAH/PAA layer on the S_8 was attributed to the weak positive/negative charges and high ionic strength of these polymer solutions which sufficiently screened the long-range electrostatic repulsions and thereby enhanced the hydrophobic attractions of adsorbed chains to the cathode surface.[144] Furthermore, the spin-assisted polyelectrolyte adsorption generated thinner and uniform surfaces compared to those formed by the dipping method, because the spinning of the substrates imposed shear forces on the adsorbing polymer chains such that they densely cover the surface.[145-147] In this process, the surface of the sulfur cathode is too rough and porous to observe the adsorbed priming layer through SEM.

After the deposition of the priming layer (PAH/PAA) on the sulfur cathode, PEO/PAA multilayers were alternatively adsorbed by the dipping method using PEO and PAA solutions, both of which were prepared by adding 1 M of LiTFSI and

adjusting the solution pH at 2.5 to induce hydrogen bonding between ether oxygens of PEO and protonated carboxylic acids of PAA.[148-149] By following the multilayer deposition procedure mentioned above, we were able to prepare robust conformal multilayered polymer coatings (optimally around 1-2 microns from 5-LBL bilayers on top of sulfur cathodes (thickness 50 microns deposited on Al foil).

In order to confirm the uniform polymer layers on heterogeneous surfaces of the sulfur cathodes, the LbL multilayer deposition was performed on each of the cathode components. The surface of a sulfur cathode is typically composed of 3 different materials, sulfur powders (60 wt%), carbon black (20 wt%), and polyvinylidene fluoride (pvdf) binders (20 wt%), which are presumably randomly distributed on the surface. The cathode components were separated into two different substrates, S_8 substrates and carbon+binder substrates, and the multilayer deposition procedure described above for the S_8 cathode coating was performed. The polymer adsorption behavior on different substrates was investigated by contact angle measurements (**Figure 5.2g**). All of the substrates tested were initially hydrophobic (104.1, 164.9, and 144.4 ° for S8, carbon+binder, and sulfur+carbon+binder substrates (i.e., S_8 cathode), respectively), but during the sequential deposition of multilayers up to PEO/PAA 5 bilayers, the contact angles of 3 different initial substrates significantly decreased to 24.7, 13.4, and 16.2 °, respectively. Even lower water contact angles of carbon+binder substrates and S8 cathode, when compared to the sulfur only substrate, could be partly explained by much more porous and rough surface morphologies of them (**Figure 5.3**). The surface and cross-sectional SEM images of a bare sulfur

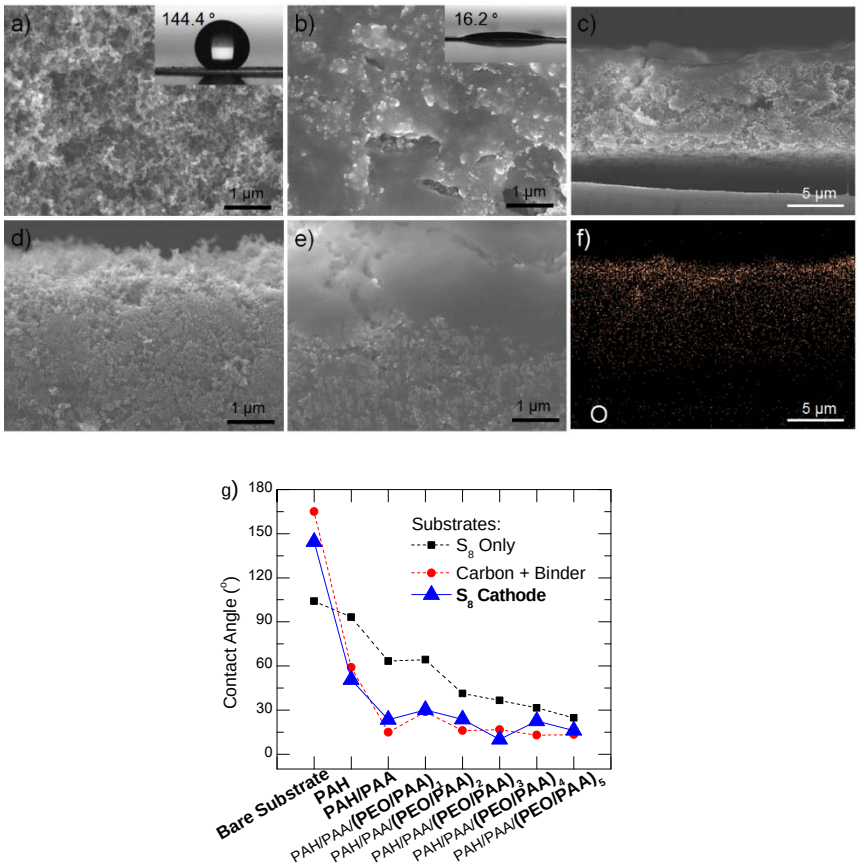

Figure 5.2 SEM images and photo images of water droplets on: a) a pristine S8 cathode, and b) a PAH/PAA/(PEO/PAA)5 multilayer-coated cathode. A cross-sectional SEM image of: d) a pristine S8 cathode, and e) a PAH/PAA/(PEO/PAA)5 multilayer-coated cathode. c) A cross-sectional SEM image of a PAH/PAA/(PEO/PAA)5 multilayer-coated cathode for EDS analysis. f) An Oxygen (orange) elemental map by EDS of the PAH/PAA/(PEO/PAA)5 multilayer-coated cathode. g) The changes in contact angle as a function of adsorbed polymer layers on the substrates of S8-only, carbon + binder, and S8 + carbon + binder (i.e., S8 cathode).

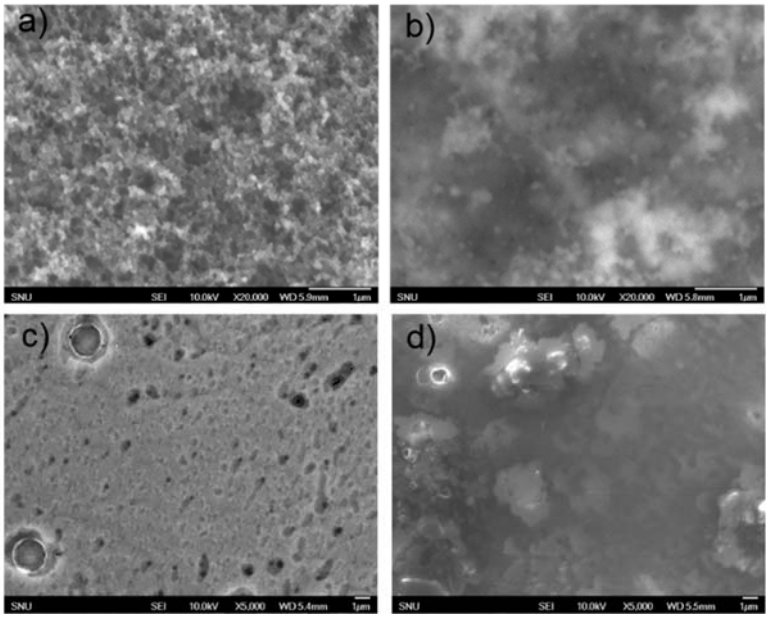

Figure 5.3 SEM images of a) an as-prepared carbon+binder substrate, b) a 5 bilayer-coated carbon+binder substrate, c) a bare sulfur substrate, d) a 5 bilayer-coated sulfur substrate.

cathode confirms the porous and rough surface morphologies, in which carbon black particles with approximately 50 nm in diameter mostly cover the electrode surface (**Figure 5.2b** and **e**). After the PEO/PAA 5 bilayer deposition, the surface is conformally passivated by the polymer multilayers of 2 μm in thickness as observed in the SEM image, leading us to believe that the polymers deeply penetrated inside the cathode through the pores (**Figure 5.2c** and **f**). The LbL coatings of PEO/PAA deposited in the absence of PAH/PAA priming layers, however, did not show such drastic morphological changes, nor uniform increased film thickness (**Figure 5.4 and 5.5**). The successful conformal coating on the S8 cathodes with PAH/PAA/(PEO/PAA)n multilayers were also confirmed using SEM-EDS and XPS (**Figure 5.6 and 5.7**).

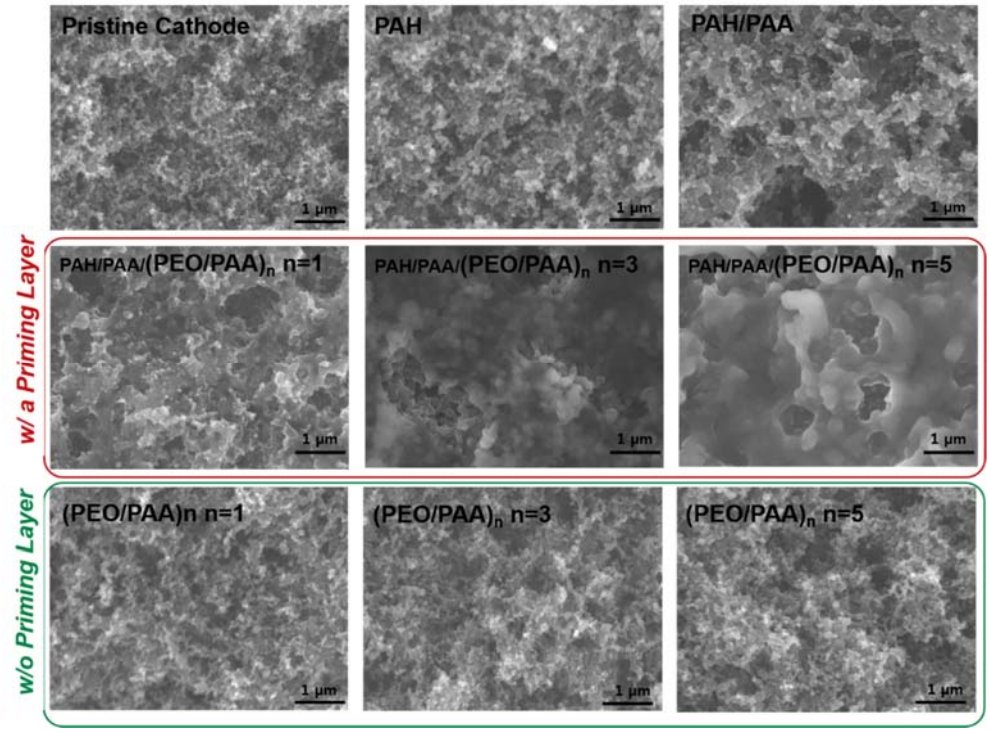

Figure 5.4 SEM images of sulfur cathodes showing the morphological changes during the deposition of (PEO/PAA)n, n=1, 3, and 5, with and without priming layer of (PAH/PAA).

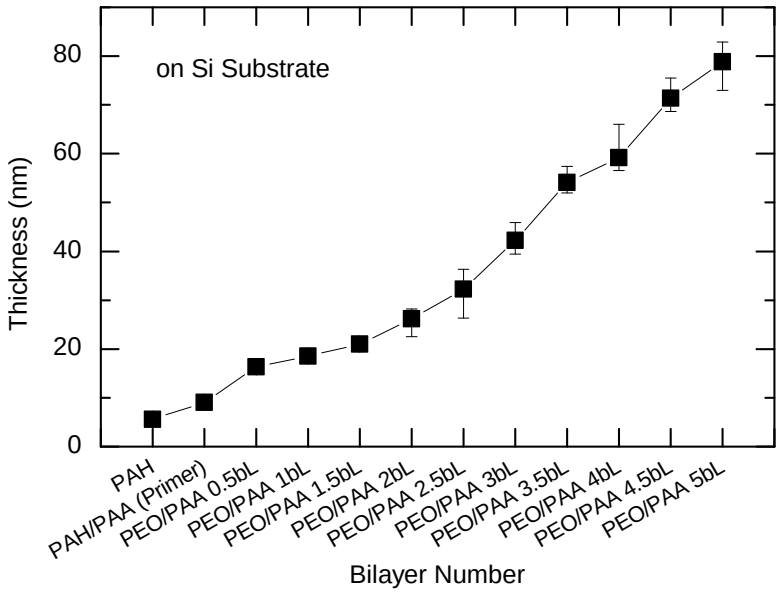

Figure 5.5 Multilayer thickness growth as a function of bilayer numbers during the LbL deposition of PAH/PAA/(PEO/PAA)n multilayers on Si wafer substrates.

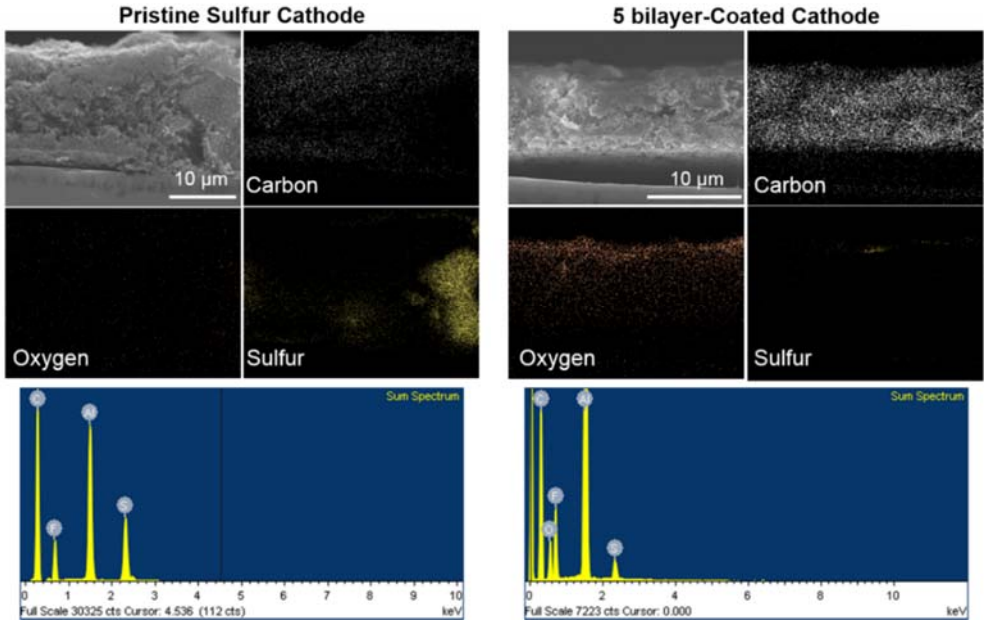

Figure 5.6 Elemental maps and EDS spectrafor a pristine sulfur cathode and a (PEO/PAA) 5 bilayer-coated sulfur cathode.

Element [wt%]	Bare Cathode	PEO/PAA 5 bi-layer Cathode
C	72.41	53.07
O	-	10.72
F	15.07	18.67
Al	7.95	16.54
S	4.24	1.00
Totals	99.67	100.00

Table 5.1 Weight fraction of elements estimated from EDS spectra on a pristine sulfur cathode and a (PEO/PAA) 5 bilayer-coated sulfur cathode.

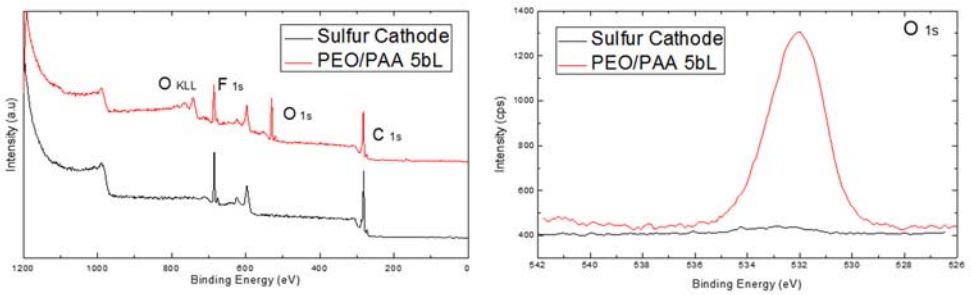

Figure 5.7 XPS spectra of a pristine sulfur cathode and a (PEO/PAA) 5 bilayer-coated sulfur cathode.

5.3.2 Elctrochemical Characterizations

The electrochemical stability of the multilayer-coated cathodes was investigated integration into 2032 coin cell Li-S batteries and galvanostatic cycling studies of these devices at 0.5 C rate (1 C = 1675 mAg^{-1}). The electrolyte system used in these studies were 1M LiTFSI in dioxolane/glyme with 0.33 M LiNO3. The charge/discharge voltage profiles of the sulfur cathodes with different numbers of polymer bilayers are shown in **Figure 5.8a-d**. The region of the upper plateau at ~2.4 V in the discharge profile is believed to originate from the dissolution reaction, where solid sulfur is reduced to soluble polysulfides (S_8 to S_n^{2-}, n=8-4) upon lithiation (**Figure 5.9**).[150] In this region, the decrease in the specific capacity during initial 10 cycles is denoted as "ΔQ", which mainly results from the irreversible loss of active sulfur due to the formation of soluble polysulfides, thus ΔQ is directly related to the surface protecting or passivation characteristics of the sulfur cathodes. The ΔQ value of the bare cathode without surface passivation is the largest (164 mAhg-1) and this ΔQ value decreases to 106, 92, and 81 $mAhg^{-1}$ with 1, 3, and 5 bilayers of surface coating on the sulfur cathodes. Such decrease in the ΔQ value as a function of bilayer number indicates the effective suppression of polysulfide dissolution into electrolytes by the (PEO/PAA)n multilayer coatings. Meanwhile, a slight increase in the charge-discharge overpotential was found with 5 bilayers coated on the cathode in **Figure 5.8d**. The slight increase in the overpotential is believed to be due to the reduction in lithium ion conductivity through the thicker

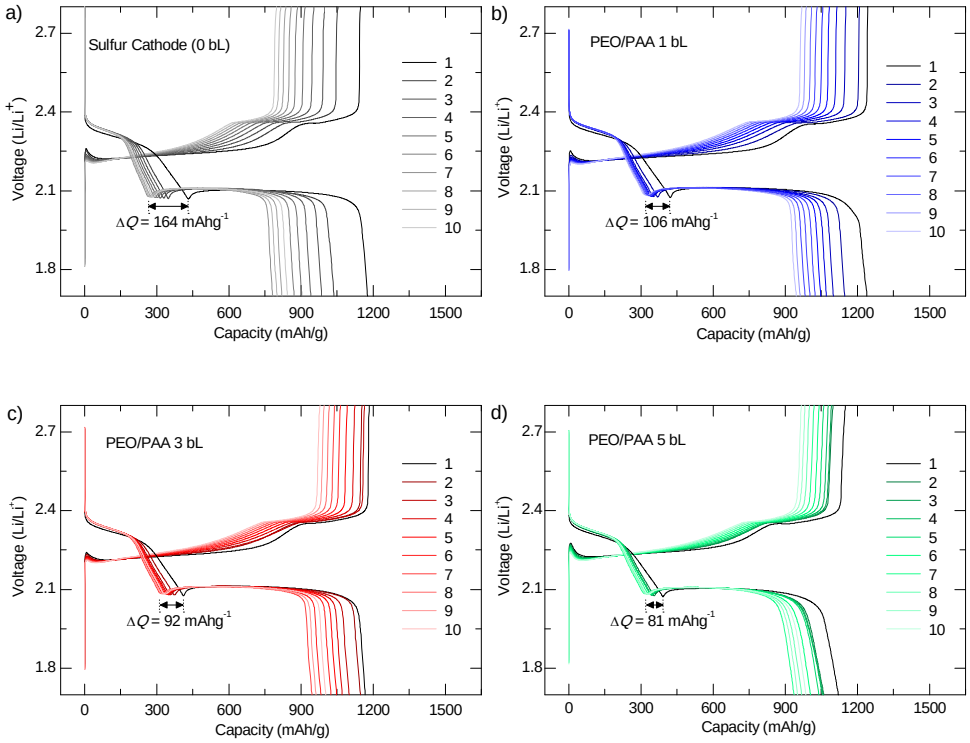

Figure 5.8 a) The charge/discharge voltage profiles of a pristine sulfur cathode and b)-d)1, 3, and 5 bilayer-coated sulfur cathodes.

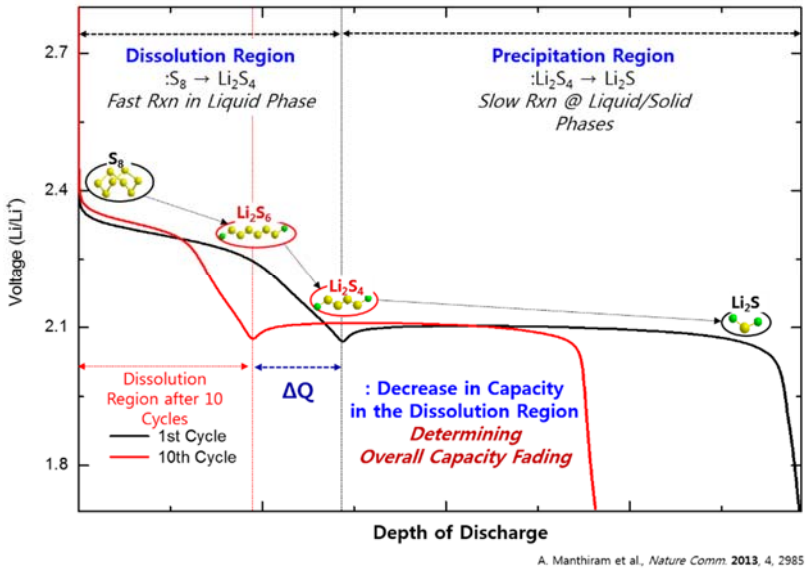

Figure 5.9 A schematic description of the specific capacity decrease in dissolution region, indicated with the discharge voltage profiles.

multilayers deposited on the cathode. In this regard, it is noted that there is a trade-off point between ΔQ and the overpotential, suggesting that there is an optimum number of bilayers for the effective surface passivation.

The discharge capacities of sulfur cathodes with different number of (PEO/PAA)n bilayers are presented in **Figure 5.10a**. As hinted from the decrease in ΔQ, the (PEO/PAA)n multilayer passivated cathodes retain much higher specific capacity up to 100 cycles, while the pristine sulfur cathode shows the rapid capacity fading even after first 10 cycles. As mentioned above, there is an optimum (PEO/PAA) bilayer deposited on the sulfur cathode to reveal the best electrochemical performance. In our system, 3 (PEO/PAA) bilayers coated on the cathode exhibit the best capacity retention (806 $mAhg^{-1}$) even after 100 cycles (i.e., 70.27 % capacity retention with respect to the initial capacity), while 42.46 %, 48.24 %, and 64.37 % capacity retentions were obtained for pristine cathode, 1-bilayer, and 5-bilayer coated cathodes, respectively. On the other hands, the cycling performance of (PAH/PAA)n multilayer-coated cathodes is worse than (PEO/PAA)n multilayer-coated cathodes, presumably due to the slow Li+ diffusion through the electrostatic multilayers of (PAH/PAA)n,[137-139] compared to that through the hydrogen bonded multilayers of (PEO/PAA)n. The structural and surficial stabilities of the (PEO/PAA)n multilayer-coated cathodes during the cycles were also confirmed using EIS and SEM (**Figure 5.11** and **5.12**, respectively).

The influence of C-rate (0.1 to 2.0 C, 10 cycles for each) on the capacity retention behavior of the multilayer-coated cathodes was investigated in **Figure 10b**. The

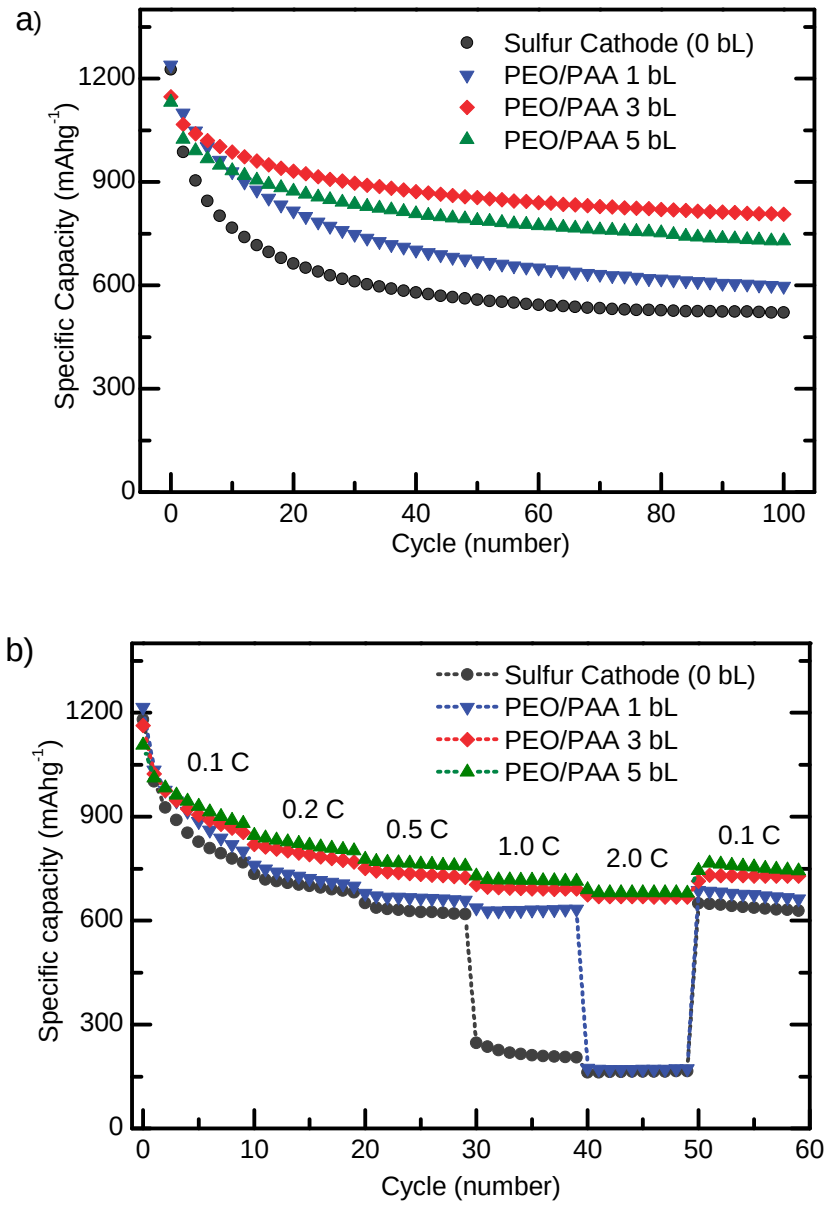

Figure 5.10 a) Cyclic performance of a pristine sulfur cathode and 1, 3, and 5 bilayer-coated sulfur cathodes. b) The C-rate capability of a pristine sulfur cathode and (PEO/PAA) 1, 3, and 5 bilayer-coated sulfur cathodes.

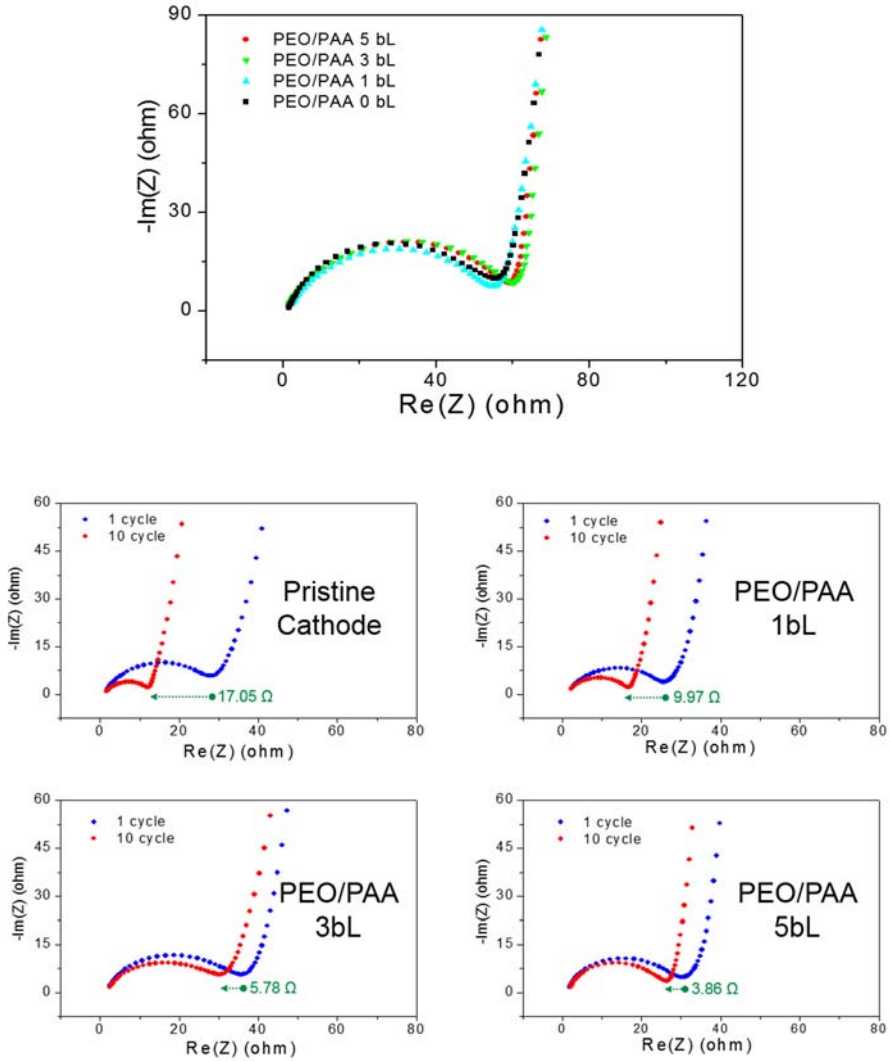

Figure 5.11 Electrochemical impedance spectroscopic (EIS) data on a pristine sulfur cathode and 1, 3, and 5 bilayer-coated sulfur cathode measured before cycling, and EIS data on a pristine sulfur cathode and 1, 3, and 5 bilayer-coated sulfur cathode measured after an initial one cycle and 10 cycles.

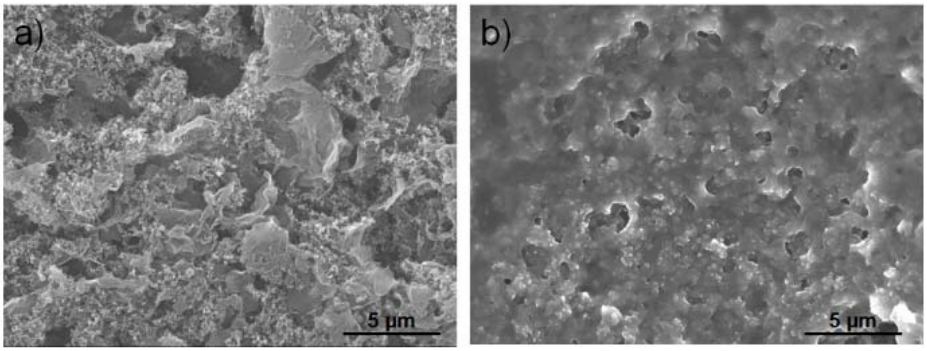

Figure 5.12 SEM images of: a) a pristine sulfur cathode and b) a 5 bilayer-coated cathode after 10 cycles.

abrupt decreases in the capacities were observed over 1.0 C with the pristine S8 cathode, and at 2.0 C with one bilayer-coated cathode. The polysulfide diffusion with insufficient protection on the surfaces of these cathodes results in the gradual decomposition of electrical contacts between the carbon framework and sulfur products during repeated cycles, and that leads to the limited utilization of active sulfur, particularly, at high C-rate. On the other hand, three and five bilayer-coated cathodes retained high capacity retention, even at 2 C, which was clear evidence of the effective protection from the polysulfide diffusion by the sufficient multilayer coatings on S8 cathodes.

The cycling performance of the different cathodes was also tested without the addition of $LiNO_3$ in the electrolytes (**Figure 5.13**), which is known to be the common additive to suppress the shuttle effect of polysulfides, although all the other electrochemical characterizations in this work were conducted with $LiNO_3$ salts. The Li-S batteries without $LiNO_3$ salts are prone to the chemical reaction between polysulfides and Li anode,[43] thus the cycling in the absence of $LiNO_3$ salts gives us insight on the effect of the passivation multilayers on the loss of polysulfides during repeated cycles. Furthermore, recent reports have cited concerns on the long term cycling issues using $LiNO_3$ additives, further prompting removal of these salts and evaluating device performance with LBL cathode coatings The "bare" S_8 cathode without passivation bilayers shows a drastic decrease in the specific capacity (141.32 mAhg-1) as well as poor coulombic efficiency (28.17 % at 84th cycle) and the battery function is stopped after 84 cycles due to the polysulfide shuttle effect.

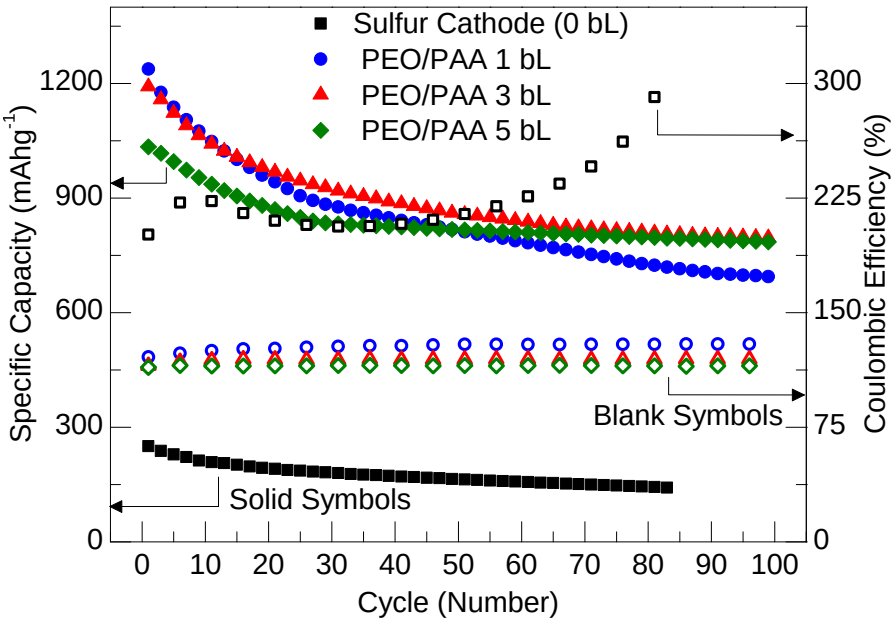

Figure 5.13 Cyclic performance and coulombic efficiency at 0.5 C of a pristine sulfur cathode and 1, 3, and 5 bilayer-coated sulfur cathodes without $LiNO_3$ salts in the electrolytes. (coulombic efficiency = charge capacity/discharge capacity)

However, we observe the suppression of polysulfide by the LBL coating of PEO/PAA bilayers as evidenced by significant retention of charge capacity out to 100 cycles (618.5 $mAhg^{-1}$, 744.9 $mAhg^{-1}$, and 715.3 $mAhg^{-1}$ at the 100th cycle for 1, 3, and 5 (PEO/PAA) bilayers, respectively). Moreover, high coulombic efficiency of the multilayer-coated cathodes (77.1 %, 83.83 %, and 86.70 % after 100 cycles for 1, 3, and 5 bilayers, respectively) is directly attributed to the effective passivation of the polysulfide shuttling.

The suppression of polysulfide dissolution was also confirmed in the experiment with excess electrolytes of beaker cells, assembled with a pristine S8 cathode or a multilayer-coated cathode (**Figure 5.14**), where the extent of polysulfide dissolution was found to be significantly lowered with the multilayer-coating, as noted by optical absorbance spectroscopy (with absorptions at 430 nm (Sx2- (x = 4-8)) and 620 nm (S3·-)).

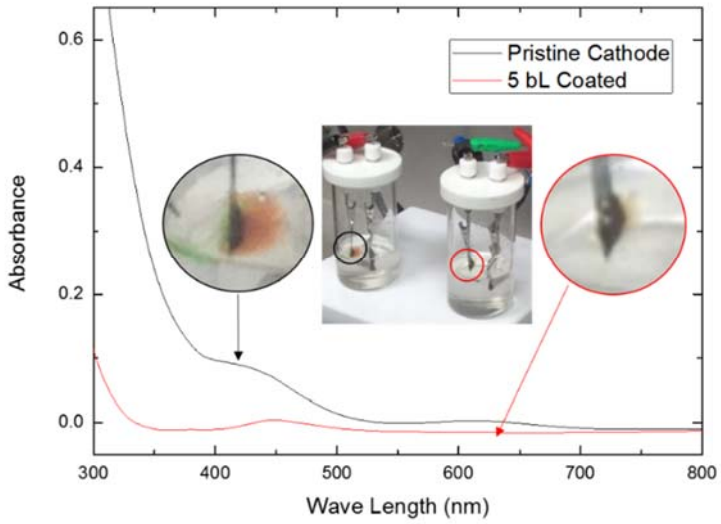

Figure 5.14 UV-Vis Spectra and Photo images of the electrolyte solutions, at 5 mins after applying a constant voltage at 1.5 V to the beaker cells, assembled with pristine sulfur cathode, and 5-bilayer-coated cathode.

5.4. Conclusions

In conclusion, (PEO/PAA) multilayers deposited on sulfur cathodes by the LbL method effectively improve the capacity retention of lithium-sulfur batteries, by successful blocking of intermediate polysulfides dissolving into electrolyte solution.

We think that these simple and inexpensive cathode passivation methods are quite practical and scalable for the large scale production of sulfur copolymer cathodes in industry, and expected to be widely utilized in different types of electrochemical devices.

Bibliography

(1) Mandeville, C. W. Sulfur: A Ubiquitous and Useful Tracer in Earth and Planetary Sciences. *Elements* **2010,** *6*, 75-80.

(2) Hedenquist, J. W.; Lowenstern, J. B. The Role of Magmas in the Formation of Hydrothermal Ore-Deposits. *Nature* **1994,** *370*, 519-527.

(3) Manning, C. E. Sulfur Surprises in Deep Geological Fluids. *Science* **2011,** *331*, 1018-1019.

(4) Metrich, N.; Mandeville, C. W. Sulfur in Magmas. *Elements* **2010,** *6*, 81-86.

(5) Schauder, R.; Muller, E. Polysulfide as a Possible Substrate for Sulfur-Reducing Bacteria. *Arch. Microbiol.* **1993,** *160*, 377-382.

(6) Bamford, V. A.; Bruno, S.; Rasmussen, T.; Appia-Ayme, C.; Cheesman, M. R.; Berks, B. C.; Hemmings, A. M. Structural basis for the oxidation of thiosulfate by a sulfur cycle enzyme. *EMBO J.* **2002,** *21*, 5599-5610.

(7) United States. Bureau of Mines.; Geological Survey (U.S.). *Mineral commodity summaries*; 0160-5151; U.S. Dept. of the Interior, Bureau of Mines: Washington, D.C., 2009; p 160.

(8) Liu, J. G.; Ueda, M. High refractive index polymers: fundamental research and practical applications. *J. Mater. Chem.* **2009,** *19*, 8907-8919.

(9) Bureau, B.; Zhang, X. H.; Smektala, F.; Adam, J. L.; Troles, J.; Ma, H. L.; Boussard-Pledel, C.; Lucas, J.; Lucas, P.; Le Coq, D.; Riley, M. R.; Simmons, J. H. Recent advances in chalcogenide glasses. *J. Non-Cryst. Solids* **2004,** *345*, 276-283.

(10) Lucas, J. Infrared glasses. *Current Opinion in Solid State & Materials Science* **1999,** *4*,

181-187.

(11) Aggarwal, I. D.; Sanghera, J. S. Development and applications of chalcogenide glass optical fibers at NRL. *Journal of Optoelectronics and Advanced Materials* **2002,** *4*, 665-678.

(12) Guillevic, E.; Zhang, X. H.; Pain, T.; Calvez, L.; Adam, J. L.; Lucas, J.; Guilloux-Viry, M.; Ollivier, S.; Gadret, G. Optimization of chalcogenide glass in the As-Se-S system for automotive applications. *Opt. Mater.* **2009,** *31*, 1688-1692.

(13) You, N. H.; Higashihara, T.; Ando, S.; Ueda, M. Highly Refractive Polymer Resin Derived from Sulfur-Containing Aromatic Acrylate. *Journal of Polymer Science Part a-Polymer Chemistry* **2010,** *48*, 2604-2609.

(14) Dislich, H. Plastics as Optical-Materials. *Angewandte Chemie-International Edition in English* **1979,** *18*, 49-59.

(15) Lu, C. L.; Yang, B. High refractive index organic-inorganic nanocomposites: design, synthesis and application. *J. Mater. Chem.* **2009,** *19*, 2884-2901.

(16) Lee, S.; Shin, H. J.; Yoon, S. M.; Yi, D. K.; Choi, J. Y.; Paik, U. Refractive index engineering of transparent ZrO2-polydimethylsiloxane nanocomposites. *J. Mater. Chem.* **2008,** *18*, 1751-1755.

(17) Tao, P.; Li, Y.; Rungta, A.; Viswanath, A.; Gao, J. N.; Benicewicz, B. C.; Siegel, R. W.; Schadler, L. S. TiO2 nanocomposites with high refractive index and transparency. *J. Mater. Chem.* **2011,** *21*, 18623-18629.

(18) Nakayama, N.; Hayashi, T. Preparation and characterization of TiO2 and polymer nanocomposite films with high refractive index. *J. Appl. Polym. Sci.* **2007,** *105*, 3662-3672.

(19) Lu, C. L.; Cui, Z. C.; Wang, Y.; Li, Z.; Guan, C.; Yang, B.; Shen, J. C. Preparation and characterization of ZnS-polymer nanocomposite films with high refractive index. *J. Mater. Chem.* **2003,** *13*, 2189-2195.

(20) Lu, C. L.; Guan, C.; Liu, Y. F.; Cheng, Y. R.; Yang, B. PbS/polymer nanocomposite optical materials with high refractive index. *Chem. Mater.* **2005,** *17*, 2448-2454.

(21) Weibel, M.; Caseri, W.; Suter, U. W.; Kiess, H.; Wehrli, E. Preparation of Polymer Nanocomposites with "Ultrahigh" Refractive Index. *Polym. Adv. Technol.* **1991,** *2*, 75-80.

(22) Althues, H.; Palkovits, R.; Rumplecker, A.; Simon, P.; Sigle, W.; Bredol, M.; Kynast, U.; Kaskel, S. Synthesis and characterization of transparent luminescent ZnS : Mn/PMMA nanocomposites. *Chem. Mater.* **2006,** *18*, 1068-1072.

(23) Lee, S.; Lee, B.; Kim, B. J.; Park, J.; Yoo, M.; Bae, W. K.; Char, K.; Hawker, C. J.; Bang, J.; Cho, J. Free-Standing Nanocomposite Multilayers with Various Length Scales, Adjustable Internal Structures, and Functionalities. *J. Am. Chem. Soc.* **2009,** *131*, 2579-2587.

(24) Tamborra, M.; Striccoli, M.; Comparelli, R.; Curri, M. L.; Petrella, A.; Agostiano, A. Optical properties of hybrid composites based on highly luminescent CdS nanocrystals in polymer. *Nanotechnology* **2004,** *15*, S240-S244.

(25) Beal, J. H. L.; Etchegoin, P. G.; Tilley, R. D. Transition Metal Polysulfide Complexes as Single-Source Precursors for Metal Sulfide Nanocrystals. *J. Phys. Chem. C* **2010,** *114*, 3817-3821.

(26) Bu, W. B.; Chen, Z. X.; Chen, F.; Shi, J. L. Oleic Acid/Oleylamine Cooperative-Controlled Crystallization Mechanism for Monodisperse Tetragonal Bipyramid NaLa(MoO4)(2) Nanocrystals. *J. Phys. Chem. C* **2009,** *113*, 12176-12185.

(27) Cademartiri, L.; Montanari, E.; Calestani, G.; Migliori, A.; Guagliardi, A.; Ozin, G. A. Size-dependent extinction coefficients of PbS quantum dots. *J. Am. Chem. Soc.* **2006,** *128*, 10337-10346.

(28) Joo, J.; Na, H. B.; Yu, T.; Yu, J. H.; Kim, Y. W.; Wu, F. X.; Zhang, J. Z.; Hyeon, T. Generalized and facile synthesis of semiconducting metal sulfide nanocrystals. *J. Am. Chem.*

Soc. **2003,** *125*, 11100-11105.

(29) Moreels, I.; Justo, Y.; De Geyter, B.; Haustraete, K.; Martins, J. C.; Hens, Z. Size-Tunable, Bright, and Stable PbS Quantum Dots: A Surface Chemistry Study. *ACS Nano* **2011,** *5*, 2004-2012.

(30) Si, H. Y.; Yuan, D.; Chen, J. S.; Chow, G. M. Synthesis of PbS nanocrystals from sulfur-amine solutions at room temperature. *Rsc Advances* **2011,** *1*, 817-822.

(31) Bakueva, L.; Musikhin, S.; Hines, M. A.; Chang, T. W. F.; Tzolov, M.; Scholes, G. D.; Sargent, E. H. Size-tunable infrared (1000-1600 nm) electroluminescence from PbS quantum-dot nanocrystals in a semiconducting polymer. *Appl. Phys. Lett.* **2003,** *82*, 2895-2897.

(32) Konstantatos, G.; Howard, I.; Fischer, A.; Hoogland, S.; Clifford, J.; Klem, E.; Levina, L.; Sargent, E. H. Ultrasensitive solution-cast quantum dot photodetectors. *Nature* **2006,** *442*, 180-183.

(33) McDonald, S. A.; Konstantatos, G.; Zhang, S. G.; Cyr, P. W.; Klem, E. J. D.; Levina, L.; Sargent, E. H. Solution-processed PbS quantum dot infrared photodetectors and photovoltaics. *Nat. Mater.* **2005,** *4*, 138-U14.

(34) Liu, G.; Niu, P.; Yin, L. C.; Cheng, H. M. alpha-Sulfur Crystals as a Visible-Light-Active Photocatalyst. *J. Am. Chem. Soc.* **2012,** *134*, 9070-9073.

(35) Zhuo, S. F.; Huang, Y.; Liu, C. B.; Wang, H.; Zhang, B. Sulfur copolymer nanowires with enhanced visible-light photoresponse. *Chem. Commun.* **2014,** *50*, 11208-11210.

(36) Yamin, H.; Gorenshtein, A.; Penciner, J.; Sternberg, Y.; Peled, E. Lithium Sulfur Battery - Oxidation Reduction-Mechanisms of Polysulfides in Thf Solutions. *J. Electrochem. Soc.* **1988,** *135*, 1045-1048.

(37) Levillain, E.; Gaillard, F.; Leghie, P.; Demortier, A.; Lelieur, J. P. On the understanding

of the reduction of sulfur (S-8) in dimethylformamide (DMF). *J. Electroanal. Chem.* **1997,** *420*, 167-177.

(38) Levillain, E.; Demortier, A.; Lelieur, J. P. Reduction of S-3(-) and S-6(2-) Polysulfide Ions in Liquid-Ammonia. *J. Electroanal. Chem.* **1995,** *394*, 205-210.

(39) Leghie, P.; Lelieur, J. P.; Levillain, E. Comments on the mechanism of the electrochemical reduction of sulphur in dimethylformamide. *Electrochem. Commun.* **2002,** *4*, 406-411.

(40) Qian, L.; Tian, X. Q.; Yang, L.; Mao, J. F.; Yuan, H. Y.; Xiao, D. High specific capacitance of CuS nanotubes in redox active polysulfide electrolyte. *Rsc Advances* **2013,** *3*, 1703-1708.

(41) Licht, S.; Hodes, G.; Manassen, J. Numerical-Analysis of Aqueous Polysulfide Solutions and Its Application to Cadmium Chalcogenide Polysulfide Photoelectrochemical Solar-Cells. *Inorg. Chem.* **1986,** *25*, 2486-2489.

(42) Dirlam, P. T.; Simmonds, A. G.; Shallcross, R. C.; Arrington, K. J.; Chung, W. J.; Griebel, J. J.; Hill, L. J.; Glass, R. S.; Char, K.; Pyun, J. Improving the Charge Conductance of Elemental Sulfur via Tandem Inverse Vulcanization and Electropolymerization. *Acs Macro Letters* **2015,** *4*, 111-114.

(43) Mikhaylik, Y. V.; Akridge, J. R. Polysulfide shuttle study in the Li/S battery system. *J. Electrochem. Soc.* **2004,** *151*, A1969-A1976.

(44) Chen, H. W.; Dong, W. L.; Ge, J.; Wang, C. H.; Wu, X. D.; Lu, W.; Chen, L. W. Ultrafine Sulfur Nanoparticles in Conducting Polymer Shell as Cathode Materials for High Performance Lithium/Sulfur Batteries. *Scientific Reports* **2013,** *3*.

(45) Fu, Y. Z.; Manthiram, A. Orthorhombic Bipyramidal Sulfur Coated with Polypyrrole Nanolayers As a Cathode Material for Lithium-Sulfur Batteries. *J. Phys. Chem. C* **2012,** *116*,

8910-8915.

(46) Jayaprakash, N.; Shen, J.; Moganty, S. S.; Corona, A.; Archer, L. A. Porous Hollow Carbon@Sulfur Composites for High-Power Lithium-Sulfur Batteries. *Angewandte Chemie-International Edition* **2011,** *50*, 5904-5908.

(47) Lee, K. T.; Black, R.; Yim, T.; Ji, X. L.; Nazar, L. F. Surface-Initiated Growth of Thin Oxide Coatings for Li-Sulfur Battery Cathodes. *Advanced Energy Materials* **2012,** *2*, 1490-1496.

(48) Li, W. Y.; Zhang, Q. F.; Zheng, G. Y.; Seh, Z. W.; Yao, H. B.; Cui, Y. Understanding the Role of Different Conductive Polymers in Improving the Nanostructured Sulfur Cathode Performance. *Nano Lett.* **2013,** *13*, 5534-5540.

(49) Moon, S.; Jung, Y. H.; Jung, W. K.; Jung, D. S.; Choi, J. W.; Kim, D. K. Encapsulated Monoclinic Sulfur for Stable Cycling of Li-S Rechargeable Batteries. *Adv. Mater.* **2013,** *25*, 6547-6553.

(50) Xiao, L. F.; Cao, Y. L.; Xiao, J.; Schwenzer, B.; Engelhard, M. H.; Saraf, L. V.; Nie, Z. M.; Exarhos, G. J.; Liu, J. A Soft Approach to Encapsulate Sulfur: Polyaniline Nanotubes for Lithium-Sulfur Batteries with Long Cycle Life. *Adv. Mater.* **2012,** *24*, 1176-1181.

(51) Evers, S.; Nazar, L. F. Graphene-enveloped sulfur in a one pot reaction: a cathode with good coulombic efficiency and high practical sulfur content. *Chem Commun (Camb)* **2012,** *48*, 1233-5.

(52) Ji, L.; Rao, M.; Zheng, H.; Zhang, L.; Li, Y.; Duan, W.; Guo, J.; Cairns, E. J.; Zhang, Y. Graphene oxide as a sulfur immobilizer in high performance lithium/sulfur cells. *J. Am. Chem. Soc.* **2011,** *133*, 18522-5.

(53) Lin, T. Q.; Tang, Y. F.; Wang, Y. M.; Bi, H.; Liu, Z. Q.; Huang, F. Q.; Xie, X. M.; Jiang, M. H. Scotch-tape-like exfoliation of graphite assisted with elemental sulfur and graphene-

sulfur composites for high-performance lithium-sulfur batteries. *Energy & Environmental Science* **2013,** *6*, 1283-1290.

(54) Wang, H. L.; Yang, Y.; Liang, Y. Y.; Robinson, J. T.; Li, Y. G.; Jackson, A.; Cui, Y.; Dai, H. J. Graphene-Wrapped Sulfur Particles as a Rechargeable Lithium-Sulfur Battery Cathode Material with High Capacity and Cycling Stability. *Nano Lett.* **2011,** *11*, 2644-2647.

(55) Wang, Y. X.; Huang, L.; Sun, L. C.; Xie, S. Y.; Xu, G. L.; Chen, S. R.; Xu, Y. F.; Li, J. T.; Chou, S. L.; Dou, S. X.; Sun, S. G. Facile synthesis of a interleaved expanded graphite-embedded sulphur nanocomposite as cathode of Li-S batteries with excellent lithium storage performance. *J. Mater. Chem.* **2012,** *22*, 4744-4750.

(56) Zu, C. X.; Manthiram, A. Hydroxylated Graphene-Sulfur Nanocomposites for High-Rate Lithium-Sulfur Batteries. *Advanced Energy Materials* **2013,** *3*, 1008-1012.

(57) Chen, H.; Wang, C.; Dong, W.; Lu, W.; Du, Z.; Chen, L. Monodispersed sulfur nanoparticles for lithium-sulfur batteries with theoretical performance. *Nano Lett.* **2015,** *15*, 798-802.

(58) Wang, Z. Y.; Dong, Y. F.; Li, H. J.; Zhao, Z. B.; Wu, H. B.; Hao, C.; Liu, S. H.; Qiu, J. S.; Lou, X. W. Enhancing lithium-sulphur battery performance by strongly binding the discharge products on amino-functionalized reduced graphene oxide. *Nature Communications* **2014,** *5*.

(59) Wu, H. W.; Huang, Y.; Zong, M.; Fu, H. T.; Sun, X. Self-assembled graphene/sulfur composite as high current discharge cathode for lithium-sulfur batteries. *Electrochim. Acta* **2015,** *163*, 24-31.

(60) Zheng, S. Y.; Wen, Y.; Zhu, Y. J.; Han, Z.; Wang, J.; Yang, J. H.; Wang, C. S. In Situ Sulfur Reduction and Intercalation of Graphite Oxides for Li-S Battery Cathodes. *Advanced Energy Materials* **2014,** *4*.

(61) Schneider, T.; Baldauf, A.; Ba, L. A.; Jamier, V.; Khairan, K.; Sarakbi, M. B.; Reum, N.; Schneider, M.; Roseler, A.; Becker, K.; Burkholz, T.; Winyard, P. G.; Kelkel, M.; Diederich, M.; Jacob, C. Selective Antimicrobial Activity Associated with Sulfur Nanoparticles. *J. Biomed. Nanotechnol.* **2011,** *7*, 395-405.

(62) Choudhury, S. R.; Mandal, A.; Chakravorty, D.; Gopal, M.; Goswami, A. Evaluation of physicochemical properties, and antimicrobial efficacy of monoclinic sulfur-nanocolloid. *J. Nanopart. Res.* **2013,** *15*.

(63) Bahrin, L. G.; Apostu, M. O.; Birsa, L. M.; Stefan, M. The antibacterial properties of sulfur containing flavonoids. *Bioorg. Med. Chem. Lett.* **2014,** *24*, 2315-2318.

(64) Weld, J. T.; Gunther, A. The Antibacterial Properties of Sulfur. *J. Exp. Med.* **1947,** *85*, 531-542.

(65) Libenson, L.; Hadley, F. P.; Mcilroy, A. P.; Wetzel, V. M.; Mellon, R. R. Antibacterial Effect of Elemental Sulfur. *J. Infect. Dis.* **1953,** *93*, 28-35.

(66) Shafaei-Fallah, M.; He, J. Q.; Rothenberger, A.; Kanatzidis, M. G. Ion-Exchangeable Cobalt Polysulfide Chalcogel. *J. Am. Chem. Soc.* **2011,** *133*, 1200-1202.

(67) Ma, S. L.; Shim, Y.; Islam, S. M.; Subrahmanyam, K. S.; Wang, P. L.; Li, H.; Wang, S. C.; Yang, X. J.; Kanatzidis, M. G. Efficient Hg Vapor Capture with Polysulfide Intercalated Layered Double Hydroxides. *Chem. Mater.* **2014,** *26*, 5004-5011.

(68) Oh, Y.; Morris, C. D.; Kanatzidis, M. G. Polysulfide Chalcogels with Ion-Exchange Properties and Highly Efficient Mercury Vapor Sorption. *J. Am. Chem. Soc.* **2012,** *134*, 14604-14608.

(69) Greer, S. C. The Dielectric-Constant of Liquid Sulfur. *J. Chem. Phys.* **1986,** *84*, 6984-6988.

(70) Kreuzer, H. J. Physics and chemistry in high electric fields. *Surf. Interface Anal.* **2004,**

36, 372-379.

(71) Germain, J.; Rolandi, M.; Backer, S. A.; Frechet, J. M. J. Sulfur as a Novel Nanopatterning Material: An Ultrathin Resist and a Chemically Addressable Template for Nanocrystal Self-Assembly. *Adv. Mater.* **2008,** *20*, 4526-4529.

(72) Briseno, A. L.; Mannsfeld, S. C. B.; Lu, X. M.; Xiong, Y. J.; Jenekhe, S. A.; Bao, Z. N.; Xia, Y. N. Fabrication of field-effect transistors from hexathiapentacene single-crystal nanowires. *Nano Lett.* **2007,** *7*, 668-675.

(73) Briseno, A. L.; Miao, Q.; Ling, M. M.; Reese, C.; Meng, H.; Bao, Z. N.; Wudl, F. Hexathiapentacene: Structure, molecular packing, and thin-film transistors. *J. Am. Chem. Soc.* **2006,** *128*, 15576-15577.

(74) Schmidt, M. Elemental Sulfur - Challenge to Theory and Practice. *Angewandte Chemie-International Edition in English* **1973,** *12*, 445-455.

(75) Tobolsky, A. V. Polymeric Sulfur and Related Polymers. *Journal of Polymer Science Part C-Polymer Symposium* **1966**, 71-78.

(76) Tobolsky, A. V.; Eisenberg, A. Equilibrium Polymerization of Sulfur. *J. Am. Chem. Soc.* **1959,** *81*, 780-782.

(77) Tobolsky, A. V.; Macknight, W.; Beevers, R. B.; Gupta, V. D. The Glass Transition Temperature of Polymeric Sulphur. *Polymer* **1963,** *4*, 423-427.

(78) Bacon, R. F.; Fanelli, R. The viscosity of sulfur. *J. Am. Chem. Soc.* **1943,** *65*, 639-648.

(79) Fairbrother, F.; Gee, G.; Merrall, G. T. The Polymerization of Sulfur. *Journal of Polymer Science* **1955,** *16*, 459-469.

(80) Ding, R.; Leonov, A. I. A kinetic model for sulfur accelerated vulcanization of a natural rubber compound. *J. Appl. Polym. Sci.* **1996,** *61*, 455-463.

(81) Loo, C. T. High-Temperature Vulcanization of Elastomers .3. Network Structure of

Efficiently Vulcanized Natural-Rubber Mixes. *Polymer* **1974,** *15*, 729-737.

(82) Coleman, M. M.; Shelton, J. R.; Koenig, J. L. Sulfur Vulcanization of Hydrocarbon Diene Elastomers. *Industrial & Engineering Chemistry Product Research and Development* **1974,** *13*, 154-165.

(83) Meltzer, T. H.; Dermody, W. J.; Tobolsky, A. V. Fraction of Effective Sulfur Crosslinking in Polybutadiene Rubber Vulcanizates. *J. Appl. Polym. Sci.* **1965,** *9*, 3041-&.

(84) Blight, L. B.; Currell, B. R.; Nash, B. J.; Scott, R. T. M.; Stillo, C. Chemistry of the Modification of Sulfur by the Use of Dicyclopentadiene and of Styrene. *British Polymer Journal* **1980,** *12*, 5-11.

(85) Grant, D.; Vanwazer, J. R. Exchange of Parts between Molecules at Equilibrium .V. Alkyl-Terminated Chain Polysulfides + Polyselenides. *J. Am. Chem. Soc.* **1964,** *86*, 3012-3017.

(86) Kishore, K.; Ganesh, K. Synthesis, Characterization, and Thermal-Degradation Studies on Group Via Derived Weak-Link Polymers. *Macromolecules* **1993,** *26*, 4700-4705.

(87) Saville, R. W. The Reactions of Amines and Sulphur with Olefins .4. The Chemical and Thermal Decompositions of Nn'-Thiobisamines and Their Reactions with Olefins. *J. Chem. Soc.* **1958**, 2880-2888.

(88) Bateman, L.; Moore, C. G.; Porter, M. The Reaction of Sulphur and Sulphur Compounds with Olefinic Substances .11. The Mechanism of Interaction of Sulphur with Mono-Olefins and 1-5-Dienes. *J. Chem. Soc.* **1958**, 2866-2879.

(89) Shumane, M.; Gradwell, M. H. S.; McGill, W. J. Dimethylammonium dimethyldithiocarbamate-accelerated sulfur vulcanization. II. Vulcanization of rubbers and model compound 2,3-dimethyl-2-butene. *J. Appl. Polym. Sci.* **2001,** *82*, 3074-3083.

(90) Rosenthal, E. Q.; Puskas, J. E.; Wesdemiotis, C. Green Polymer Chemistry: Living

Dithiol Polymerization via Cyclic Intermediates. *Biomacromolecules* **2012,** *13*, 154-164.

(91) Goehtals, E. J.; Sillis, C. Oxidation of Dithiols to Polydisulfides by Means of Dimethylsulfoxide. *Makromolekulare Chemie-Macromolecular Chemistry and Physics* **1968,** *119*, 249-&.

(92) Block, E. Liquid sulfur as a reagent for solvent-free reactions: Simple and rapid synthesis of polysulfanes with 20 or more sulfur atoms with characterization by UPLC-(Ag+)-coordination ion spray-MS. *Abstr. Pap. Am. Chem. Soc.* **2013,** *246*.

(93) Wang, K.; Groom, M.; Sheridan, R.; Zhang, S. Z.; Block, E. Liquid sulfur as a reagent: synthesis of polysulfanes with 20 or more sulfur atoms with characterization by UPLC-(Ag+)-coordination ion spray-MS. *J. Sulfur Chem.* **2013,** *34*, 55-66.

(94) Ding, Y.; Hay, A. S. Copolymerization of elemental sulfur with cyclic(arylene disulfide) oligomers. *Journal of Polymer Science Part a-Polymer Chemistry* **1997,** *35*, 2961-2968.

(95) Ahmed, A.; Blanchard, L. P. Copolymerization of Elemental Sulfur with Styrene. *J. Appl. Polym. Sci.* **1984,** *29*, 1225-1239.

(96) Pujol, J. M.; Brossas, J.; Catala, J. M. Synthesis of Polybutadiene Polysulfide. *Journal of Polymer Science Part a-Polymer Chemistry* **1988,** *26*, 1573-1586.

(97) Pujol, J. M.; Brossas, J.; Catala, J. M. Synthesis of Telechelic Dithiol Oligomers Containing Sulfur Atoms-Moisture Barrier Properties. *J. Appl. Polym. Sci.* **1991,** *42*, 3091-3100.

(98) Penczek, S.; Duda, A. Anionic Copolymerization of Elemental Sulfur. *Pure Appl. Chem.* **1981,** *53*, 1679-1687.

(99) Duda, A.; Penczek, S. Anionic Copolymerization of Elemental Sulfur with Propylene Sulfide. *Macromolecules* **1982,** *15*, 36-40.

(100) Ji, X. L.; Lee, K. T.; Nazar, L. F. A highly ordered nanostructured carbon-sulphur

cathode for lithium-sulphur batteries. *Nat. Mater.* **2009,** *8*, 500-506.

(101) Ross, G. W. The Reaction of Sulphur and Sulphur Compounds with Olefinic Substances .10. The Kinetics of the Reaction of Sulphur with Cyclohexene and Other Olefins. *J. Chem. Soc.* **1958**, 2856-2866.

(102) Chung, W. J.; Griebel, J. J.; Kim, E. T.; Yoon, H.; Simmonds, A. G.; Ji, H. J.; Dirlam, P. T.; Glass, R. S.; Wie, J. J.; Nguyen, N. A.; Guralnick, B. W.; Park, J.; Somogyi, A.; Theato, P.; Mackay, M. E.; Sung, Y. E.; Char, K.; Pyun, J. The use of elemental sulfur as an alternative feedstock for polymeric materials. *Nat Chem* **2013,** *5*, 518-24.

(103) Chung, W. J.; Simmonds, A. G.; Griebel, J. J.; Kim, E. T.; Suh, H. S.; Shim, I. B.; Glass, R. S.; Loy, D. A.; Theato, P.; Sung, Y. E.; Char, K.; Pyun, J. Elemental sulfur as a reactive medium for gold nanoparticles and nanocomposite materials. *Angew. Chem. Int. Ed. Engl.* **2011,** *50*, 11409-12.

(104) Simmonds, A. G.; Griebel, J. J.; Park, J.; Kim, K. R.; Chung, W. J.; Oleshko, V. P.; Kim, J.; Kim, E. T.; Glass, R. S.; Soles, C. L.; Sung, Y.-E.; Char, K.; Pyun, J. Inverse Vulcanization of Elemental Sulfur to Prepare Polymeric Electrode Materials for Li–S Batteries. *ACS Macro Letters* **2014**, 229-232.

(105) Griebel, J. J.; Nguyen, N. A.; Namnabat, S.; Anderson, L. E.; Glass, R. S.; Norwood, R. A.; Mackay, M. E.; Char, K.; Pyun, J. Dynamic Covalent Polymers via Inverse Vulcanization of Elemental Sulfur for Healable Infrared Optical Materials. *Acs Macro Letters* **2015,** *4*, 862-866.

(106) Griebel, J. J.; Namnabat, S.; Kim, E. T.; Himmelhuber, R.; Moronta, D. H.; Chung, W. J.; Simmonds, A. G.; Kim, K. J.; van der Laan, J.; Nguyen, N. A.; Dereniak, E. L.; Mackay, M. E.; Char, K.; Glass, R. S.; Norwood, R. A.; Pyun, J. New Infrared Transmitting Material via Inverse Vulcanization of Elemental Sulfur to Prepare High Refractive Index Polymers.

Adv. Mater. **2014,** *26*, 3014-3018.

(107) Lova, P.; Manfredi, G.; Boarino, L.; Comite, A.; Laus, M.; Patrini, M.; Marabeli, F.; Soci, C.; Comoretto, D. Polymer Distributed Bragg Reflectors for Vapor Sensing. *Acs Photonics* **2015,** *2*, 537-543.

(108) Frezza, L.; Patrini, M.; Liscidini, M.; Comoretto, D. Directional Enhancement of Spontaneous Emission in Polymer Flexible Microcavities. *J. Phys. Chem. C* **2011,** *115*, 19939-19946.

(109) Bailey, J.; Sharp, J. S. Infrared Dielectric Mirrors Based on Thin Film Multilayers of Polystyrene and Polyvinylpyrrolidone. *Journal of Polymer Science Part B-Polymer Physics* **2011,** *49*, 732-739.

(110) Robbiano, V.; Giordano, M.; Martella, C.; Di Stasio, F.; Chiappe, D.; de Mongeot, F. B.; Comoretto, D. Hybrid Plasmonic-Photonic Nanostructures: Gold Nanocrescents Over Opals. *Advanced Optical Materials* **2013,** *1*, 389-396.

(111) Bailey, J.; Sharp, J. S. Thin film polymer photonics: Spin cast distributed Bragg reflectors and chirped polymer structures. *European Physical Journal E* **2010,** *33*, 41-49.

(112) Simmonds, A. G.; Griebel, J. J.; Park, J.; Kim, K. R.; Chung, W. J.; Oleshko, V. P.; Kim, J.; Kim, E. T.; Glass, R. S.; Soles, C. L.; Sung, Y. E.; Char, K.; Pyun, J. Inverse Vulcanization of Elemental Sulfur to Prepare Polymeric Electrode Materials for Li-S Batteries. *Acs Macro Letters* **2014,** *3*, 229-232.

(113) Griebel, J. J.; Li, G. X.; Glass, R. S.; Char, K.; Pyun, J. Kilogram Scale Inverse Vulcanization of Elemental Sulfur to Prepare High Capacity Polymer Electrodes for Li-S Batteries. *Journal of Polymer Science Part a-Polymer Chemistry* **2015,** *53*, 173-177.

(114) Chung, W. J.; Griebel, J. J.; Kim, E. T.; Yoon, H.; Simmonds, A. G.; Ji, H. J.; Dirlam, P. T.; Glass, R. S.; Wie, J. J.; Nguyen, N. A.; Guralnick, B. W.; Park, J.; Somogyi, A.; Theato,

P.; Mackay, M. E.; Sung, Y. E.; Char, K.; Pyun, J. The use of elemental sulfur as an alternative feedstock for polymeric materials. *Nature Chem.* **2013,** *5*, 518-524.

(115) Thomson, J. W.; Nagashima, K.; Macdonald, P. M.; Ozin, G. A. From Sulfur-Amine Solutions to Metal Sulfide Nanocrystals: Peering into the Oleylamine-Sulfur Black Box. *J. Am. Chem. Soc.* **2011,** *133*, 5036-5041.

(116) Davis, R. E.; Nakshbendi, H. F. Sulfur in Amine Solvents. *J. Am. Chem. Soc.* **1962,** *84*, 2085-2090.

(117) Hodgson, W. G.; Buckler, S. A.; Peters, G. Free Radicals in Amine Solutions of Elemental Sulfur. *J. Am. Chem. Soc.* **1963,** *85*, 543-546.

(118) Mori, K.; Nakamura, Y. Reaction of Sulfur Compound Activated by Amine .2. Reaction of Sulfur and Some Aliphatic Primary Amines. *J. Org. Chem.* **1971,** *36*, 3041-&.

(119) Dirlam, P. T.; Simmonds, A. G.; Kleine, T. S.; Nguyen, N. A.; Anderson, L. E.; Klever, A. O.; Florian, A.; Costanzo, P. J.; Theato, P.; Mackay, M. E.; Glass, R. S.; Char, K.; Pyun, J. Inverse vulcanization of elemental sulfur with 1,4-diphenylbutadiyne for cathode materials in Li-S batteries. *Rsc Advances* **2015,** *5*, 24718-24722.

(120) Kim, E. T.; Chung, W. J.; Lim, J.; Johe, P.; Glass, R. S.; Pyun, J.; Char, K. One-pot synthesis of PbS NP/sulfur-oleylamine copolymer nanocomposites via the copolymerization of elemental sulfur with oleylamine. *Polymer Chemistry* **2014,** *5*, 3617-3623.

(121) Liu, J.; Jeong, H.; Liu, J.; Lee, K.; Park, J. Y.; Ahn, Y. H.; Lee, S. Reduction of functionalized graphite oxides by trioctylphosphine in non-polar organic solvents. *Carbon* **2010,** *48*, 2282-2289.

(122) Hong, J.; Char, K.; Kim, B. S. Hollow Capsules of Reduced Graphene Oxide Nanosheets Assembled on a Sacrificial Colloidal Particle. *Journal of Physical Chemistry Letters* **2010,** *1*, 3442-3445.

(123) Kovtyukhova, N. I.; Ollivier, P. J.; Martin, B. R.; Mallouk, T. E.; Chizhik, S. A.; Buzaneva, E. V.; Gorchinskiy, A. D. Layer-by-layer assembly of ultrathin composite films from micron-sized graphite oxide sheets and polycations. *Chem. Mater.* **1999,** *11*, 771-778.

(124) Li, F.; Park, S.; Ling, D.; Park, W.; Han, J. Y.; Na, K.; Char, K. Hyaluronic acid-conjugated graphene oxide/photosensitizer nanohybrids for cancer targeted photodynamic therapy. *Journal of Materials Chemistry B* **2013,** *1*, 1678-1686.

(125) Yang, K. K.; Liang, S.; Zou, L. F.; Huang, L. W.; Park, C.; Zhu, L. S.; Fang, J. Y.; Fu, Q.; Wang, H. Intercalating Oleylamines in Graphite Oxide. *Langmuir* **2012,** *28*, 2904-2908.

(126) Chung, S. H.; Manthiram, A. High-Performance Li-S Batteries with an Ultra-lightweight MWCNT-Coated Separator. *Journal of Physical Chemistry Letters* **2014,** *5*, 1978-1983.

(127) Gu, M.; Lee, J.; Kim, Y.; Kim, J. S.; Jang, B. Y.; Lee, K. T.; Kim, B. S. Inhibiting the shuttle effect in lithium-sulfur batteries using a layer-by-layer assembled ion-permselective separator. *Rsc Advances* **2014,** *4*, 46940-46946.

(128) Huang, J. Q.; Zhang, Q.; Peng, H. J.; Liu, X. Y.; Qian, W. Z.; Wei, F. Ionic shield for polysulfides towards highly-stable lithium-sulfur batteries. *Energy & Environmental Science* **2014,** *7*, 347-353.

(129) Su, Y. S.; Manthiram, A. Lithium-sulphur batteries with a microporous carbon paper as a bifunctional interlayer. *Nature Communications* **2012,** *3*.

(130) Yao, H. B.; Yan, K.; Li, W. Y.; Zheng, G. Y.; Kong, D. S.; Seh, Z. W.; Narasimhan, V. K.; Liang, Z.; Cui, Y. Improved lithium-sulfur batteries with a conductive coating on the separator to prevent the accumulation of inactive S-related species at the cathode-separator interface. *Energy & Environmental Science* **2014,** *7*, 3381-3390.

(131) Zhou, G. M.; Pei, S. F.; Li, L.; Wang, D. W.; Wang, S. G.; Huang, K.; Yin, L. C.; Li, F.;

Cheng, H. M. A Graphene-Pure-Sulfur Sandwich Structure for Ultrafast, Long-Life Lithium-Sulfur Batteries. *Adv. Mater.* **2014,** *26*, 625-631.

(132) Hong, T. K.; Lee, D. W.; Choi, H. J.; Shin, H. S.; Kim, B. S. Transparent, Flexible Conducting Hybrid Multi layer Thin Films of Multiwalled Carbon Nanotubes with Graphene Nanosheets. *ACS Nano* **2010,** *4*, 3861-3868.

(133) Kong, B. S.; Geng, J. X.; Jung, H. T. Layer-by-layer assembly of graphene and gold nanoparticles by vacuum filtration and spontaneous reduction of gold ions. *Chem. Commun.* **2009**, 2174-2176.

(134) Lee, S. W.; Kim, B. S.; Chen, S.; Shao-Horn, Y.; Hammond, P. T. Layer-by-Layer Assembly of All Carbon Nanotube Ultrathin Films for Electrochemical Applications. *J. Am. Chem. Soc.* **2009,** *131*, 671-679.

(135) Lingstrom, R.; Wagberg, L. Polyelectrolyte multilayers on wood fibers: Influence of molecular weight on layer properties and mechanical properties of papers from treated fibers. *J. Colloid Interface Sci.* **2008,** *328*, 233-242.

(136) Yoo, D.; Shiratori, S. S.; Rubner, M. F. Controlling bilayer composition and surface wettability of sequentially adsorbed multilayers of weak polyelectrolytes. *Macromolecules* **1998,** *31*, 4309-4318.

(137) DeLongchamp, D. M.; Hammond, P. T. Fast ion conduction in layer-by-layer polymer films. *Chem. Mater.* **2003,** *15*, 1165-1173.

(138) DeLongchamp, D. M.; Hammond, P. T. Highly ion conductive poly(ethylene oxide)-based solid polymer electrolytes from hydrogen bonding layer-by-layer assembly. *Langmuir* **2004,** *20*, 5403-5411.

(139) Farhat, T. R.; Hammond, P. T. Designing a new generation of proton-exchange membranes using layer-by-layer deposition of polyelectrolytes. *Adv. Funct. Mater.* **2005,** *15*,

945-954.

(140) Seong, H.; Baek, J.; Pak, K.; Im, S. G. A Surface Tailoring Method of Ultrathin Polymer Gate Dielectrics for Organic Transistors: Improved Device Performance and the Thermal Stability Thereof. *Adv. Funct. Mater.* **2015,** *25*, 4462-4469.

(141) Kwak, M. J.; Oh, M. S.; Yoo, Y.; You, J. B.; Kim, J.; Yu, S. J.; Im, S. G. Series of Liquid Separation System Made of Homogeneous Copolymer Films with Controlled Surface Wettability. *Chem. Mater.* **2015,** *27*, 3441-3449.

(142) You, J. B.; Kim, S. Y.; Park, Y. J.; Ko, Y. G.; Im, S. G. A Vapor-Phase Deposited Polymer Film to Improve the Adhesion of Electroless-Deposited Copper Layer onto Various Kinds of Substrates. *Langmuir* **2014,** *30*, 916-921.

(143) Baxamusa, S. H.; Im, S. G.; Gleason, K. K. Initiated and oxidative chemical vapor deposition: a scalable method for conformal and functional polymer films on real substrates. *Phys. Chem. Chem. Phys.* **2009,** *11*, 5227-5240.

(144) Park, J.; Hammond, P. T. Polyelectrolyte multilayer formation on neutral hydrophobic surfaces. *Macromolecules* **2005,** *38*, 10542-10550.

(145) Cho, J.; Char, K. Effect of layer integrity of spin self-assembled multilayer films on surface Wettability. *Langmuir* **2004,** *20*, 4011-4016.

(146) Cho, J.; Char, K.; Hong, J. D.; Lee, K. B. Fabrication of highly ordered multilayer films using a spin self-assembly method. *Adv. Mater.* **2001,** *13*, 1076-+.

(147) Cho, J.; Lee, S. H.; Kang, H. M.; Char, K.; Koo, J.; Seung, B. H.; Lee, K. B. Quantitative analysis on the adsorbed amount and structural characteristics of spin self-assembled multilayer films. *Polymer* **2003,** *44*, 5455-5459.

(148) Seo, J.; Lutkenhaus, J. L.; Kim, J.; Hammond, P. T.; Char, K. Development of surface morphology in multilayered films prepared by layer-by-layer deposition using poly(acrylic

acid) and hydrophobically modified poly(ethylene oxide). *Macromolecules* **2007,** *40*, 4028-4036.

(149) Seo, J.; Lutkenhaus, J. L.; Kim, J.; Hammond, P. T.; Char, K. Effect of the layer-by-layer (LbL) deposition method on the surface morphology and wetting behavior of hydrophobically modified PEO and PAA LbL films. *Langmuir* **2008,** *24*, 7995-8000.

(150) Su, Y. S.; Fu, Y. Z.; Cochell, T.; Manthiram, A. A strategic approach to recharging lithium-sulphur batteries for long cycle life. *Nature Communications* **2013,** *4*.

국문 초록

황은 자연환경과 밀접한 관계 속에서 상호작용하기 때문에 인류의 삶에 큰 영향을 미친다. 또한 황은 전 세계적인 원유정제 과정 속에서 폐기물로서 과잉 생산되고 있는 실정이다. 따라서 황을 활용할 수 있는 화학적 기법을 개발하는 연구의 필요성이 대두된다. 황은 기능성 신소재로서의 많은 독특한 특성을 지니고 있으나, 기계적 / 화학적으로 취약한 성질 때문에 가공되어 활용되지 못해왔다.

본 박사학위 논문은 황의 분자구조 개질 및 내부 나노재료 복합화, 표면 개질을 통해 기능성 및 가공성을 향상시킴으로써 광학소자 및 차세대 배터리 양극재 등 다양한 분야로의 활용에 관한 연구로서, 1장에서는 황의 물리화학적 특성 및 기능성에 대한 소개 및 응용분야 적용을 위한 해결과제를 제시한다.

2장에서는 황 본연의 우수한 기능성을 담지하면서 가공성을 획기적으로 향상시킨 황 공중합체를 합성하였고, 향상된 열가소성 및 용해성 등에 대해 분석하였다. 황 공중합체의 향상된 물리화학적 특성을 이용한 용융공정 및 용액 공정 기술을 개발하였고, 이를 광학적, 전기화학적 에너지 저장 소재 등에 활용하여 기존의 유기 고분자 물질에 비해 획기적으로 향상된 성능을 구현하였다.

3장과 4장에서는 각각, 황 공중합체의 기능성을 한 층 더 향상시키기 위해, 무기나노입자 및 그래핀과의 하이브리드화를 진행하였다. 올레일 아민의 독특한 이중 반응성을 활용함으로써, 황-올레일 아민 공중합체가 형성되는 동시에, 아민 작용기가 무기나노입자나 산화 그래핀 표면에 결합하여, 나노 규모의 하이브리드 물질을 합성하였다. 특히, 합성된 그래핀-황 공중합체 하이브리드 재료는 황 공중합체의 전기전도성을 획기적으로 향상시킴으로써, 리튬-황 이차전지 전극으로 활용하였을 때, 기존에 비해 개선된 출력성능을 보였다.

5장에서는, 황 및 황 공중합체 기반의 양극재 표면의 직접적인 개질을 통한 리튬-황 이차전지 전극의 성능 개선에 대한 연구를 진행하였다. 다층박막 적층법을 활용하여, 황 양극재 표면에 균질한 박막을 형성하여, 이에 따른 표면 특성 변화를 분석하였다. 황 표면의 확산방지막 형성을 통해, 안정적인 전기화학 반응을 지속시킴으로써 리튬-황 이차전지의 수명 연장에 기여할 수 있음을 보고하였다.

이러한 일련의 연구 결과들을 바탕으로, 황의 분자구조적 측면과 나노미터 및 마이크로미터 수준의 복합적 개질을 통해 황을 활용한 광학소자 및 배터리 전극의 성능을 획기적으로 향상시킬 수 있음을 보였다.

주요어 : 황 공중합체, 하이브리드, 표면 개질, 리튬-황 전지, 컨포멀 코팅

학번 : 2010-22808